Alaska University Transportation Center

Use of H2Ri Wicking Fabric to Prevent Frost Boils in the Dalton Highway Beaver Slide Area, Alaska
Final Report

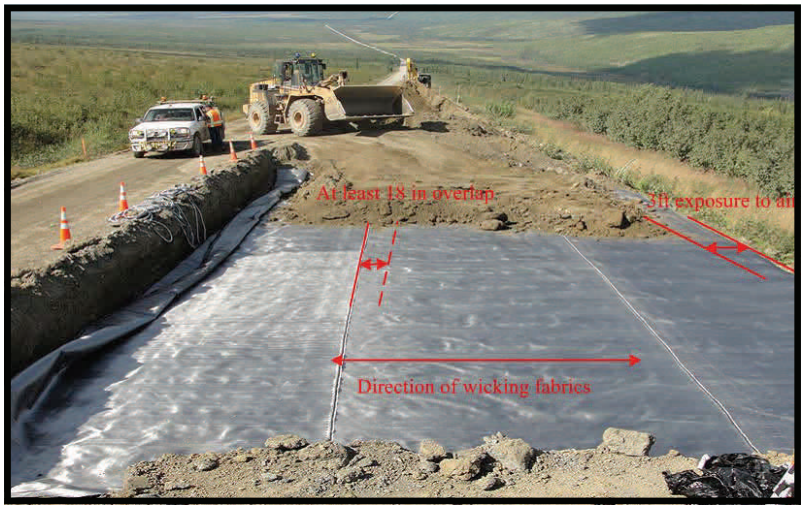

Prepared By:
Xiong Zhang, Ph.D., P.E.
Dept. of Civil and Environmental Engineering
University of Alaska Fairbanks
Wendy Presler, Graduate Student

December 2012

Prepared By:

Alaska University Transportation Center
Duckering Building Room 245
P.O. Box 755900
Fairbanks, AK 99775-5900

INE/AUTC 12.23

REPORT DOCUMENTATION PAGE

Form approved OMB No.

1. AGENCY USE ONLY (LEAVE BLANK)	2. REPORT DATE	3. REPORT TYPE AND DATES COVERED
	August 2012	Final Report (07/01/2010-2/15/2012)

4. TITLE AND SUBTITLE

Use of H2Ri Wicking Fabric to Prevent Frost Boils in the Dalton Highway Beaver Slide Area, Alaska

5. FUNDING NUMBERS

AUTC#510020/ RR10.02
DTRT06-G-0011

6. AUTHOR(S)
Xiong Zhang, Ph.D., P.E.
Wendy Presler, Graduate Student
Dept. of Civil and Environmental Engineering
University of Alaska Fairbanks

7. PERFORMING ORGANIZATION NAME(S) AND ADDRESS(ES)
Alaska University Transportation Center
P.O. Box 755900
Fairbanks, AK 99775-5900

8. PERFORMING ORGANIZATION REPORT NUMBER

INE/AUTC 12.23

9. SPONSORING/MONITORING AGENCY NAME(S) AND ADDRESS(ES)
Research and Innovative Technology Administration (RITA), U.S. Dept. of Transportation
1200 New Jersey Ave, SE, Washington, DC 20590
TenCate Geosynthetics North America, 365 South Holland Drive, Pendergrass, GA 30567

10. SPONSORING/MONITORING AGENCY REPORT NUMBER

11. SUPPLENMENTARY NOTES
Performed in cooperation with TENCATE GEOSYTHETICS (North America), Alaska Department of Transportation & Public Facilities, and Geo-Watersheds Scientific.

12a. DISTRIBUTION / AVAILABILITY STATEMENT

No restrictions

12b. DISTRIBUTION CODE

13. ABSTRACT (Maximum 200 words)

Many roads in Alaska, such as the Dalton Highway, experience degradation during spring thaw due to the downslope running of shallow groundwater. The water flow down the slope and pools up in the road embankments, where it freezes, causing frost boils and subsequent road damage. One good example of this damage occurred at Beaver Slide, near mile 110.5 of the Dalton Highway. The frost boils have resulted in extremely unsafe driving conditions and frequent accidents. Past repair efforts indicate conventional road construction methods do not work. The Mirafi Nylon Wicking Fabric, developed by Tencate Geosynthetics (North America), offers a potential solution. Featuring high specific surface area and high permeability, preliminary laboratory tests of MNWF indicate that it has great promise as a cost-effective means to solve the frost boil 8 problems on northern road systems. This proposed project aims to verify the theory, testing MNWF at Beaver Slide using moisture and temperature sensors to gather measurements for one year. Upon evaluation, researchers expect improved performance of pavement at installation sites. Data will be gathered regarding soil properties at the site; observed thermal and moisture changes and pavement performance over a one-year period; analysis of frost boil mechanisms; and evaluation of MNWF effectiveness to mitigate frost boil problems. Research results may lead to incorporation of MNWF in the geotechnical engineering curriculum at UAF. Further, recommendations developed from the research will be useful in ensuring a reliable and economic design of roads in arctic environments.

14- KEYWORDS: Slope stability (Jbgpx), Embankments (Pdxe), Permafrost (Rbespfp)

15. NUMBER OF PAGES

111

16. PRICE CODE

N/A

17. SECURITY CLASSIFICATION OF REPORT	18. SECURITY CLASSIFICATION OF THIS PAGE	19. SECURITY CLASSIFICATION OF ABSTRACT	20. LIMITATION OF ABSTRACT
Unclassified	Unclassified	Unclassified	N/A

Notice

This document is disseminated under the sponsorship of the U.S. Department of Transportation in the interest of information exchange. The U.S. Government assumes no liability for the use of the information contained in this document.

The U.S. Government does not endorse products or manufacturers. Trademarks or manufacturers' names appear in this report only because they are considered essential to the objective of the document.

Quality Assurance Statement

The Federal Highway Administration (FHWA) provides high-quality information to serve Government, industry, and the public in a manner that promotes public understanding. Standards and policies are used to ensure and maximize the quality, objectivity, utility, and integrity of its information. FHWA periodically reviews quality issues and adjusts its programs and processes to ensure continuous quality improvement.

Author's Disclaimer

Opinions and conclusions expressed or implied in the report are those of the author. They are not necessarily those of the Alaska DOT&PF or funding agencies.

SI* (MODERN METRIC) CONVERSION FACTORS

APPROXIMATE CONVERSIONS TO SI UNITS

Symbol	When You Know	Multiply By	To Find	Symbol
		LENGTH		
in	inches	25.4	millimeters	mm
ft	feet	0.305	meters	m
yd	yards	0.914	meters	m
mi	miles	1.61	kilometers	km
		AREA		
in^2	square inches	645.2	square millimeters	mm^2
ft^2	square feet	0.093	square meters	m^2
yd^2	square yard	0.836	square meters	m^2
ac	acres	0.405	hectares	ha
mi^2	square miles	2.59	square kilometers	km^2
		VOLUME		
fl oz	fluid ounces	29.57	milliliters	mL
gal	gallons	3.785	liters	L
ft^3	cubic feet	0.028	cubic meters	m^3
yd^3	cubic yards	0.765	cubic meters	m^3
		NOTE: volumes greater than 1000 L shall be shown in m^3		
		MASS		
oz	ounces	28.35	grams	g
lb	pounds	0.454	kilograms	kg
T	short tons (2000 lb)	0.907	megagrams (or "metric ton")	Mg (or "t")
		TEMPERATURE (exact degrees)		
^oF	Fahrenheit	5 (F-32)/9 or (F-32)/1.8	Celsius	^oC
		ILLUMINATION		
fc	foot-candles	10.76	lux	lx
fl	foot-Lamberts	3.426	$candela/m^2$	cd/m^2
		FORCE and PRESSURE or STRESS		
lbf	poundforce	4.45	newtons	N
lbf/in^2	poundforce per square inch	6.89	kilopascals	kPa

APPROXIMATE CONVERSIONS FROM SI UNITS

Symbol	When You Know	Multiply By	To Find	Symbol
		LENGTH		
mm	millimeters	0.039	inches	in
m	meters	3.28	feet	ft
m	meters	1.09	yards	yd
km	kilometers	0.621	miles	mi
		AREA		
mm^2	square millimeters	0.0016	square inches	in^2
m^2	square meters	10.764	square feet	ft^2
m^2	square meters	1.195	square yards	yd^2
ha	hectares	2.47	acres	ac
km^2	square kilometers	0.386	square miles	mi^2
		VOLUME		
mL	milliliters	0.034	fluid ounces	fl oz
L	liters	0.264	gallons	gal
m^3	cubic meters	35.314	cubic feet	ft^3
m^3	cubic meters	1.307	cubic yards	yd^3
		MASS		
g	grams	0.035	ounces	oz
kg	kilograms	2.202	pounds	lb
Mg (or "t")	megagrams (or "metric ton")	1.103	short tons (2000 lb)	T
		TEMPERATURE (exact degrees)		
^oC	Celsius	1.8C+32	Fahrenheit	^oF
		ILLUMINATION		
lx	lux	0.0929	foot-candles	fc
cd/m^2	$candela/m^2$	0.2919	foot-Lamberts	fl
		FORCE and PRESSURE or STRESS		
N	newtons	0.225	poundforce	lbf
kPa	kilopascals	0.145	poundforce per square inch	lbf/in^2

*SI is the symbol for the International System of Units. Appropriate rounding should be made to comply with Section 4 of ASTM E380.
(Revised March 2003)

TABLE OF CONTENT

LIST OF FIGURES

LIST OF TABLES

ACKNOWLEDGMENTS

The authors wish to express their appreciation to the people who helped in this research project. The discussions with Jeff Currey (AKDOT&PF Northern Region Geotechnical Engineer), Dwight Stuller, and Billy Connor made the project possible. TenCate Geosynthetics provided research funding for the preliminary laboratory tests and the H2Ri needed for the field implementation. Special thanks go to David M. Jones, Brett Odgers, and Bruce Lacina for their continuous support during the whole process. Billy Connor at the Alaska University Transportation Center (AUTC) provided funding for the instrumentation and valuable input from the beginning to the end of this project.

The Dalton Highway Maintenance and Operations section of Alaska DOT&PF provided the equipment and personnel to construct the test section. William Bunch, Robert Buggey, Brad King, and Glenn Hollett were the crew members that helped with the construction of the test section. Michael R. Lilly and Jeff Bosworth from Geo-Watersheds Scientific helped with installation of the thermal and moisture sensors, as well as construction of the data-acquisition station. William Russell helped facilitate the field trips for data acquisition. Acknowledgment is extended to graduate students Lin Li and Ruiqiang Song for their contributions in field and laboratory testing and data analysis for the project.

ABSTRACT

EXECUTIVE SUMMARY

Beaver Slide is the name of a downhill stretch of road near mile 110.5 on the Dalton Highway, heading north. The road gradient is approximately 11%, and the road prism is on a side hill. The embankment is about 4 feet on the high (west) side and 9 feet on the low (east) side. Each year, frost boils and soft spots appear in late April and remain all summer. The soft areas heal if there are periods with no rain, but as soon as a significant amount of rain falls, they reappear. The soft areas go away after freeze-up. Frost boils cause extremely unsafe driving conditions and frequent accidents. Past repair efforts indicate that conventional road construction methods do not work. TenCate Geosynthetics (North America) recently developed a wicking fabric called H2Ri. The fabric has high specific surface area (consequently high wettability and high capillary action) and high permeability. Preliminary laboratory tests indicate its promise as a cost-effective means for solving the frost boil problems of northern road systems. The purpose of the proposed project was to verify the effectiveness of H2Ri in mitigating frost boils that occur in roads in Alaska. A test section was built at the Beaver Slide area of the Dalton Highway with the installation of two layers of H2Ri. The test section was instrumented with sensors to measure changes in moisture and temperature over two years. Results were analyzed to evaluate the wicking fabric's effectiveness in mitigating frost boils.

The obtained data indicate that there are two mechanisms for the formation of frost boils (also referred to as "soft spots") at Beaver Slide: (a) frost heave and subsequent thaw weakening, which occur in early spring, and (b) upward pressurized water flow to the road surface during lengthy rainy periods, similar to Artesian water, from mid-summer to fall. The test section was built at a site where soft spots had occurred most frequently in previous years. Surface observations made by the Alaska Department of Transportation and Public Facilities Maintenance and Operations (M&O) road crew for the Dalton Highway indicate that use of H2Ri eliminated the damage caused by both formation mechanisms. The test section performed well over the two-year study. During this time, no soft spots or frost boils occurred in the test section treated with H2Ri, though they were observed past both the upper and lower ends of the test section during early spring or a particularly rainy period. The M&O road crew reports that it is clear where the road was treated with H2Ri based on the road surface performance.

The animation of change in volumetric water content indicated that water flows along the direction of the wicking fabric to the shoulder of the road. Field observations found that soil at the shoulder was damp. The animation of change in volumetric water content and temperature in the road structure indicated that formation of frost boils in early spring is due to thaw weakening only, since the soil above the elevation of the ditch line is still frozen when frost boils appear.

The H2Ri wicking fabric successfully eliminated frost heave and thaw weakening in the first 3.5 feet below the road surface (below the second layer of H2Ri). Observed volumetric moisture content indicated that the soils never reached saturation. In the D-1 material used in

the Beaver Slide area, no frost heave was observed at all. However, in soils 7 feet below the centerline of the road surface, which is beyond the treated zone, excess water due to frost heave was indicated, though it occurred too deep to cause damage to the road structure.

Results indicate that H2Ri, if used properly, is a good material for draining water from the road structure. The material has high ability to absorb water from surrounding soils; it also has high ability to transport water under differential water pressure. The pressure difference is generated by exposing the H2Ri wicking fabric to the atmosphere.

The obtained data indicate that the instrumented sensors functioned well and that data were consistent with each other. The whole data-acquisition system performed well over the two-year study and could be used for longer monitoring periods if needed.

CHAPTER 1: INTRODUCTION

BACKGROUND

Beaver Slide is a stretch of road near mile 110.5 of the Dalton Highway (Figure 1.1), about five miles south of the Arctic Circle. A general area map of the Beaver Slide site is shown in Figure 1. The road is downhill heading north, and its gradient is approximately 11%. The road prism is on a side hill (Figure 2). The embankment is about 4 feet on the high (west) side and 9 feet on the low (east) side. Each spring, shallow groundwater flows downslope and into the road embankment, causing frost boils and subsequent road damage. Frost boils that occurred in May 2010 are shown in Figure 2. When truck drivers see soft spots, they tend to brake, which adds load and worsens road conditions. Frost boils result in extremely unsafe driving conditions and sometimes are the cause of accidents. Past Alaska Department of Transportation & Public Facilities (AKDOT&PF) road maintenance indicates that conventional repair methods do not last. French drains were installed by AKDOT&PF at a skew to drain water from the road section. Another repair method involved removing the existing road section and replacing it with better material, a repair that was extremely costly. Both of these methods were only a local repair, as the problem moved downslope.

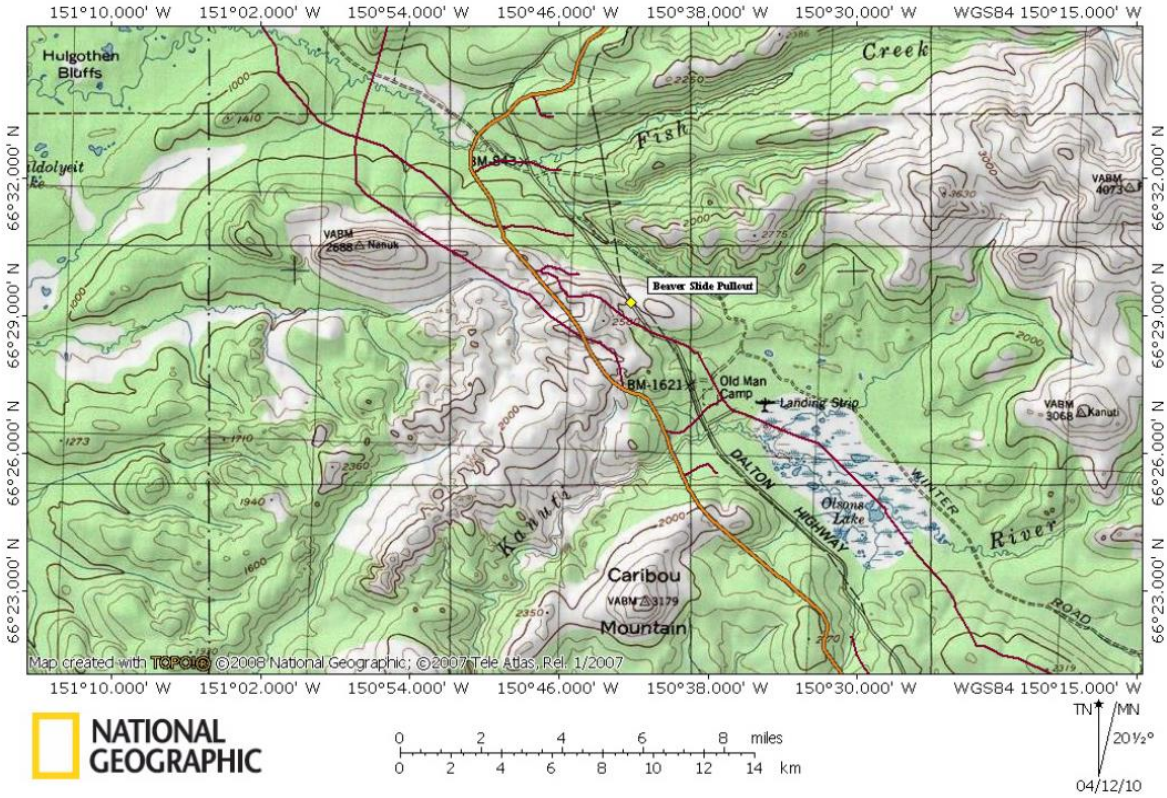

Figure 1. Dalton Highway Beaver Slide study site general area map

Figure 2. Frost boils at Beaver Slide on May 12, 2012 (looking north)

A material called H2Ri Nylon Wicking Fabric recently developed by TenCate Geosynthetics (North America) has high specific surface area (consequently high wettability and high capillary action) and high permeability. Preliminary laboratory tests indicate it has great promise as a cost-effective means for solving the problem of frost boils. The purpose of the proposed project was to verify the effectiveness of H2Ri in mitigating frost boils in roads in Alaska. A test section was built at Beaver Slide with the installation of two layers of H2Ri. The test section was instrumented with sensors to measure changes in moisture and temperature over two years, and the results were analyzed.

OBJECTIVES

The main objectives of this project were (1) to construct a test section with the installation of two layers of H2Ri and instrumentation for moisture and temperature sensors; (2) to systematically monitor moisture and temperature changes in the test section for a period of two years; and (3) to analyze field observation results and evaluate the effectiveness of H2Ri in reducing frost boils and improving the performance of roads in Alaska.

RESEARCH METHODOLOGY

To achieve the objectives of this study, the following major tasks were proposed:

- Task 1: Construction of the test section and soil sampling
- Task 2: Laboratory characterization of soil properties
- Task 3: Field monitoring performance of the test section

- Task 4: Data processing and analyses
- Task 5: Draft of final report and recommendations

To meet the objectives of this study, the following major tasks were conducted:

Task 1: Construction of the test section and soil sampling

A problem area at the Beaver Slide was selected to construct the proposed test section. The test section was about 60 feet long and included the installation of two layers of H2Ri at depths of 3.5 feet and 2.5 feet below the road surface. Twenty-two moisture sensors were installed at four different elevations and seven different locations to measure moisture changes in the embankment through two full freeze-thaw seasons. The same number of thermistors was installed at the same locations as the moisture sensors to monitor temperature changes in the road structure. A data collection station was also built to house the data-acquisition system. TenCate Geosynthetics provided the H2Ri needed for field implementation. The Dalton Highway M&O section of AKDOT&PF provided the equipment and labor to construct the test section. Michael R. Lilly from Geo-Watersheds Scientific helped with installation of the thermal and moisture sensors as well as construction of the data-acquisition station. The Alaska University Transportation Center provided the funding needed for instrumentation and field monitoring. The test section was constructed in such a way that one lane was built by folding excess fabric at the centerline while the other lane was kept open for safe traffic flow. The existing embankment material was reused for construction of the test section and collected for laboratory tests to characterize soil properties. A detailed description of the construction of the test section is given in Chapter 3.

Task 2: Laboratory characterization of soil properties

Laboratory tests were performed to characterize soil properties including sieve analysis (AASHTO T27-99), moisture content, and plasticity index (ASTM D 4318) to obtain the liquid limit, plastic limit, and plasticity index for the fines only. Compaction tests were performed for the three materials to obtain the optimum moisture content (OMC) and maximum dry density (MDD). Suction tests (i.e., the pressure plate test, ASTM D2325-68, for suction less than 1,500 kPa and salt concentration tests for suction higher than 1,500 kPa) were performed to obtain the soil water characteristic curve at room temperature, to evaluate the water-storage characteristics of the base materials, and to examine the mechanism of H2Ri to remove water from the road structure. The test results are presented in Chapter 4.

Task 3: Field monitoring of moisture and temperature changes and performance of the test section

Soil moisture content and temperatures were measured at different depths at different locations of the test section for two years (August 2010 to August 2012). Hourly data measurements and storage were made by the data-acquisition system. The research team went to the site to collect data every three to five months, depending on weather and thermal conditions at the test section. Visual observations were made to evaluate the performance of the test section. The analysis results are presented in Chapter 4.

Task 4: Data processing and analyses

Results from the laboratory tests and field monitoring of the moisture and thermal changes in the test section were analyzed to identify the source and movement of water, as well as related frost boil mechanisms. The effectiveness of using H2Ri to prevent frost boils was evaluated. The analysis results are presented in Chapter 4.

Task 5: Draft of final report and recommendations

A final report was drafted upon completion of data analyses. The report includes a literature survey and investigation of the results of other researchers (presented in Chapter 2), a description of the project's research methods and approach, test procedures and results, findings, and suggestions for further study. Recommended uses of H2Ri for road projects in Alaska are provided as well.

CHAPTER 2: LITERATURE REVIEW

Since frost boils are mainly related to frost heave and thaw weakening, a literature review was made on methods used to mitigate these two problems. Frost heave and thaw weakening cause extensive damage to road structures in Alaska and other northern regions. The formation of ice lenses in a road structure is shown in Figure 3. The three conditions necessary for the formation of ice lenses and thus frost heave are (1) frost-susceptible (FS) soil, (2) subfreezing temperatures, and (3) water (must be available from the groundwater table, infiltration, or an aquifer, or held within the voids of fine-grained soil).

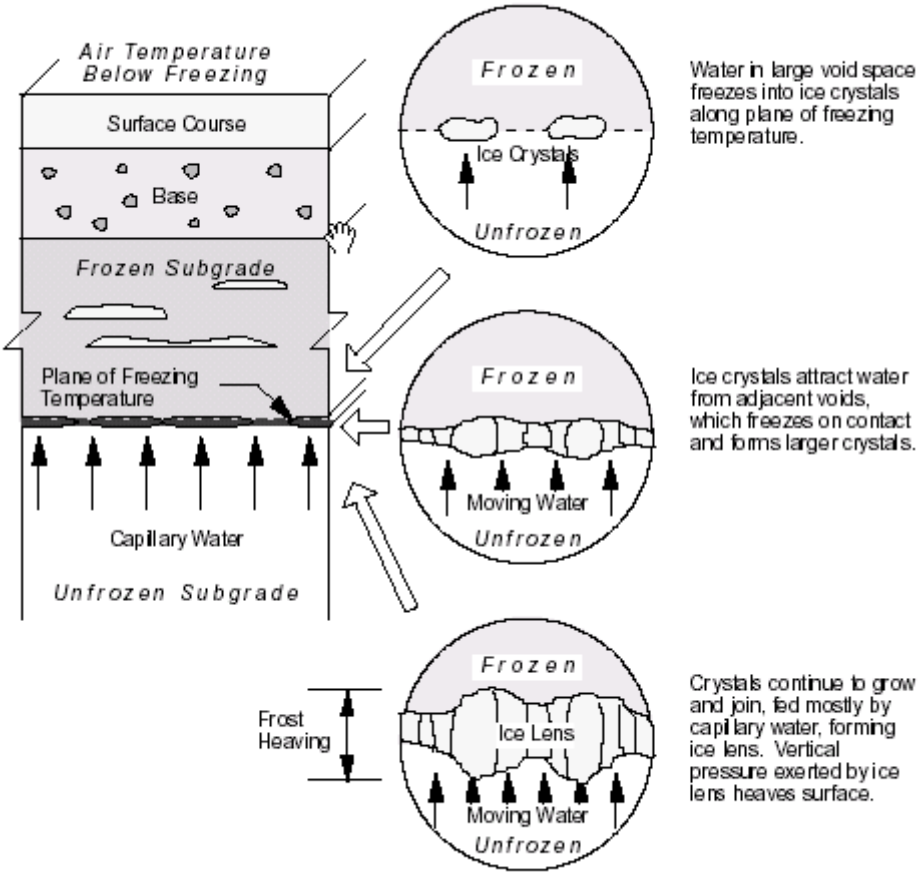

Figure 3. Formation of ice lenses in a pavement structure

Unfortunately, all three conditions are met in many places in Alaska. Removing any one of these three conditions will eliminate or at least minimize frost heave and thaw weakening. Numerous techniques have been developed to mitigate damage to roads and airfields caused by frost heave and thaw weakening. The best-known and most widely employed technique involves removing frost-susceptible (FS) soils and replacing them with non-frost-susceptible (NFS) soils of adequate thickness to reduce strain in frost-susceptible soil layers to an acceptable level *(Removal of condition #1).* AKDOT&PF stipulates that D-1 material with a fines content of less than 6% be used as base course material (AKDOT&PF, 2004). Other methods include use of insulation to reduce the freeze and thaw depth (Esch 1994) *(Removal of condition #2).* In areas where removal of FS soils and reduction of subfreezing

temperatures are difficult and expensive, removal of water could lead to savings in construction costs. By breaking the capillary flow path, frost action is less severe *(Removal of condition #3).*

A capillary barrier is a layer of coarse-grained soils or geosynthetics in a fine-grained soil that (i) reduces upward capillary flow of soil water due to the suction gradient generated by evaporation or freezing, and/or (ii) reduces or prevents water from infiltrating from the overlying fine-pored unsaturated soil into the soil below the capillary barrier (Henry and Holtz 2001). In the latter case, if the capillary barrier is sloped, the infiltrating water flows in the fine soil downward along the interface with the capillary barrier.

Granular capillary barriers have been used successfully to reduce frost heave of roads. Taber (1929) found that placing a layer of coarse sand above the water supply in frost-susceptible soil specimens being frozen from the top down eliminated frost heave. Taber (1929) noted that frost heaving requires substantially more water than is naturally available in the soil pores. Casagrande (1938) and Beskow (1946) described placing a layer of sand or gravel above the water table in road construction to reduce frost heave of overlying fine-grained soil. Later, Rengmark (1963) and Taivenen (1963) documented using a sand layer above the water table to help prevent frost heave in overlying frost-susceptible soil.

Geotextiles and geocomposites were evaluated as capillary barriers to reduce frost damage in pavement structures. Geosynthetic drainage nets (geonets) have been found to serve as excellent capillary barriers under most conditions because of their large pore size. The performance of nonwoven geotextiles as a capillary barrier appears to be compromised by soil intrusion into their interiors, decreasing the pore size and increasing the affinity of the material to water. Hoover et al. (1981) and Allen et al. (1983) independently performed experiments indicating that certain geotextiles reduced frost heave when the material was placed horizontally in upright, cylindrical soil specimens that were frozen from the top down, with water freely available at the base. Henry (1998) noted the importance of the surface properties of geotextiles; that is, that hydrophobic geotextiles were much more effective in reducing frost heave than hydrophilic geotextiles. Henry (1996) concluded that properly selected geotextiles reduce frost heave in soils by functioning as capillary barriers. Henry summarized guidelines for granular capillary barriers, suggesting their use as preliminary guidelines for geotextile capillary barriers:

1. Their thickness should exceed the height of the capillary rise of water in them.
2. They should be placed above the water table and as deep in the soil as practical—below the depth of frost penetration, if possible.
3. Drainage should be placed below them.
4. They should be protected from contamination with fine-grained soil by the use of filters on the top and bottom.

Henry concluded that geotextiles probably can be used for a combination of functions to reduce frost-related damage, besides serving as capillary barriers during freezing and

reinforcing or separating and filtering subgrade layers, or both, during thaw. Figure 4 shows a capillary barrier installed according to guidance presented in Henry (1996).

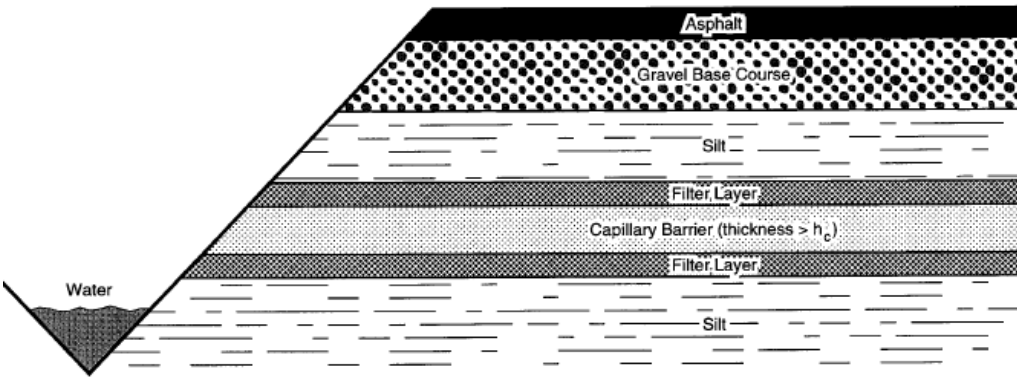

Figure 4. Sketch depicting a capillary barrier installed according to guidance presented in past work (Henry 1996)

In recent years, the Geocomposite Capillary Barrier Drain (GCBD) was proposed as a promising method to reduce frost damage in pavement structures. A typical example of this method is the NCHRP-IDEA Project 68 "Geocomposite barrier drain for limiting moisture changes in pavement subgrades and base courses" (Henry and Stormont 2002). A GCBD consists of a capillary barrier layer sandwiched between transport layers (Figure 5). The function of the capillary barrier layer is to impede unsaturated flow, either upward or downward. A capillary barrier is formed by a layer of relatively coarse or large-pore material. Such a material, although conductive under saturated conditions, will have very low or nonexistent hydraulic conductivity under most suctions. The effectiveness of a capillary barrier is related to the dimensions of its pores: in general, the larger the pores, the lower the suctions at which the material will remain nonconductive.

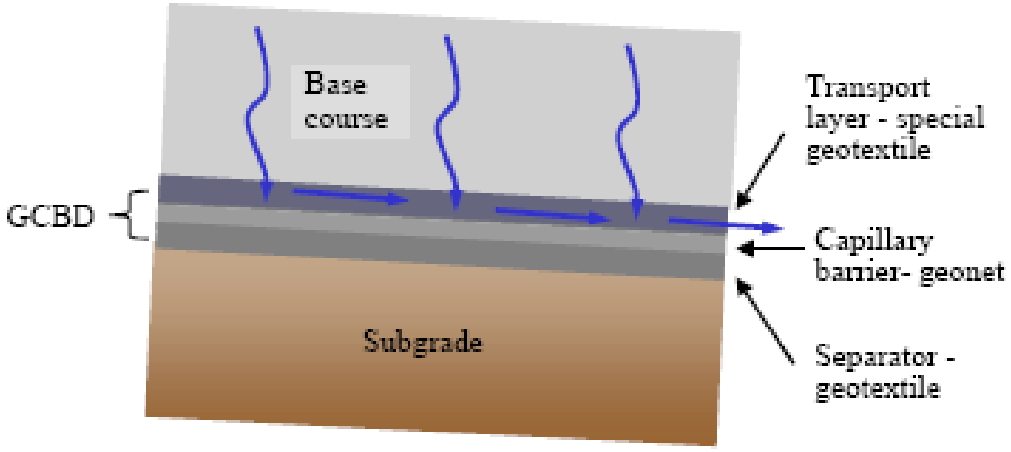

Figure 5. GCBD between base course and subgrade, illustrating how water laterally drains in the transport layer (Henry and Stormont, 2002)

The GCBD is similar to drains commonly used to minimize the impacts of frost. However, conventional drainage systems are not wholly effective in reducing water-related problems in partially saturated soils (Beskow 1991), where soil above the groundwater table

is unsaturated, and frost heave occurs through the capillary rise of water. The GCBD is designed as a capillary break and drainage system that can suck water out of soil—that is, provide drainage while the soil is unsaturated. The key to the success of such a system is a material that has high wettability (which means it can absorb water from unsaturated soils) and high permeability (i.e., it can transport the absorbed water out of the pavement structure quickly).

The transport layer used in Henry and Stormont (2002) was a heavy woven, multifilament material with a mass per unit area of 2370 g/m^2, a thickness of 3.2 mm, and an O_{95} size of 0.075 mm. The infiltration test results indicated that the use of the GCBD to limit moisture changes in pavement subgrades and bases was promising. At infiltration rates that typically occur in the field and are of concern to transportation agencies, the GCBD drained water from overlying base material that was not saturated—base aggregate that is used in New Mexico and in New Hampshire. Furthermore, the GCBD prevented the moistening of the subgrade at many of the infiltration rates tested. Whether the capillary barrier will reduce or prevent frost heave by preventing upward flow during freezing was not tested.

All of the capillary barrier methods just discussed were attempts to cut off capillary water flow by generating a horizontal layer with very low unsaturated permeability under suction. The whole structure is permeable for downward rainfall infiltration. This type of capillary barrier requires that thickness exceeds the height of the capillary rise of water in it, as discussed previously. In addition, the barrier provides conditions suitable for water vapor flow because of its high porosity and comparatively low equilibrium degrees of saturation. Guthrie and Hermansson (2006) reported test results indicating that granular base materials became saturated due to water vapor flow during freezing. An impermeable capillary barrier such as a geomembrane seems to be a better option for reducing frost heave in soils.

At present, few references can be found regarding the use of an impermeable layer to reduce the frost heave problem. The major concern might be that though an impermeable layer can completely cut off capillary water flow during frost heave, it also prevents natural drainage of rainfall infiltration and would permanently trap water within the soil layers above it. This phenomenon may occur if the impermeable layer is placed horizontally in the pavement structure, but was not observed in the large-scale infiltration test performed by Henry and Stormont (2002), when the capillary barrier was tilted in the pavement structure with a slope gradient of 5%.

Jay (2002) reported frost heave test results for the Terram Frost Blanket. The Terram Frost Blanket is composed of three layers of geosynthetics (Figure 6). The top layer is a nonwoven geotextile (polypropylene/polyethylene) that allows water from the overlying soil to enter the drainage net below. The center layer is a high-density polyethylene drainage net that allows water entering from the soil to drain away laterally to side drains. The bottom layer is a hydrophobic enhanced nonwoven geotextile that resists the capillary rise of groundwater from beneath. The hydrophobic geotextile is reported to behave like a one-way valve: it resists upward capillary rise of water, but remains permeable to downward flow. In addition, the hydrophobic geotextile allows downward drainage of rainfall infiltration and

thus does not "pond" water, but resists the upward capillary flow of groundwater that would otherwise result in frost heave. It was reported that the Terram Frost Blanket can reduce 90% of frost heave in frost-susceptible soil (see Figure 7). The samples shown in Figure 7 indicate that when capillary water flow is completely cut off, the frost heave of the soil is significantly reduced.

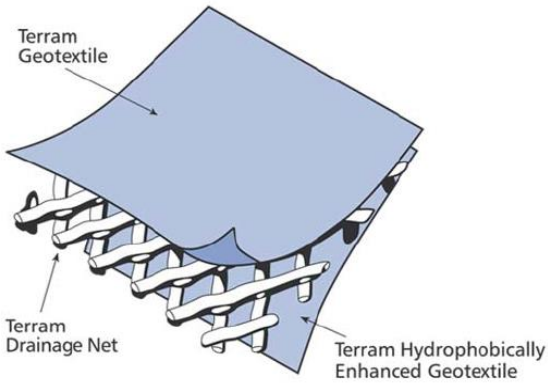

Figure 6. Components of the Terram Frost Blanket

Figure 7. Components between soil specimens in the frost heave tests

PRELIMINARY LABORATORY TESTS ON H2Ri WICKING FABRIC

The H2Ri wicking fabric recently developed by TenCate Geosynthetics (North America) is a material with high wettability similar to the fiberglass used in Henry and Stormont (2002). It has high specific surface area of 3650 cm^2/g and high permeability of $0.24s^{-1}$ (equivalent to a flow rate of 611 $l/min/m^2$). Table 1 shows the technical data sheet for the H2Ri.

TenCate Geosynthetics (North America) performed laboratory tests on H2Ri, and the tests indicated that the fabric has high ability to absorb water under unsaturated conditions. Figure 8 shows a laboratory test on H2Ri to absorb and transport water along the horizontal direction at a zero hydraulic gradient. In 983 minutes (about 16.5 hours), the wetting front of the water moved 73.3 in. horizontally at zero hydraulic gradient. Figure 9 shows that H2Ri

can wick water in the vertical direction also. In 24 minutes, the wetting front moved 6 in. in the vertical direction.

Table 1. Technical data sheet for H2Ri

Mechanical Properties	Test Method	Unit	Minimum Average Roll Value	
			MD	CD
Tensile Strength (at ultimate)	ASTM D4595	lbs/in (kN/m)	450 (78.8)	450 (78.8)
Tensile Strength (at 2% strain)	ASTM D4595	lbs/in (kN/m)	45 (7.9)	75 (13.1)
Tensile Strength (at 5% strain)	ASTM D4595	lbs/in (kN/m)	135 (23.6)	325 (56.9)
CBR Puncture Strength	ASTM D 6241	lbs (N)	2300 (10235)	
Permittivity	ASTM D4491	sec^{-1}	0.24	
Pore Size (050)	ASTM D6767	microns	85	
Pore Size (095)	ASTM D6767	microns	195	
Apparent Opening Size (AOS)[1]	ASTM D4751	U.S. Sieve (mm)	40 (0.43)	
Flow Rate	ASTM D4491	gal/min/ft^2 (l/min/m^2)	15 (611)	
Wet Front Movement [2] (24 minutes)	ASTM C1559[3]	inches	6.0 Vertical direction	
Wet Front Movement [2] (983 minutes) Zero Gradient	ASTM C1559[3]	inches	73.3 Horizontal direction	

[1] ASTM D4751: AOS is a Maximum Opening Diameter Value
[2] 'STP': Standard Temperature and Pressure
[3] Modified

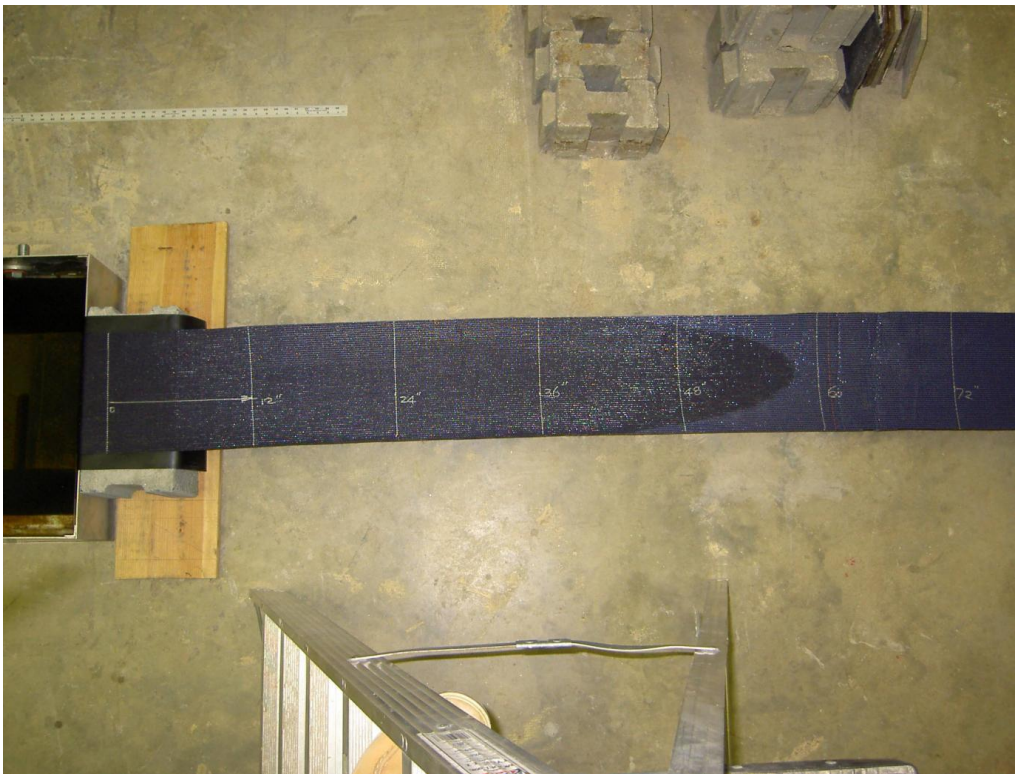

Figure 8. Water wicking of H2Ri at a zero hydraulic gradient

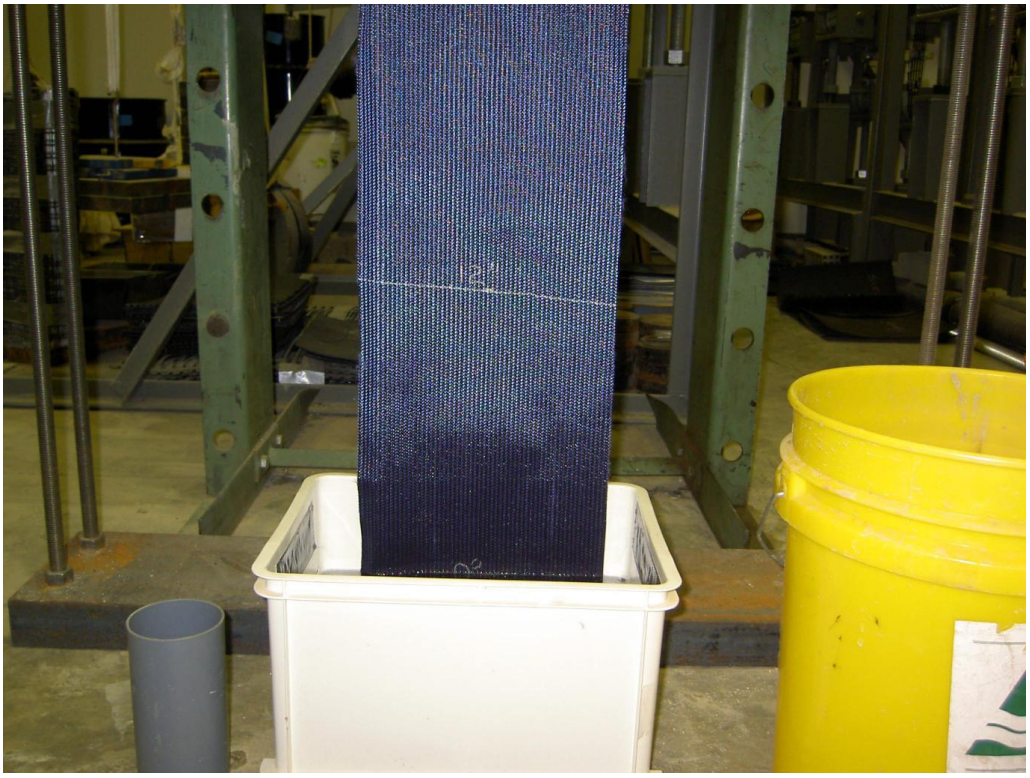

Figure 9. Water wicking of H2Ri in the vertical direction

The special characteristics of H2Ri wicking fabric make it a promising capillary barrier material to mitigate frost heave and thaw weakening problems. In 2008, TenCate Geosynthetics (North America) funded a University of Alaska Fairbanks research project entitled "Use of H2Ri Wicking Fabric to Help Prevent Frost Heaving in Alaska Pavements." The research project focused on laboratory investigation of the potential of H2Ri to serve as a capillary barrier material for frost heave and thaw weakening problems. A series of tests such as drainage tests, capillary rise tests, rainfall infiltration tests, and frost heave tests were performed. The research project generated five reports. The test results generally showed that H2Ri can potentially be used as a capillary barrier to mitigate frost heave. Although the results on frost heave were inconclusive, some definitive results on the ability of H2Ri to transport water under unsaturated conditions were observed.

Figure 10 shows the setup for laboratory rainfall-infiltration tests. Uniform sand was mixed with water into a sand slurry. The sand slurry was placed in a cylindrical plastic mold. The side of the plastic mold was tapped to densify the soils, and then the plastic mold was put upside down with an initially saturated geosynthetic and impermeable membrane placed below the slurry. Holes were hammered into the top of each plastic mold to decrease the suction caused by drainage of water that would otherwise inhibit the flow of moisture through the soil slurry. The water was allowed to drain for three days.

It was found that in the range where the soil slurry columns were sitting, in the direction of the nylon wicking fabric, H2Ri remained wet after more than three days of testing, while outside the range of where the soil slurry columns were sitting, the H2Ri wicking fabric dried out in less than one day (Figure 11). All the other geosynthetics dried out in less than one

day. Figure 12 shows a comparison of the average moisture distribution of different geosynthetics. The H2Ri (Mirafi nylon wicking fabric) clearly had the lowest moisture distribution in comparison with the other geosynthetics. An explanation for the difference is given in Figure 13. H2Ri is made of a multichannel fiber that has high air-entry value; it can maintain saturation and transport water under a high level of suction. The other geosynthetics have larger pores, which correspond to small air-entry values, become dry quickly under room relative humidity, and therefore become impermeable to water transport.

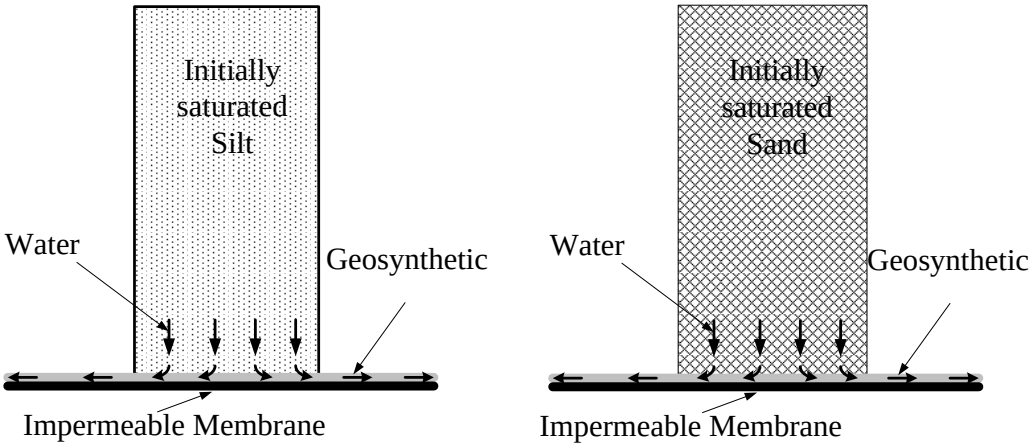

Figure 10. Modified laboratory rainfall infiltration soil column tests

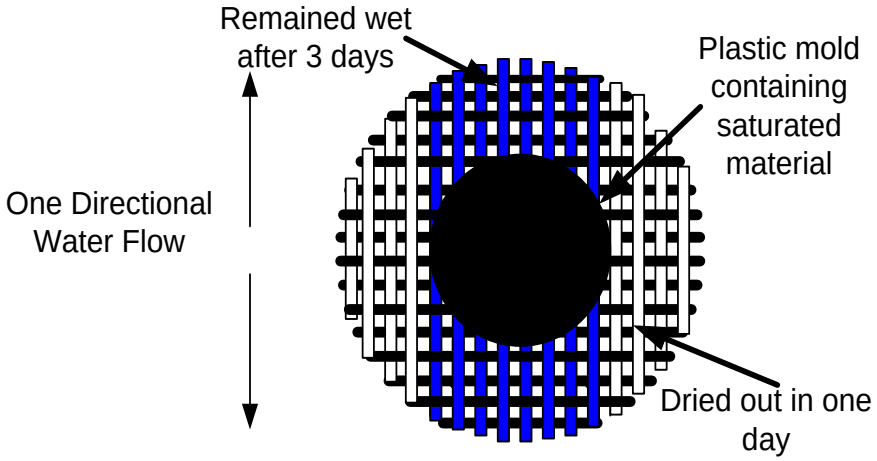

Figure 11. Water infiltration test using silt for H2Ri wicking fabric

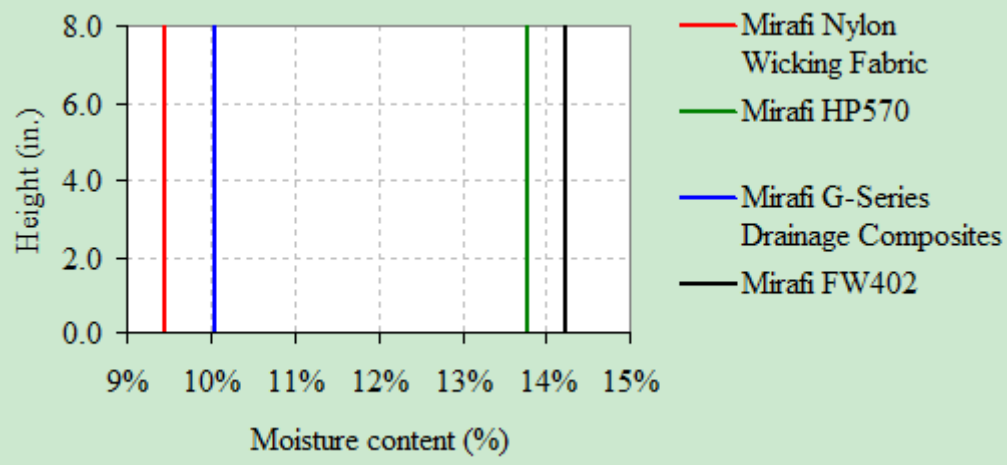

Figure 12. Results of water infiltration test using initially saturated sand

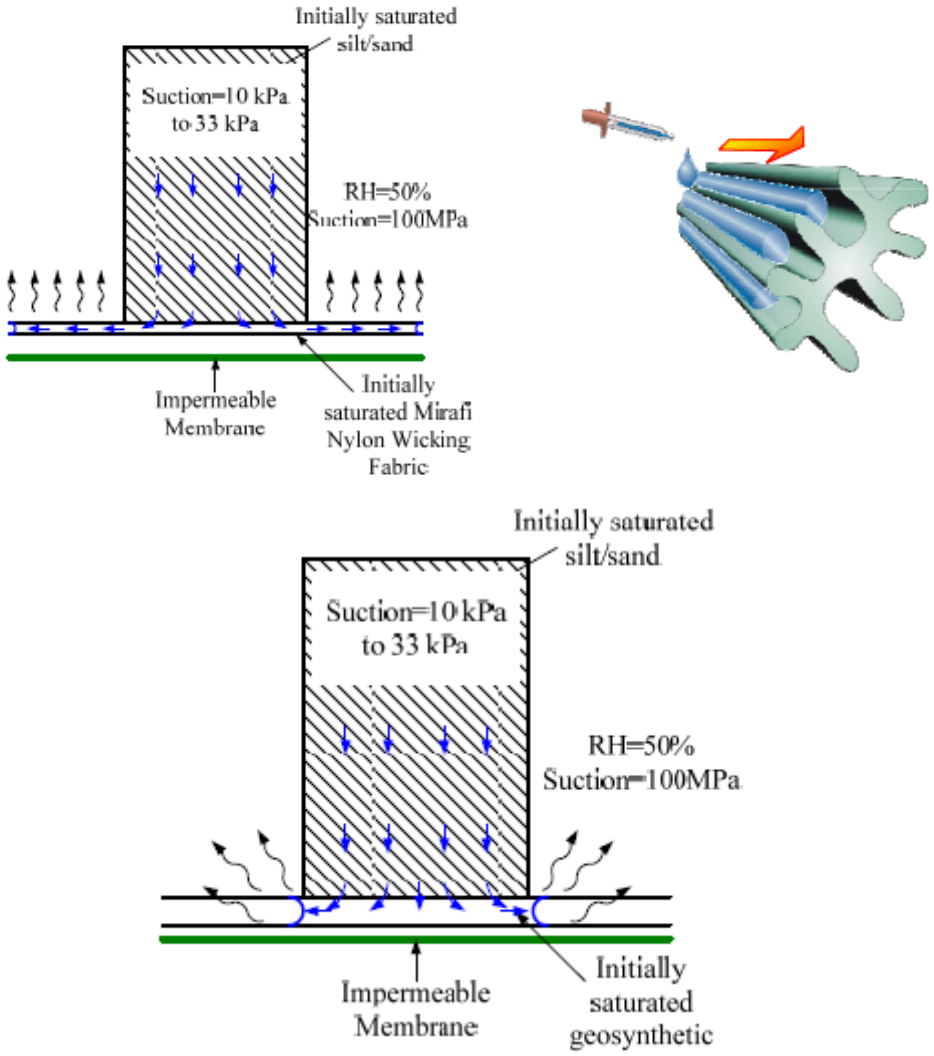

Figure 13. Water infiltration test using silt for H2Ri wicking fabric

Another typical test setup for the Rainfall Infiltration/Top Tests is shown in Figure 14. Uniform sand and water were mixed together into sand slurry and then poured into a plastic

mold to a height that would leave 1.33 in. on top. A geosynthetic was placed in the mold at this height with an excess length hanging out of the plastic mold. After the geosynthetic was firmly in place, the rest of the sand slurry was placed on top of the geosynthetic and filled to the top of the plastic mold. Aluminum foil was used to cover the soil slurry above the geosynthetic so that moisture within the slurry would not evaporate. After the tops of the molds had been covered, the experiment was allowed to sit for 5 days and then the soils were removed to measure the moisture content with depth. Figure 15 shows a comparison of average moisture distributions of the different geosynthetics. The results clearly indicate that the test with H2Ri (Mirafi nylon wicking fabric) had the lowest average moisture content. This test indicates that H2Ri can siphon water out of the soil if there is a water puddle or pocket.

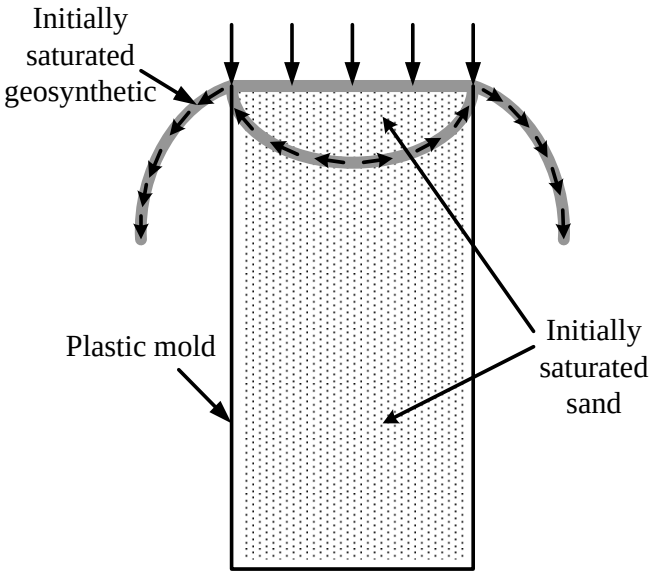

Figure 14. Experimental setup for rainfall infiltration/top tests

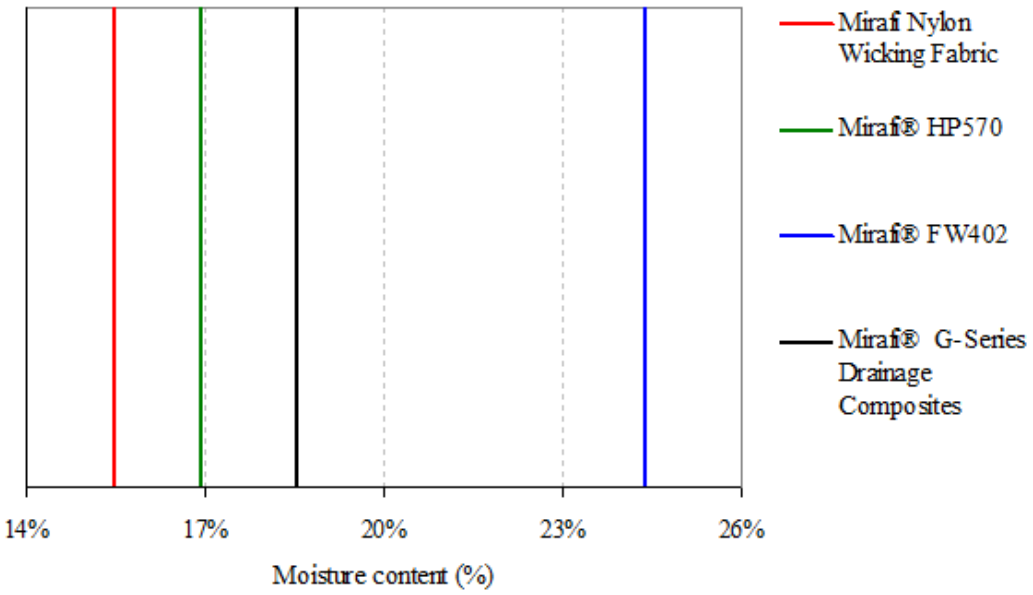

Figure 15. Results of water infiltration / top test using initially saturated sand

PRELIMINARY NUMERICAL SIMULATION OF H2Ri WICKING FABRIC PERFORMANCE IN EXPANSIVE SOIL EMBANKMENT

Preliminary numerical simulations (Zhang & Belmont, 2011) of the performance of H2Ri in expansive soils were performed by assuming the material properties of H2Ri. Figure 16 shows the configuration of the pavement section as well as the mechanical boundary conditions used in the study. The wicking fabric, if present, was installed at a depth of 1.0 m below the concrete slab. Three different wicking fabrics were considered as follows:

1. The ability of the wicking fabric to transport water is limited so that the wicking fabric works as reinforcement, similar to a geotextile. This case is referred to as "reinforcement only" in the following discussions;
2. The wicking fabric is highly permeable in all directions. This case is referred to as "single layer wicking fabric" in the following discussions; and
3. The wicking fabric is highly permeable in the direction toward the outside of the pavement only and impermeable in the other two directions. This case is referred to as "wicking fabric with impermeable layer" in the following discussions. It was used to simulate the wicking drainage board.
4. Two different conditions were considered. One is that the concrete slab is integrated and there is no moisture leakage from the slab to the subgrade, and the other is that there is leakage at the center of the slab, which caused suction in the range of 1.0 m below the centerline equal to10 kPa (field capacity).

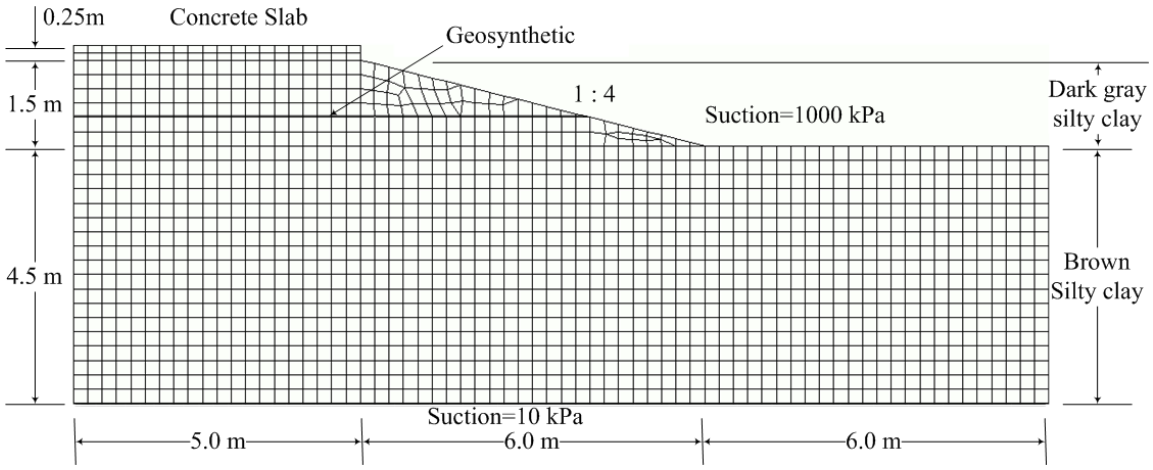

Figure 16. Configuration of pavement section

To investigate the influence of the wicking fabric on the performance of pavement structure, conditions with no inclusion of wicking fabric were also considered. Eight simulations were performed, as shown in Table 2. Figure 17 shows suction distribution in the pavement structure without and with installation of H2Ri. It can be seen from the figure that when a layer of wicking fabric is installed, the suction in the pavement structure is much higher and more uniformly distributed below the pavement structure. As a result, the

corresponding moisture content is much lower. Lower moisture content often implies high shear strength and smaller deformation.

Two parameters were used to evaluate the performance of the pavement structure. The first one was the "length of unsupported slab," which corresponds to the length of the slab not supported by the subgrade soils. This parameter is related to differential settlements caused by expansive soils under certain weather conditions. Preferably, the whole slab should be supported by subgrade soils in order to minimize the stress in the slab. The larger the "length of unsupported slab," the bigger the differential settlements. The second parameter was the Von Mises stress. A Von Mises stress is a stress-invariant used in yield criteria. It is calculated independently of the coordinate reference system, and does not carry directional stress information such as normal and shear stresses, but carries enough information to identify hot spots where failure might occur. The larger the Von Mises stress, the higher the possibility of damage. Table 2 indicates that H2Ri can reduce differential settlement and stress concentrations by changing the moisture content distribution in the pavement structure.

Table 2. Summary of the numerical simulation

Case			Max. Von Mises Stress (kPa)	Length of Unsupported Slab (m)
No Leakage	1	No Geosynthetic	2399	1.1
	3	Reinforcement Only	2668	1.1
	5	Single Layer Wicking Fabric	517.6	0.162
	7	Wicking Fabric with Impermeable Layer	**517.6**	**0.162**
With Leakage	2	No Geosynthetic	3597	1.4
	4	Reinforcement Only	3600	1.4
	6	Single Layer Wicking Fabric	3527	1.26
	8	Wicking Fabric with Impermeable Layer	**1425**	**0.079**

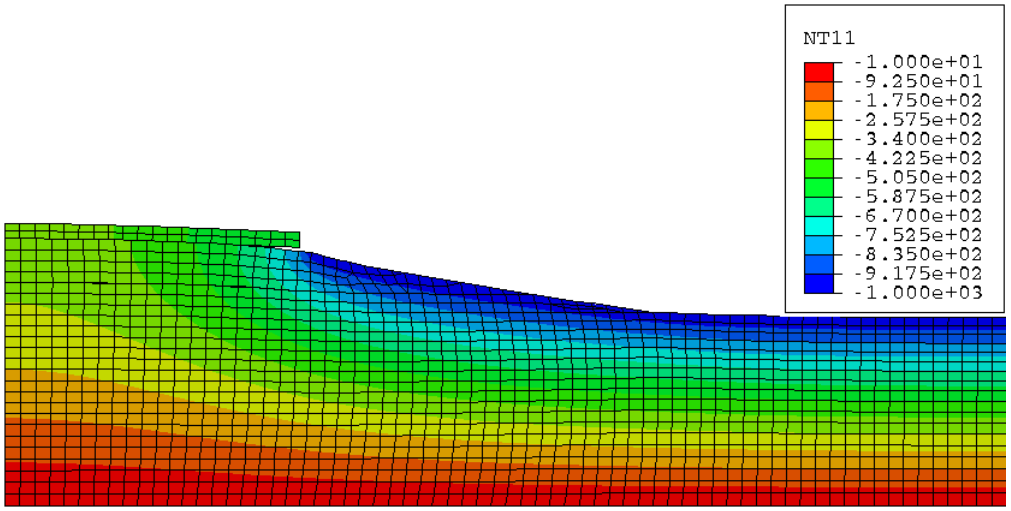

(a) Without H2Ri wicking fabric

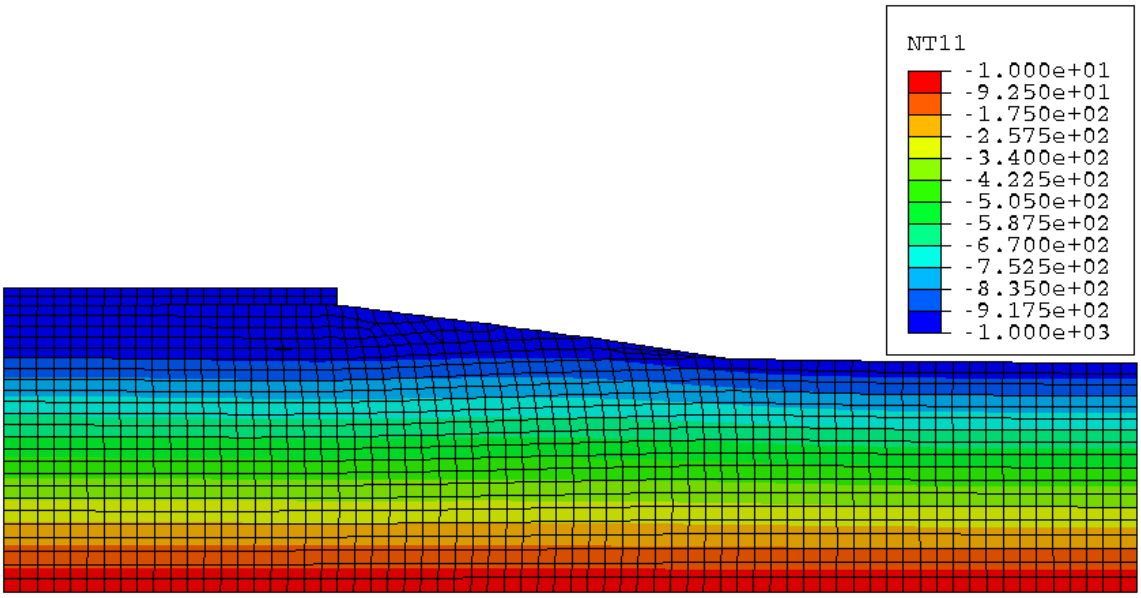

(b) With H2Ri wicking fabric

Figure 17. Simulation of pavement structure built on expansive soils without and with installation of H2Ri wicking fabric

Although laboratory tests and numerical simulation results indicated that H2Ri shows promise as a capillary barrier for the prevention of frost heave and thaw weakening, no direct evidence was available to prove that H2Ri would work in the field to improve road performance. In addition, concerns remained about whether H2Ri wicking fabric would work in the harsh climate of Alaska where water freezes easily in the winter, which could cause the wicking fabric to lose its function.

Beaver Slide is near mile 110.5 on the Dalton Highway; it trends downhill heading north. The road gradient is approximately 11%, and the road prism is on a side hill. The embankment is about 3 ft on the high (west) side and 9 ft on the low (east) side. Each spring, shallow groundwater flows downslope and into the road embankment, causing frost boils and subsequent road damage. The frost boils have resulted in hazardous driving conditions and

have even led to accidents. Past repair efforts indicate that conventional road construction methods do not work.

Beaver Slide has provided a valuable location for evaluating the effectiveness of H2Ri in mitigating frost heave and thaw weakening problems. After several discussions between engineers at DOT&PF, researchers at UAF, and representatives from TenCate Geosynthetics, it was decided that field implementation of H2Ri at the Beaver Slide site to verify the wicking fabric's effectiveness would be worthwhile. TenCate Geosynthetics provided the H2Ri needed for field implementation. The Dalton Highway M&O section of the DOT&PF provided the equipment and labor to construct the test section. Michael R. Lilly from Geo-Watersheds Scientific helped with installation of the thermal and moisture sensors as well as construction of the data-acquisition station. The AUTC provided funding for instrumentation and field monitoring. Dr. Xiong Zhang and his students performed laboratory tests and field monitoring as well as data analysis.

CHAPTER 3: CONSTRUCTION OF TEST SECTION AND INSTRUMENTATION

INTRODUCTION

This chapter describes the construction process of the test section as well as the sensor instrumentation. During construction, road materials were excavated; this process also served as a site investigation. The findings during the excavation are presented below.

The test section was constructed on August 3 and 4, 2010, and instrumentation and surveying were completed on August 5, 2010. **Error! Reference source not found.** shows the original design of the test section, which included a control section and a test section with two layers of wicking fabric. Due to limited funding, the control section was removed from the study. Since a ditch was located at the west side of the road, there was concern that wicking fabric might transport water into the road structure, which could cause damage to the road. Therefore, it was decided that the wicking fabric should be buried in the road structure instead of exposed to air on the uphill side of the road. To assure that the wicking fabric could be used for future projects, DOT&PF normal construction procedures for maintainence operations were followed, and no special requirement was made. The soils in the existing road were used for constructing the test section. To keep traffic moving, on August 3, 2010, while the lane on the east side was excavated for wicking fabric and sensor installation, the lane on the west side remained open. On August 4, 2010, while the lane on the west side was excavated for wicking fabric and sensor installation, the east side was kept open. Figure 19 shows the final configuration of the finished test section.

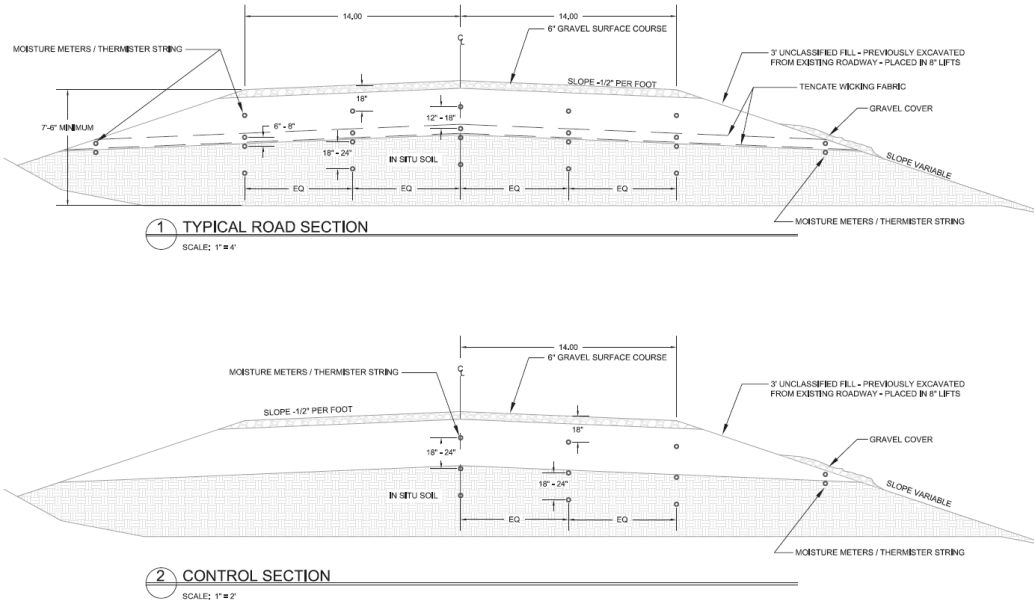

Figure 18. Original design of the test section

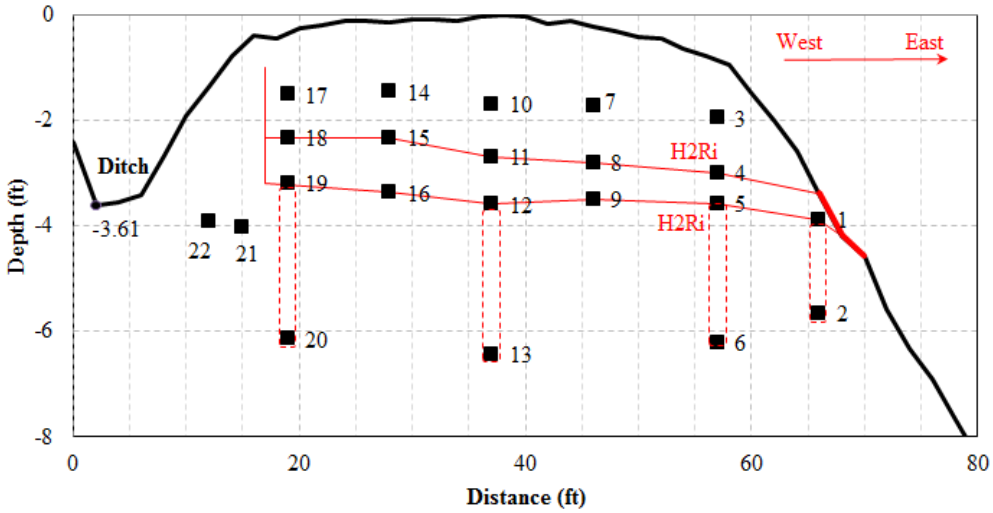

Figure 19. Final configuration of the test section (looking north)

TEST SECTION CONSTRUCTION

The construction of the test section started on August 3, 2010. A 60 feet long road section that had the most frost boils was selected for testing (Figure 20). First, the eastbound half of the existing road was excavated to a depth of 3.5 feet (Figure 21), and the bottom of the excavation was graded using a bobcat (Figure 22). The soils were generally brown to yellow sand with gravel, according to visual classification. The first 4 in. of soil was cemented and dense, most likely due to heavy traffic. Next, three pits were dug—at the center of the road, at the edge of the original road (20 feet to the center), and approximately at the edge of excavation (29 feet to the center of the road)—for installation of sensors 13, 6, and 2, respectively (see Figure 19).

Figure 20. Selection of test section (looking north)

Figure 21. Excavation of the lane on the east side of road (looking north)

Figure 22. Excavation of the lane on the east half side of road (looking north)

The excavation pits were about 1.5 feet by 1.5 feet large and 3 feet deep, as shown in Figure 23. In the excavation pit for sensor 13 (Figure 23), a 4 in. thick degraded, dark brown

vegetation layer was encountered 4 feet below the original road surface (0.5–1.0 feet below the excavation bottom). Sand with gravel was on top of the degraded vegetation layer. Under the degraded vegetation layer were crushed rocks with sand. The soils excavated from pits at sensor locations 2 and 6 were generally sand with gravel, the same as soils excavated from the first 3.5 feet of soils. No degraded vegetation layer was found in these two excavation pits.

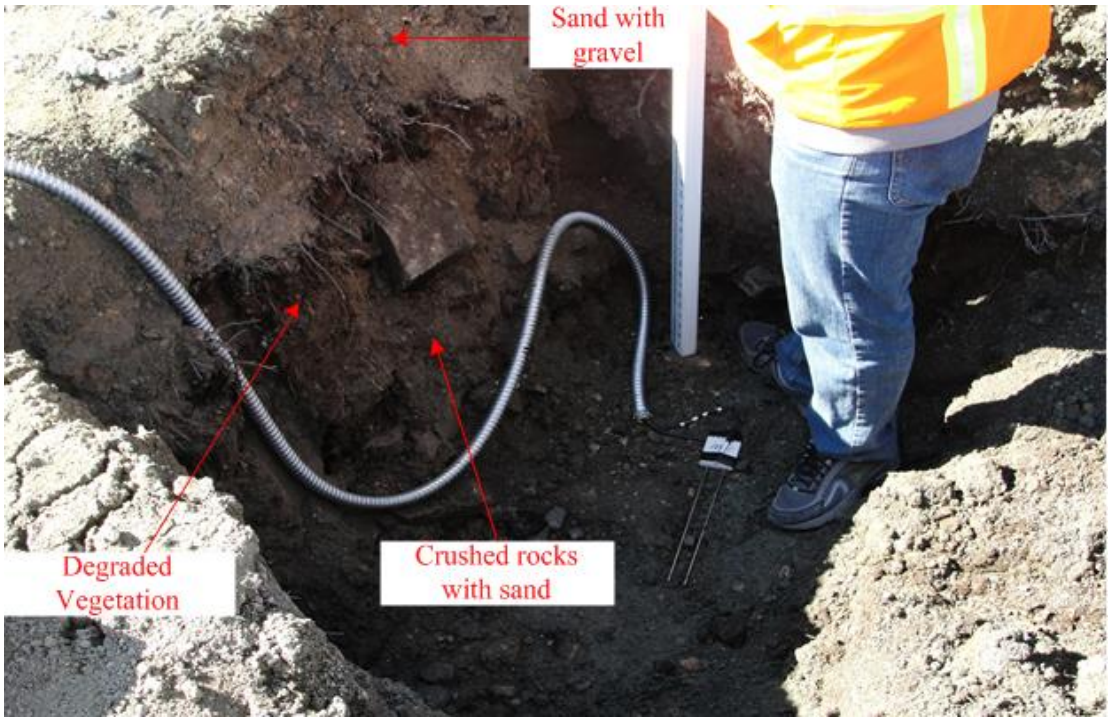

Figure 23. Excavation pit at the center of the road for sensor 13

For sensor installation, each sensor location included two sensors from Campbell Scientific Inc.: a CS107L temperature probe and a CS616-L moisture probe, as shown in Figure 24. The specifications of the two sensors can be found at the Campbell Scientific Inc. website (http://www.campbellsci.com). The sensors were taped together, and the wires were protected using aluminum conduit to prevent damage from the traffic loads. To obtain reasonable readings from the moisture probes, soils with particle sizes greater than 1 cm were taken away. The soils surrounding the sensors were hand-compacted to prevent any possible damage.

After the elevations of the sensors were recorded using a Leica NA720, the excavation pits were backfilled with soil taken from the same locations and compacted. Sensors 1, 5, 9, and 12 were then installed using the same method described for sensors 2, 6, and 13 at the corresponding locations shown in Figure 19. All the aluminum conduits holding the sensors were grouped together and buried in a ditch transverse to the test section, leading to the west side of the road where the future data station was to be located (see Figure 25).

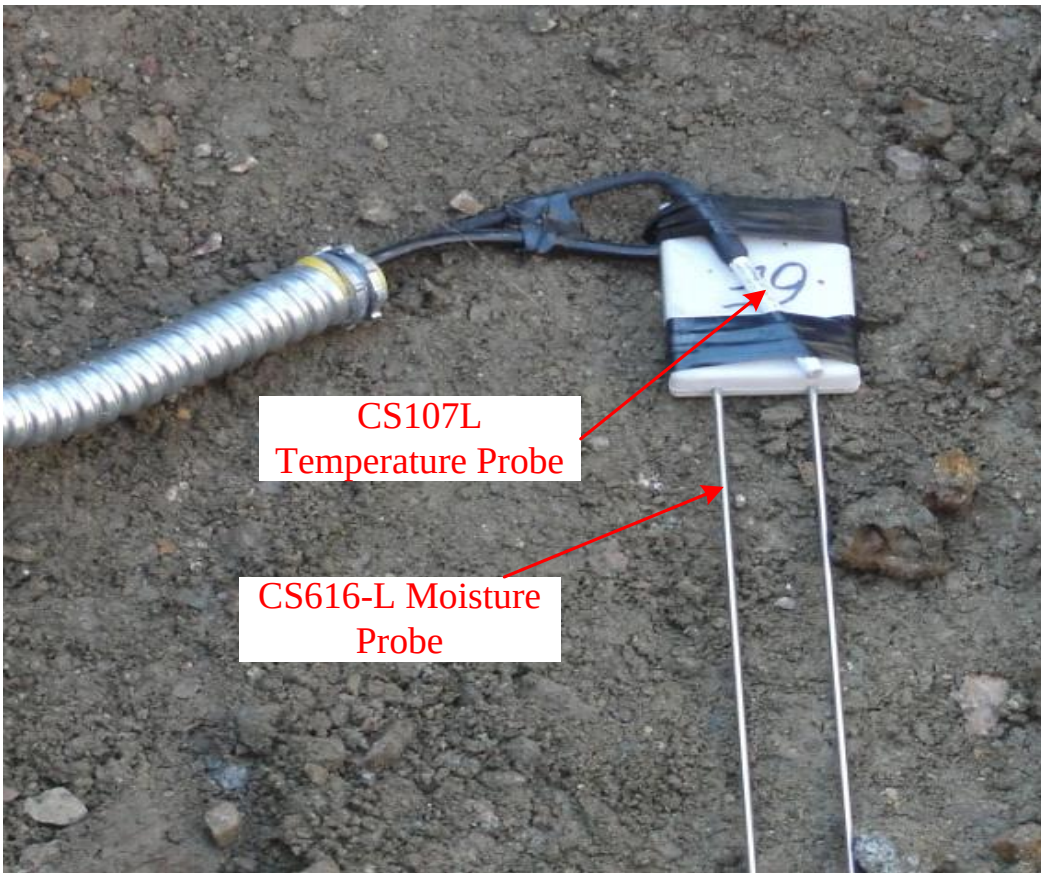

Figure 24. Enlarged view of temperature and moisture sensors

Figure 25. Installation of the aluminum conduits

Next, the wicking fabric was installed about 3.5 feet below the original road surface, as shown in Figure 26 and Figure 27. During the wicking fabric installation, a roll of wicking fabric was brought to the south (high) end of the excavation section (Figure 26). The wicking fabric was placed on the ground by pushing the roll downslope to the other end. The fabric was then cut at the lower end to the proper length, which covered the whole excavation range. Since the wicking fabric is directional, care was taken to make sure the direction of the wicking fabric was along the transverse direction of the road section so that water was transported out of the road structure horizontally to the road shoulder as shown in Figure 27.

The excavation in the east lane was about 60 feet long and 36 feet wide. Each roll of the wicking fabric was 300 feet long and 15 feet wide. In addition, according to the original design, at least 3 feet of wicking fabric was exposed to air at the shoulder. Thus, three passes were needed to cover the whole excavation area. The additional two passes of wicking fabric were placed in the same way as that for the first pass. To make sure the water would be transported from one layer of wicking fabric to another layer, a 3 ft overlap was used (see Figure 27).

Figure 26. Wicking fabric was brought into the excavation area

Figure 27. Wicking fabric installation after placement

After the wicking fabric was placed properly, the excavated soils were used to backfill the excavation area to a thickness of approximately 1 ft. The backfill was then graded and compacted on top of the wicking fabric according to the normal practice of DOT&PF (Figure 28).

Figure 28. Compaction of the backfilled soils

After the soils were compacted, sensors 4 and 8 were installed according to the method described previously at the locations shown. Due to limited space, the installation of sensor 11 was delayed until the next day. Then a second layer of wicking fabric was installed as shown in Figure 29. The wicking fabric exposed to the air was about 4 feet at the shoulder.

Figure 29. Installation of the second layer of wicking fabric

After the wicking fabric was placed properly, the excavated soils were used to backfill the excavation area to a thickness of approximately 1 ft. The backfill was then graded and compacted on top of the wicking fabric according to the normal practice of DOT&PF, and sensors 3 and 7 were installed according to the method described previously at the locations shown in Figure 30. Next, the rest of the soil was brought back to backfill the excavation in the eastbound lane to its original elevation. **Error! Reference source not found.** shows the lane on the east side of the road after construction was finished. All these activities were completed on August 3, 2010.

Construction on August 4, 2010, started with digging out the west lane of the road to a depth of approximately 3.5 ft, as shown in Figure 32. The first 3 ft of soil was still light yellow to brown sand with gravel. At 3 ft below the west edge of the original road, degraded vegetation was found similar to that found in the excavation pit at the center of the road. The same degraded dark-brown material was also found at the bottom of the west side of the excavation when grading the excavation pit (see Figure 33). To avoid the possible introduction of water from the ditch to the road section, the west road shoulder was not excavated (Figure 32).

Figure 30. Installation of sensors 3 and 7 and backfill the excavation

Figure 31. The lane on the east half of the road after construction

Figure 32. Excavation of the lane on the west side of the road

Figure 33. Degraded vegetation layer found on the bottom of the excavation

Figure 34. Installation of sensor 20

After the bottom of the excavation was graded, a pit was excavated at about 18 ft from the center of the road to install sensor 20, as shown in Figure 34 (please also refer to Figure 19). The pit was about 1.5 feet by 1.5 feet, with a depth 3 feet. During this process, groundwater was encountered at a depth of 2.5 feet (total about 6 feet below the original road surface). The soil was crushed rock with sand and silt and had high permeability. After the soils were excavated, water quickly migrated to the pit and in less than 1 hour, the bottom of the excavation pit was filled with water. As a result, sensor 20 was installed under the water, and then the pit was backfilled with soils excavated from the pit.

On the same level, sensors 16, 19, and 22 (see Figure 19) were also installed, as shown in Figure 35. The aluminum conduits for sensors 5, 6, 9, 12, 13, 16, and 19 were grouped together and buried in a small ditch in the transverse direction of the road. Figure 36 shows the location of the ditch after being backfilled. Figure 37 shows the installation of the first layer of wicking fabric on the west half of the road. Figure 38 shows the test site after installation of the first layer of wicking fabric on the west side of the road.

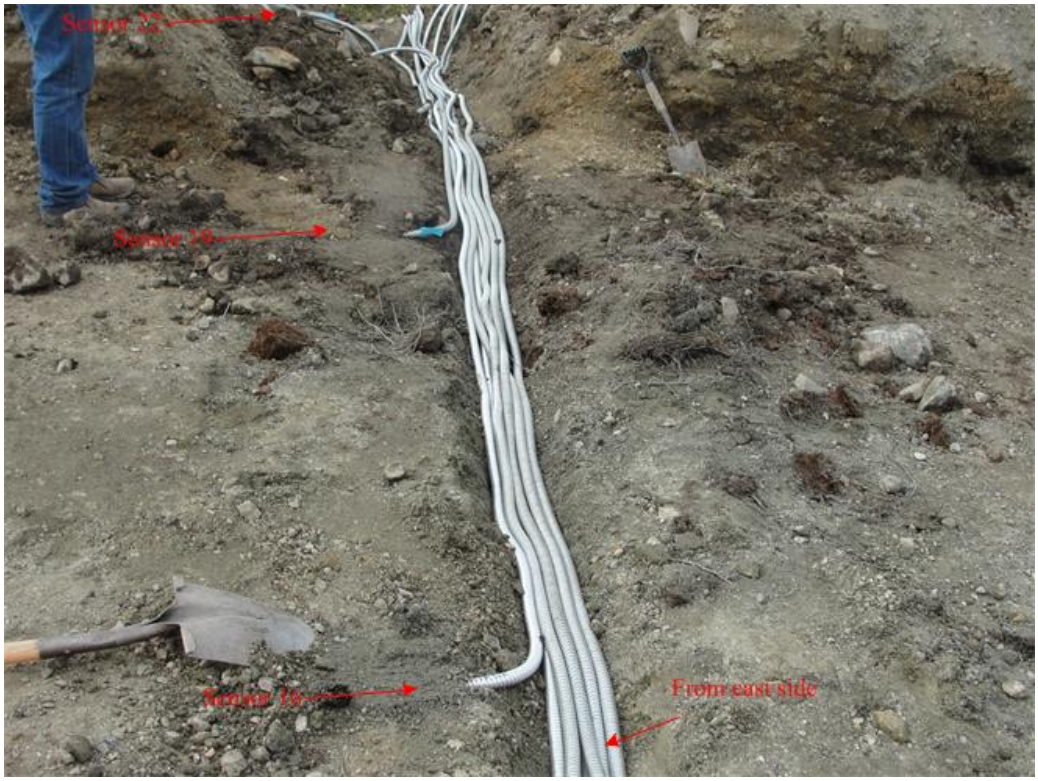

Figure 35. Installation of sensors 16, 19, and 22

Figure 36. After installation of sensors 16, 19, and 22

Figure 37. Installation of the first layer of wicking fabric on the west side of the road

Figure 38. After installation of the first layer of wicking fabric on the west side of the road

After the wicking fabrics were placed properly, the excavated soils were used to backfill the excavation area to a thickness of approximately 1 ft. The backfill was then graded and compacted on top of the wicking fabric according the normal practice of DOT&PF (see Figure 39).

Figure 39. After installation of the first layer of wicking fabric on the west side of the road

After the soils were compacted, sensors 11, 15, 18, and 21 were installed according to the method described previously at the locations shown in Figure 19. A second layer of wicking fabric was placed as shown in Figure 40, and another 1 feet thick lift of the excavated soils was placed in the excavation area, as shown in Figure 41. After the soils were graded and compacted, sensors 10, 14, and 17 were installed according to the method described previously at the locations shown in Figure 19. The remaining soil was used to backfill the excavation to its original elevation (see Figure 42).

To prevent possible degradation of the wicking fabric due to sunlight exposure, crushed rocks were brought to cover the wicking fabric on the east shoulder (see Figure 43). Figure 44 shows the coverage of the wicking fabric after completion.

Figure 40. Installation of the second layer of wicking fabric on the west side of the road

Figure 41. Installation of sensors 10, 14, and 17

Figure 42. Backfilling the excavation area to its original elevation

Figure 43. Covering the wicking fabric with crushed rocks

Figure 44. Test section after completion of construction

DATA STATION CONSTRUCTION

All the sensor cables were put into aluminum conduits to protect them from the possible damage of heavy traffic loads. The aluminum conduits were grouped together and lead to tundra on the west side of the road. A ditch was excavated to cross the existing drainage ditch and all the aluminum conduits were buried underground as shown in Figure 45. The cables were hooked into a Campbell Scientific CR1000 datalogger through two AM16/32B relay multiplexers to record the hourly temperatures and moisture content at all sensor locations. Figure 46 shows a view of the datalogger and multiplexers before and after being attached to the sensors. In addition to the temperature and moisture sensors inside the test section, an HMP45C Air Temp/Relative Humidity probe was installed to monitor the air temperature and relative humidity at the test site. The panel temperature of the datalogger was monitored by the CR1000 as well. All the data-acquisition devices were placed in an ENC14/16-NC-NM weather-resistant enclosure 14 in. by 16 in. large. The data collection box was partially buried in the tundra to protect it, but remained accessible. Figure 47 shows the finished data station on the tundra along the roadside.

Figure 45. Construction of the data collection station

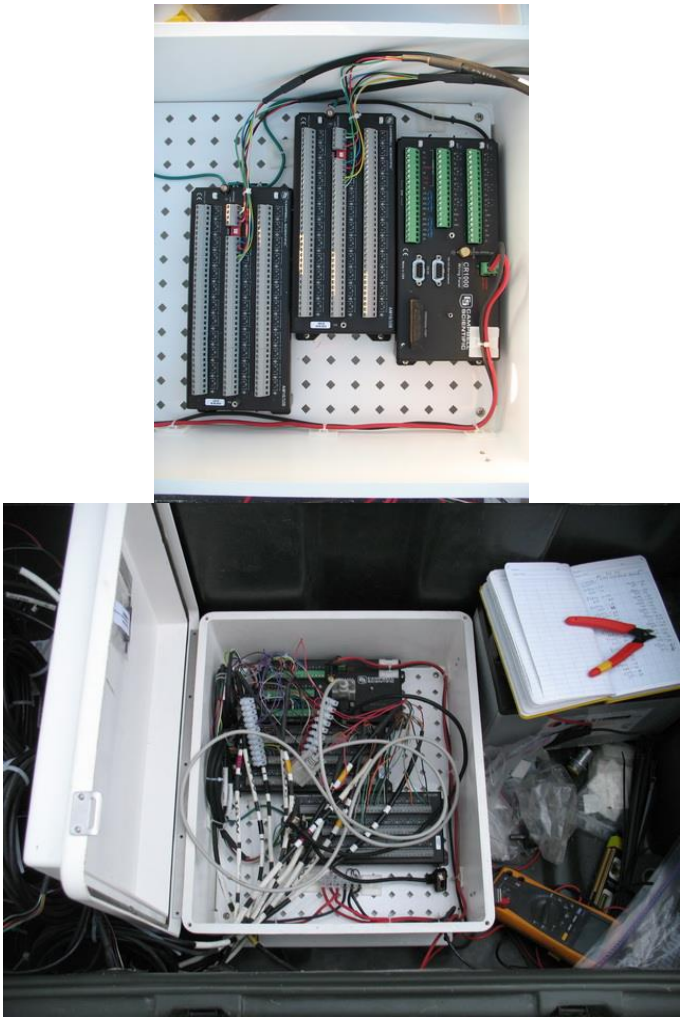

Figure 46. CR1000 Dataloggers and multiplexers for data acquisition

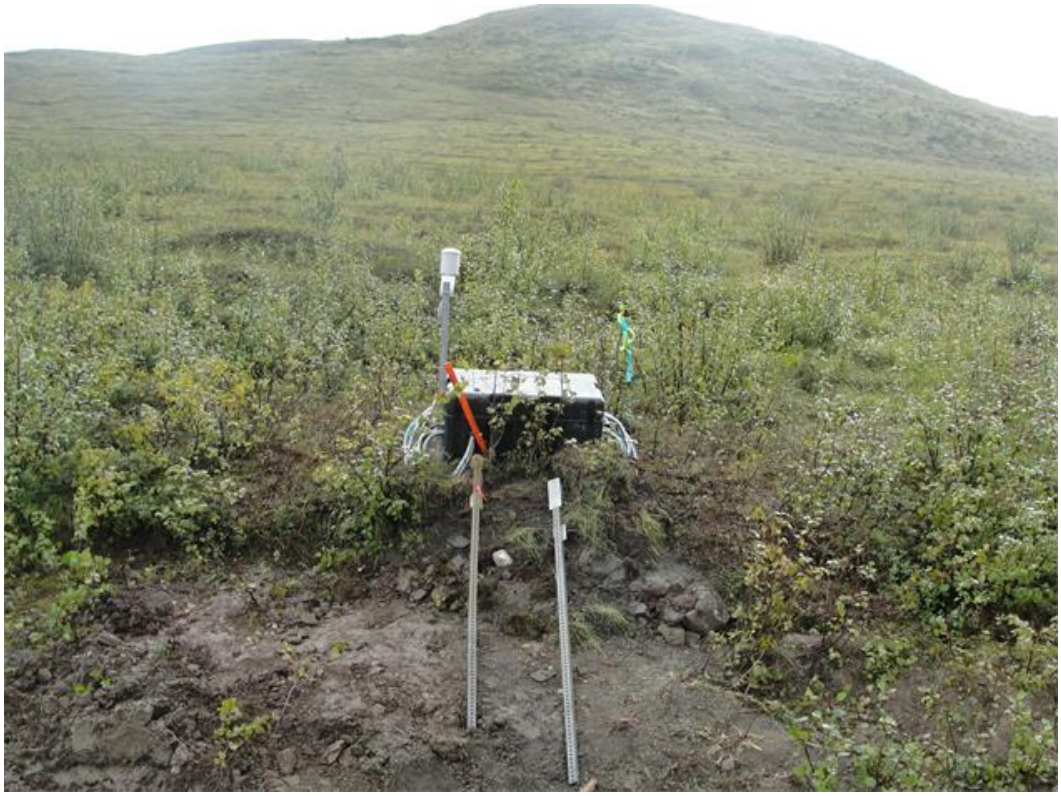

Figure 47. View of data collection station after construction

SUMMARY OF THE SURVEY

The elevations of the sensor locations as well as the shape of the test section after completion of construction were surveyed using a Leica NA720. Two benchmarks were used for the survey: one on the west side of the road in the tundra, named TBMW1; the other on the east side of the road in the tree line, named TBME1. The distance between TBMW1 and TBME1 was 102.5 ft. Figure 48 summarizes the results from the survey. The black squares represent the sensor locations. The black round points represent the surveyed profile for the road section. As shown in Figure 48, the survey extended to the tundra on the west side and to the tree line on the east side. To facilitate future analysis, a point 16 feet east of TBMW1 (near the ditch) with an elevation of 98.17 feet (top of the road center) was selected as an origin, and a coordinate system was established (see Figure 48). Figure 49 shows the sensor elevations in the new coordinate system. The black squares represent the sensor locations; the numbers beside them are the depth of the sensors to the highest points at the road center. Red lines represent the location of the H2Ri wicking fabric.

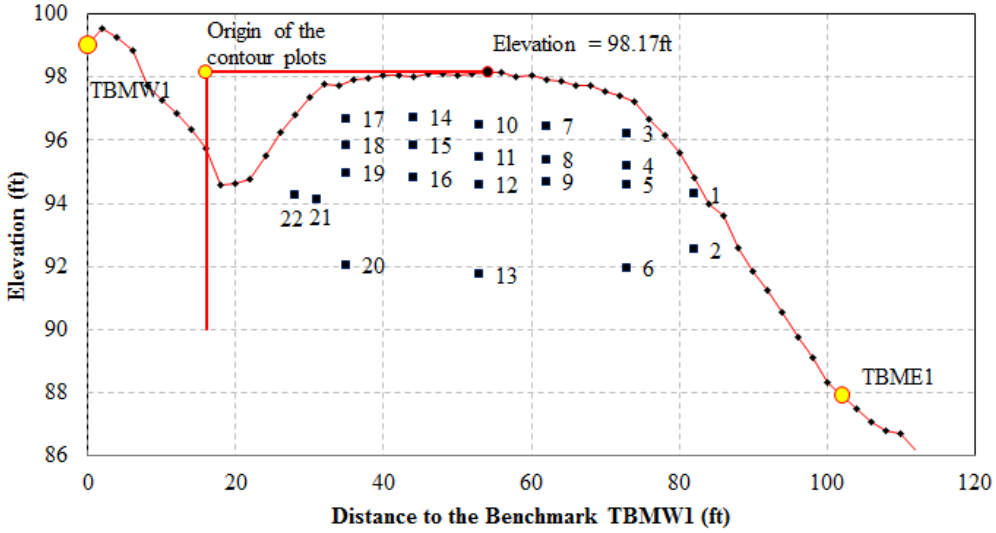

Figure 48. Summary of the survey on sensor locations and road profile

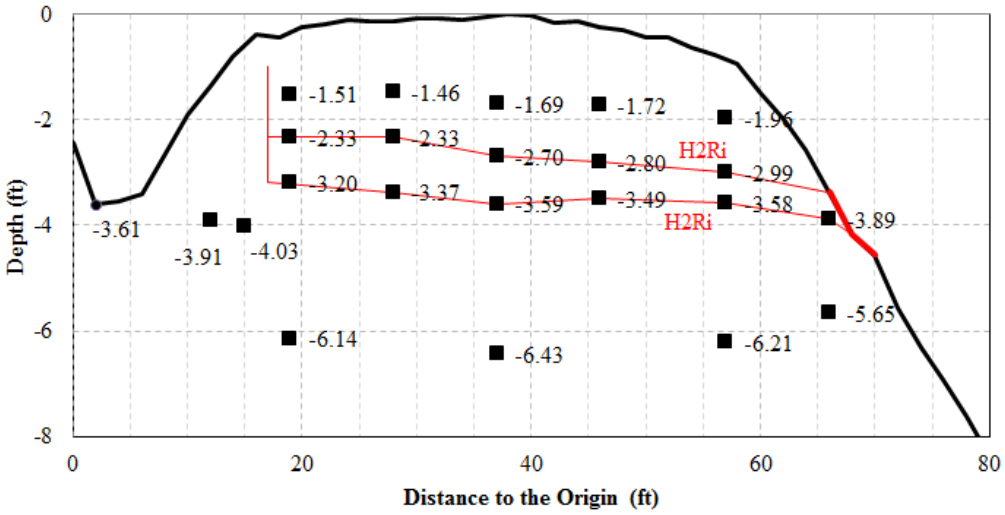

Figure 49.Sensor elevations in the new coordinate system

Soil Stratigraphy and Groundwater

Construction of the test section required excavation of the whole road at the site, and the excavation provided information for the geotechnical site investigation. Figure 50 shows the soil stratigraphy for the test section based on observations made during the construction process. It was found that the road section was built directly on the original tundra of the hill using degraded granite, which can be classified as silt with gravel according to USCS classifications. The original tundra was about 3 feet below the surface at the west edge of the road, 4.5 feet below the centerline of the road section. It was about 9 feet lower than the road surface when it extended to tree line at the west shoulder of the road. The buried vegetation had degraded to a dark yellow layer 1 to 2 in, thick. Below the degraded vegetation was in situ crushed rocks with sand.

Groundwater was easily found everywhere just below the tundra. Figure 51 shows the water found in the tundra on the slope near the data collection box. When excavating the

ditch to bury the sensor cables, we found that water seeped out of the soil surface once the tundra was removed. Additionally, water was found during the construction process in the existing ditch along the east side of the road. Figure 52 shows water in the ditch after the data collection box was installed on August 5, 2010. On the west side of the road, water was found along the tree line sporadically, as shown in Figure 53. Groundwater was also found when installing sensor 20 (see Figure 34). Figure 50 shows the approximate groundwater table based on the above observations.

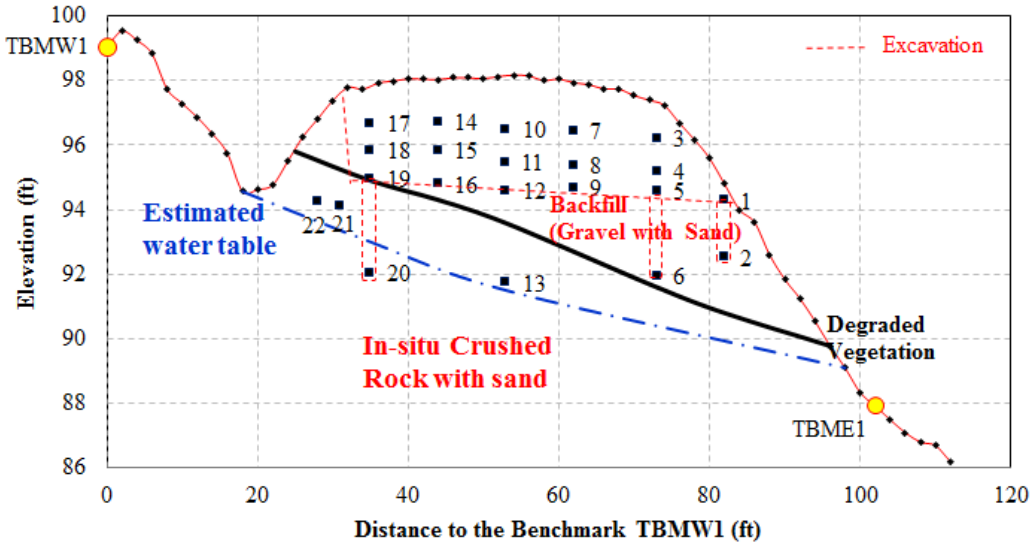

Figure 50. Soil stratigraphy at the test section

Figure 51. Water found in the tundra on the slope near the data collection box

Figure 52. Water found in the existing ditch along east side of the road on August 5, 2010

Figure 53. Water found along the tree line sporadically, on the west side of the road

Installation of the Solar Panel

The first site visit to the test section was on October 16, 2010. The preliminary test results indicated that all sensors were functioning well. However, the voltage of the battery

for the datalogger decreased from 12.5 volts to 12.2 volts in two months. Although the CR1000 would have run correctly until the battery voltage reached about 10 volts, there was concern about whether the battery could survive the harsh winter in Alaska. It was decided that it might be better to add a solar panel as a backup source of power for the datalogger. A second trip was made to the test site on March 12, 2011, to download the data and install the solar panel. Figure 54 shows the test site conditions on March 12, 2011, before installation of the solar panel. The data collection box was completely covered by snow. Figure 55 shows the data collection box after installation of the solar panel. Another visit was made on March 30, 2012, and the site conditions that day are shown in Figure 56. The solar panel was exposed to the air. Figure 57 shows the changes in battery voltage over the past two years. The data indicated that battery voltage was high enough to maintain the functionality of the datalogger.

Figure 54. Site conditions on March 12, 2011, before installation of the solar panel

Figure 55. Data collection box after installation of the solar panel

Figure 56. Site conditions on March 30, 2012

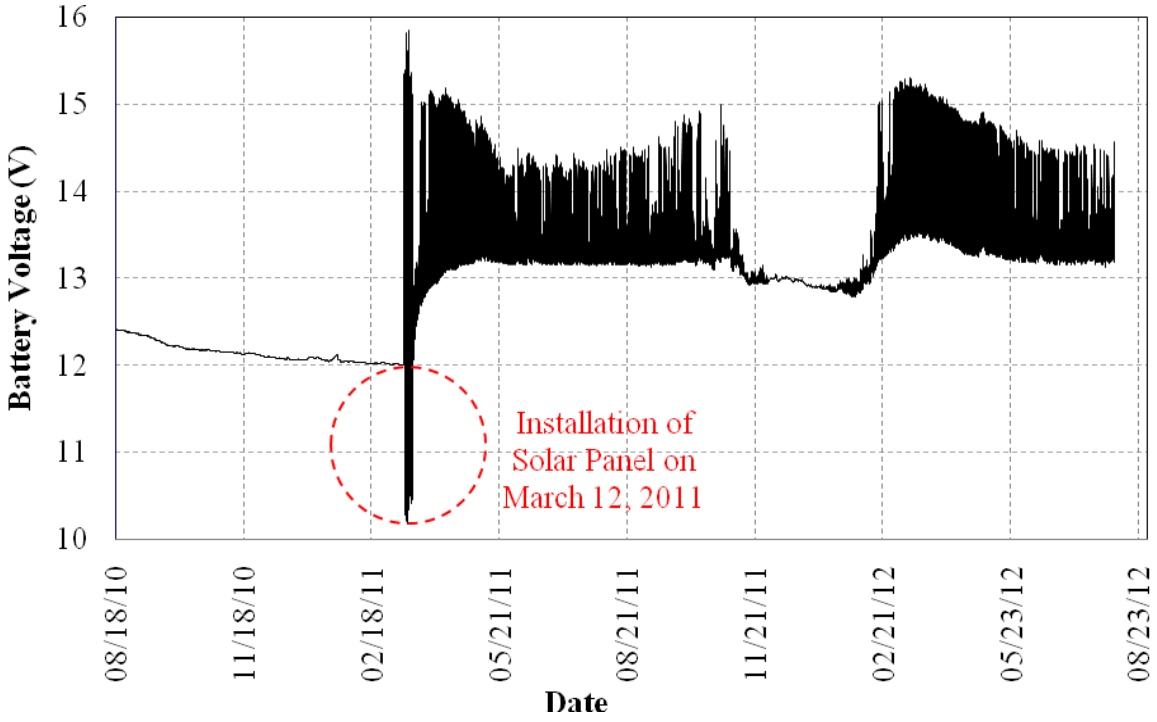

Figure 57. Battery voltage versus time curve

CHAPTER 4: RESULTS AND ANALYSIS

LABORATORY TESTS

Figure 58 shows the sieve analyses for soils taken at different locations of the road sections. The results indicate that all soils can be classified as sand with gravel according to the USCS soil classification system. While most soil samples have fines contents of less than 4%, one soil specimen has a fines contents of 6%, indicating that some soils are frost susceptible. Figure 59 shows the modified compaction test results for soils obtained from the Beaver Slide test section. The compacted soils have a maximum dry unit weight of 140.5 pcf with an optimum moisture content of 5.8%. It is worth mentioning, however, that the test section was constructed by following the normal construction process, and soils in the test section could have a lower dry unit weight since the test section was not heavily compacted.

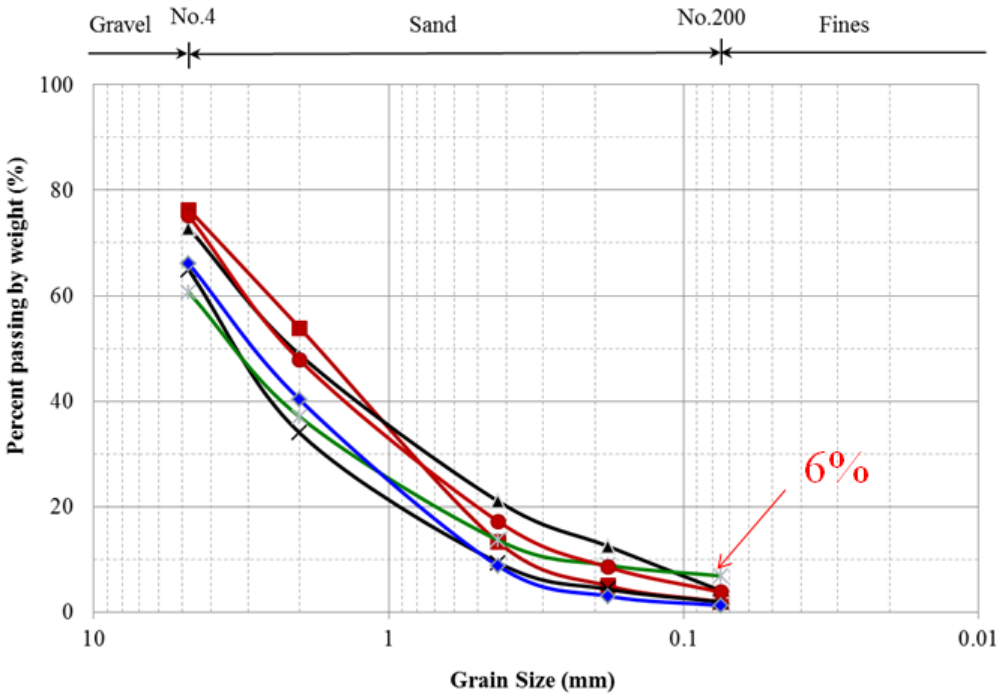

Figure 58. Sieve analyses for soils obtained from the Beaver Slide test section

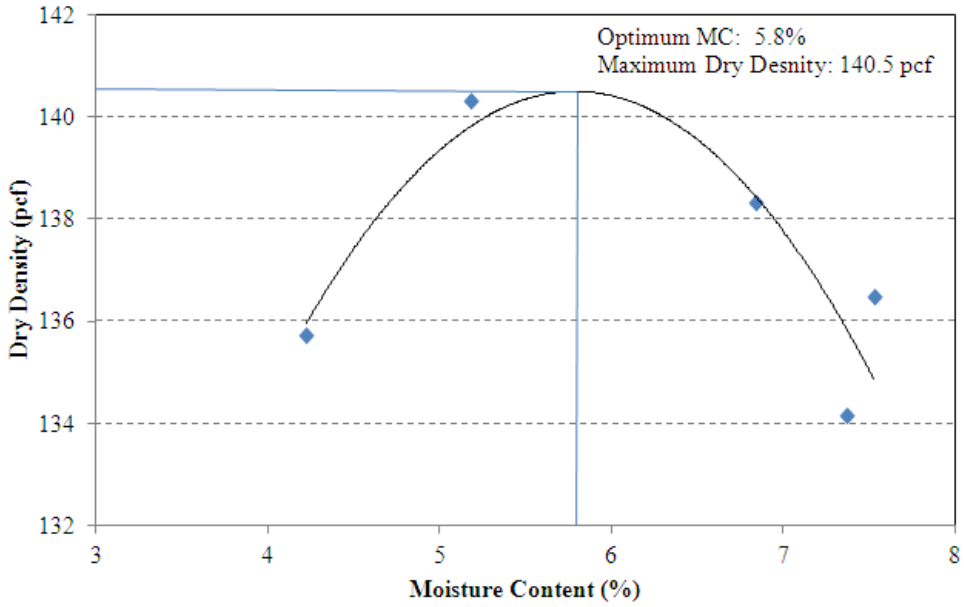

Figure 59. Modified compaction tests for soils obtained from the Beaver Slide test section

SITE CLIMATIC CONDITIONS

Figure 60 shows hourly air temperature data at the Beaver Slide test section over the two-year study period. The air temperature dropped below zero at the beginning of the third week of September each year and rose to above zero in mid or late April. The lowest temperature occurred in February 2012, at -39.21°C. Winter temperatures were generally around -20°C. The highest temperature was 24.95°C, which occurred in late May 2011. Figure 60 also indicates that hourly temperatures varied in one day, with variations as great as 30°C. The air temperature dropped to below zero on September 23, 2010, and rose above zero on April 26, 2011. In 2011, the air temperature dropped to below zero on September 24, and rose above zero on April 16, 2012. Figure 61 shows hourly relative humidity data at the Beaver Slide test section over the two-year study period. During the winter months, the relative humidity generally varied from 70% to 90%; during the summer months, the relative humidity varied more widely, from 20% to 90%. Relative humidity exceeded 99% for short periods of some summer days. We assumed these periods were rainfall events, since no rain gauge had been installed at the test section. The assumption was verified during a site visit on June 21, 2011, when rainfall occurred during the site visit, and the recorded relative humidity was between 95% and 98%. Most of the time, relative humidity was below 95%.

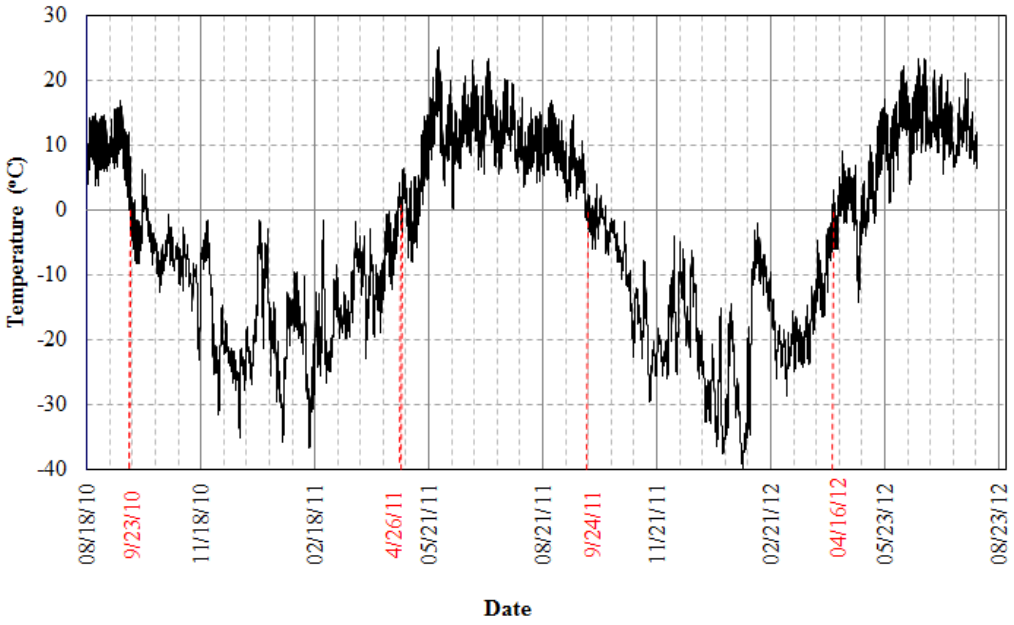

Figure 60. Hourly air temperatures at the Beaver Slide test section

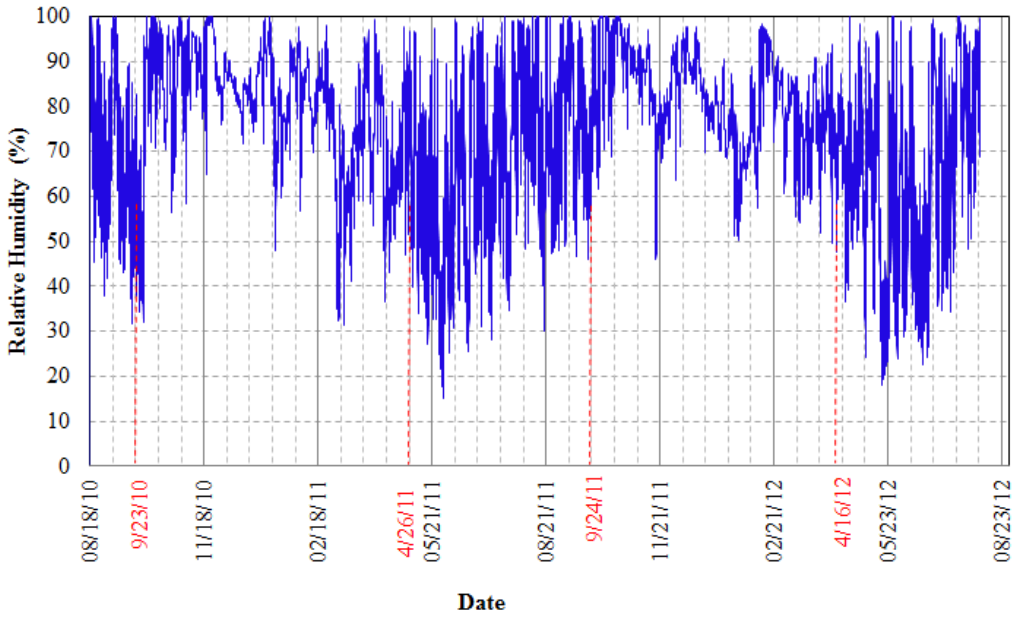

Figure 61. Hourly relative humidity at the Beaver Slide test section

TEMPERATURE CHANGES IN THE TEST SECTION

Figure 62 shows the temperature changes for sensors at 1.5 ft below the road surface during the two-year study period. Generally, changes in soil temperature follow changes in air temperature, but soil temperature changes are much less dramatic than air temperature changes, mainly due to the insulating effect of soil. Figure 62 indicates that changes in soil temperature followed changes in air temperature more closely in the summer months, from late April to early September, than in the winter months from September to April.

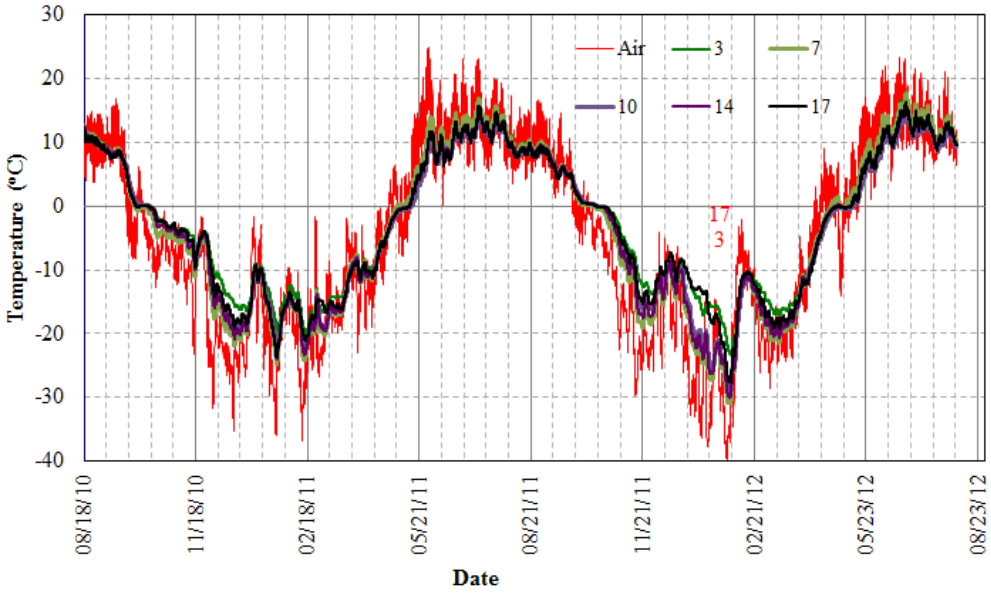

Figure 62. Temperature changes at 1.5 feet below the road surface

Soil temperatures are close to the average daily air temperature during the summer months and 5–10° warmer during the winter months, likely due to the insulation effect of snow cover. Because snow has low density and high voids, which trap a lot of air, it is good insulation and keeps the shoulders of roads relatively warm. In the winter, the soils (for example at sensors 7 and 10) at the center of the road are colder than the soils at the edges (for example at sensor 3 eastbound and sensor 10 westbound). The difference can be as much as 10°. This difference is mainly related to DOT&PF's snow removal process; during the winter, its M&O crew often pulls snow from the road surface to the two shoulders and piles it at the shoulders (please see Figure 54 for reference). The center of the road, on the other hand, is exposed to air directly and is usually colder. Except for the road lanes, all other ground surface is covered by snow, which makes the overall soil temperature in the winter higher than the ambient air temperature. Figure 62 indicates that soil temperature first dropped to 0°C on October 10, 2010, and rose to above 0°C on May 15, 2011. In 2011, soil temperature first dropped to 0°C on October 14, and rose to above 0°C on May 12, 2012.

Figure 63 shows temperature changes for sensors at about 2.5 feet below the road surface. While sensors 4, 8, 11, 15, and 18 are in the road section and covered by 2.5 feet of soils, sensor 1 is at the shoulder just 1 foot below the ground surface. Temperature changes at sensor locations 4, 8, 11, 15, and 18 followed a pattern similar to the air temperature changes, but the soil temperatures were warmer in the winter and colder in the summer due to the insulation effect of the soils. Generally, soil temperatures in the center of the road were colder than those at the edge of the road.

Soil temperatures at the sensor 1 location followed air temperature changes during the summer months and were relatively constant at -7°C during the winter months. This pattern occurred because in the summer when all the snow was gone, sensor 1 was very close to the ground surface, and in the winter, it was covered by thick snow that had been removed from

the road surface. The differences between the air temperature and the temperature at sensor 1 were due to the evaporation of water at the soil surface, which absorbs a lot of heat energy. As a result, soil temperatures were always lower than air temperatures. Figure 63 indicates that soil temperature at sensor 11 first dropped to 0°C on October 17, 2010, and rose to above 0°C on May 23, 2011. In 2011, soil temperature first dropped to 0°C on October 23, and rose to above 0°C on May 22, 2012.

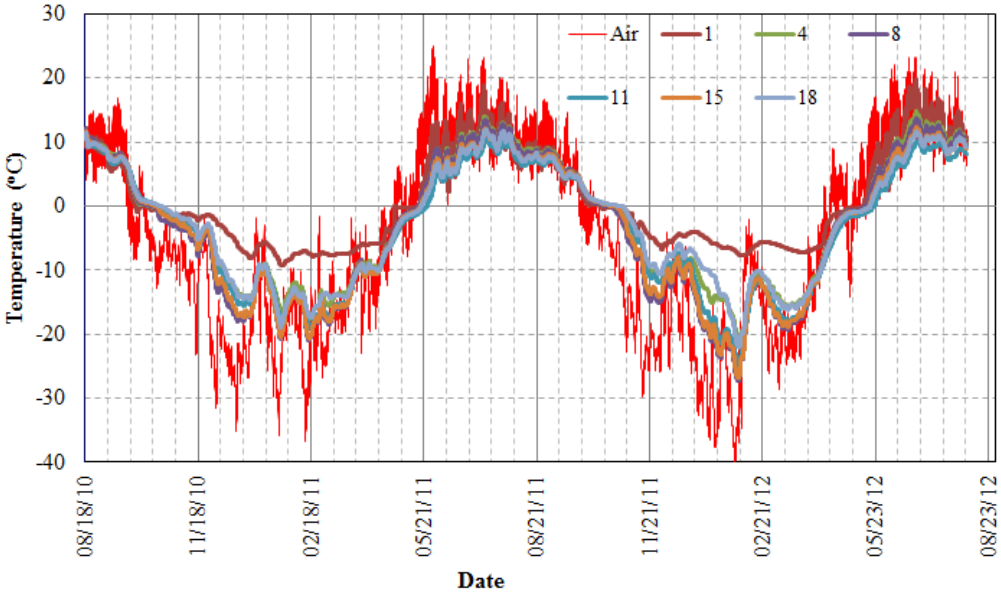

Figure 63. Temperature changes at 2.5 feet below the road surface

Figure 64 shows temperature changes for sensors at about 3.5 ft below the road surface at sensor locations 5, 9, 12, 16, 19, 21, and 22. Sensor 2 is at the shoulder with soil cover of approximately 3 ft. The temperature-change pattern is similar to that shown in Figure 63 and similar to air temperature changes. Due to the thicker soil coverage, the soil temperatures are much warmer than the air temperatures in the winter, and temperature differences at the individual sensor locations are more significant. During the winter months, the soil temperatures at different sensor locations varied from high to low in the following sensor order: 2, 22, 21, 5, 19, 16, 12, and 9. That is, soil temperatures in the center of the road section were colder than those at the edge of it. Soil at the sensor 2 location was the warmest due to DOT&PF's snow removal practice. Compared with air temperatures, soil temperatures are warmer in the winter and colder in the summer due to the insulation effect of the soils. Figure 64 indicates that soil temperature at sensor 12 first dropped to 0°C on October 25, 2010, and rose to above 0°C on May 29, 2011. In 2011, soil temperature first dropped to 0°C on October 31, and rose to above 0°C on May 29, 2012.

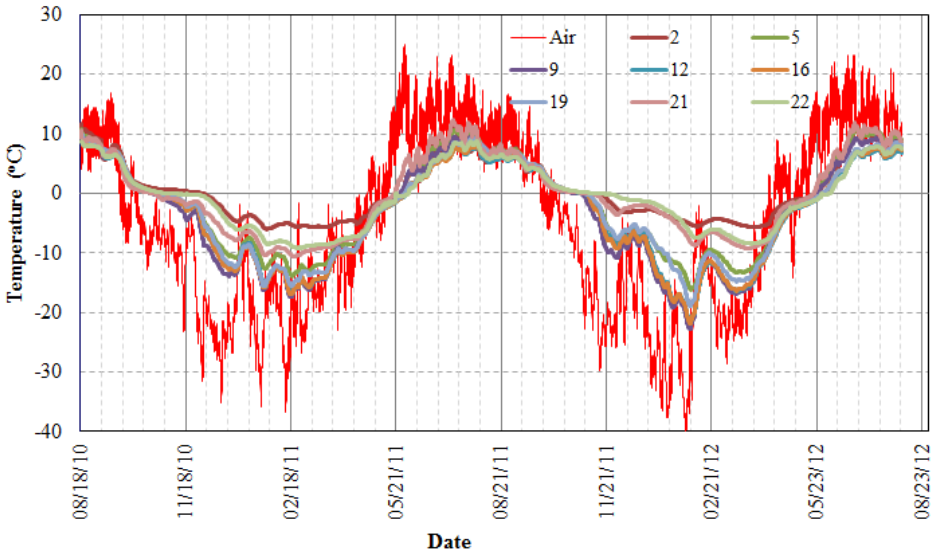

Figure 64. Temperature changes at 3.5 feet below the road surface

Figure 65 shows the temperature changes for sensors 6, 13, and 20 at about 6 ft below the road surface. The temperatures at these locations changed in a sinusoidal pattern similar to the air temperatures. However, there were clear reductions in the amplitudes of temperature variations and time lags in terms of the peak temperature values. The temperatures varied between +7°C and -11°C in the soil, while the maximum temperature variations in the air were between +23°C and -40°C. The air temperature peaked normally in late June each year and was lowest in late January, while the soil temperature 6 feet below the surface normally peaked in late July to early September and was lowest in mid-February to late March. Figure 65 indicates that soil temperature at sensor 13 first dropped to 0°C on November 9, 2010, and remained near zero until December 9, 2012, and rose to above 0°C on July 18, 2011. In 2011, soil temperature first dropped to 0°C on November 6, and rose to above 0°C on July 30, 2012.

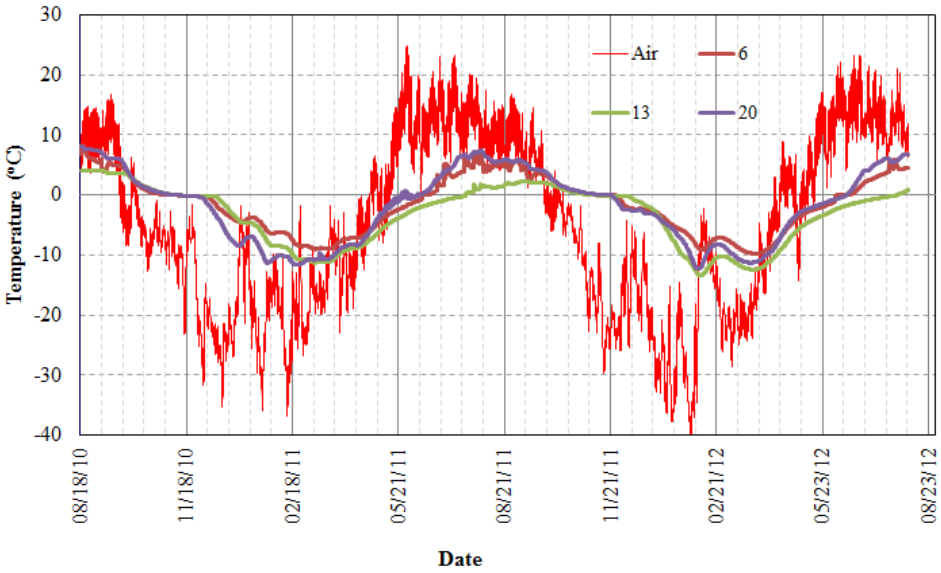

Figure 65. Temperature changes at 6 feet below the road surface

Figure 66 shows temperature changes for sensors 10 through 13 at the center of the road section but at different depths. It can be seen that at a shallow depth of 1.5 ft below the road surface, the temperature changes follow the air temperature-changing pattern closely in both amplitudes and phase. With an increase in depth, the amplitude of temperature variations is reduced and the time lag for temperature changes is bigger.

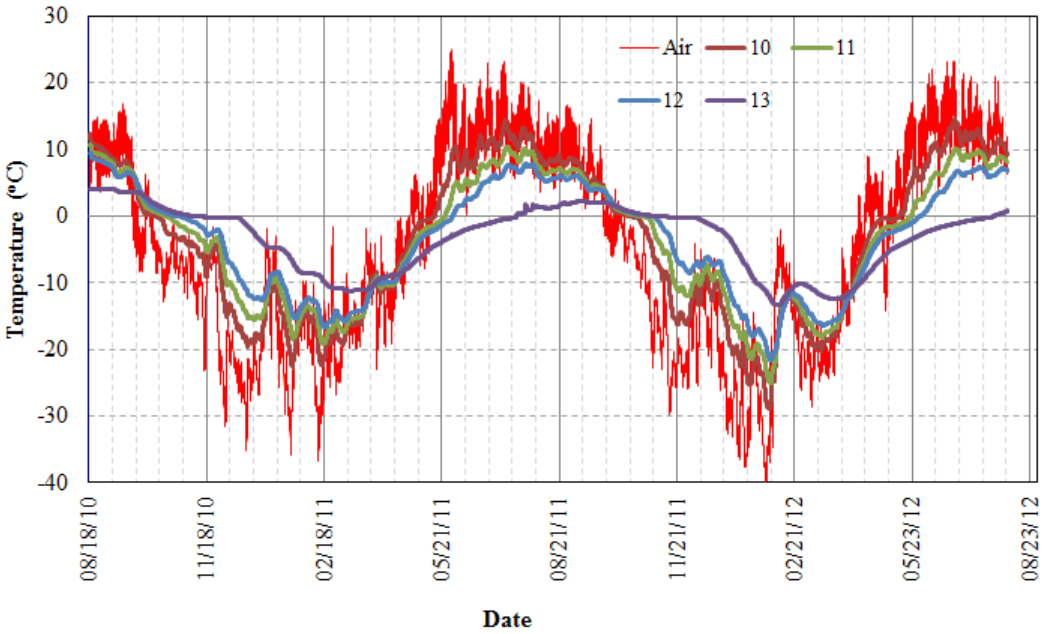

Figure 66. Temperature changes below the center of the road surface

Figure 67 shows the temperature changes for sensors 1, 2, and 22 at the shoulders of the road section. The figure indicates that during the summer months, soil temperatures follow changes in air temperature. During the winter months, the temperature changes were small and not closely related to air temperature changes, mainly due to the insulation effect of thick snow at the shoulder (see Figure 54).

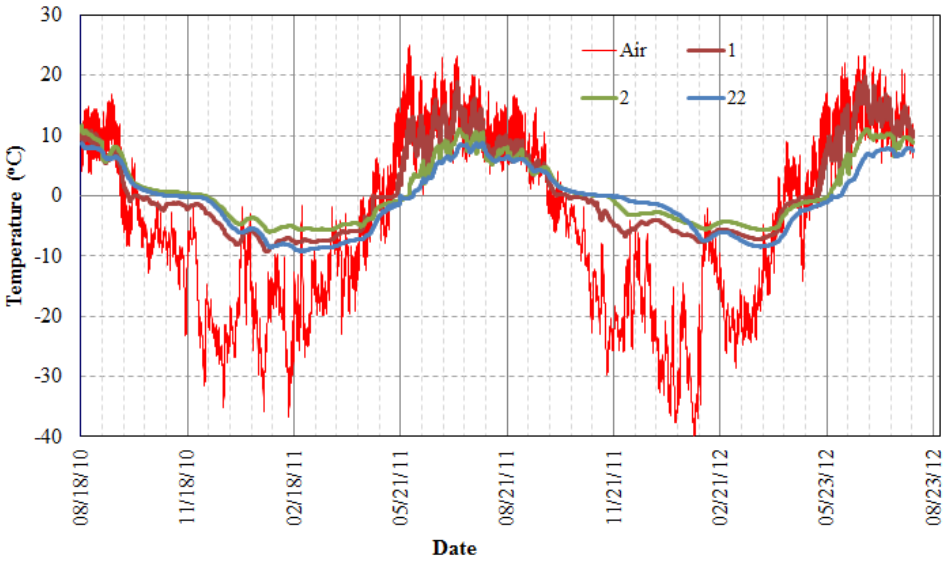

Figure 67. Temperature changes at the shoulders of the road

MOISTURE CONTENT CHANGES IN THE TEST SECTION

The CS616-L moisture probes measure unfrozen volumetric water content of the soil. At the west side of the road is a ditch line, designed to drain away the melted mountain water. It was observed that water flows in the ditch during the summer months. The bottom of the ditch is about 3.6 feet below the road surface. Of all the sensor pairs, sensor 22 was the closest to the ditch, about 3.9 feet below the road surface. Figure 68 shows the temperature and volumetric moisture content changes at the location of sensor 22.

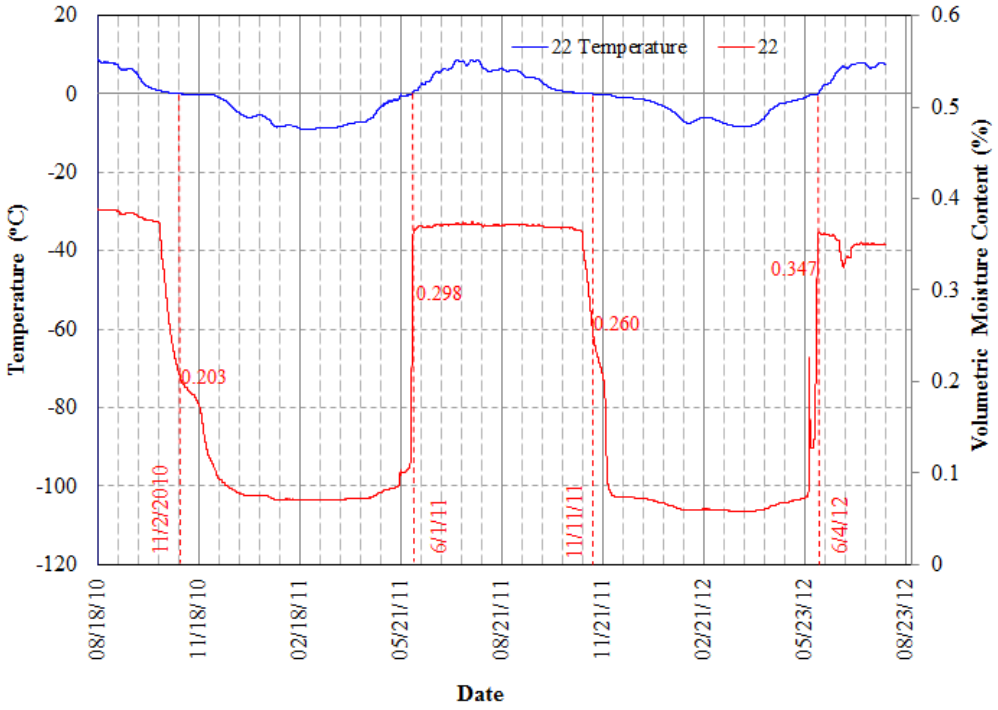

Figure 68. Temperature and volumetric moisture content changes at the location of sensor 22

It was found that the volumetric water content of the soil during the 2011 summer months was constant at 37.2% when the soil was unfrozen. During the summers of 2010 and 2012, the volumetric water content of the soil at sensor location 22 was also relatively constant. It is considered, therefore, that soils at the location of sensor 22 are always saturated during the summer months. If the soils at the test sections were relatively uniform, then their saturated volumetric water content was close to 37.2%. Consequently, sensor 22 can be used as a reference to evaluate moisture content at other locations. Figure 68 also indicates that soil volumetric water content decreased before the soil temperature dropped to 0°C. It was found that when soils at the location of sensor 22 were completely frozen, the unfrozen moisture content of the soil varied from 5.9% to 7%.

Figure 69 shows the air temperature and volumetric water content changes for sensors 3, 7, 10, 14, 17, and 22 at about 1.5 ft below the road surface, as well as the starting times for freezing and thawing processes. Initially in August 2010, all soils were unsaturated, with slight water content reduction. The moisture content at sensors 3 and 17 suddenly increased on September 6, 2010. Soils at other sensor locations, such as 7, 10, and 14, had a similar but delayed increase. The relative humidity data indicate that from 3:00 a.m. to 9:00 a.m. on

September 5, 2010, relative humidity at the site was 100%. It was concluded, therefore, that the moisture content increases during this period were due to a rainfall event. After the increase in moisture content, the moisture content at all sensor locations decreased, likely due to the drainage of water and reduced water supply. The unfrozen moisture content further decreased when the soils started freezing on October 10, 2010. Moisture probes only measure unfrozen volumetric moisture content. When soil freezes, some of the free water freezes and becomes ice. As a result, the unfrozen moisture content decreases. If soil freezes at a relatively high moisture content, the unfrozen moisture content is mainly related to temperature when the soil is frozen. After the soils froze, the values in unfrozen moisture content at all sensor locations were very close due to the similar temperature. Their changing patterns, which were controlled by the temperature changes, were nearly the same. The unfrozen moisture content varied narrowly between 7% and 12% when the temperature varied between -10°C and -20°C. In April 2011, when the temperature increased from -10°C to 0°C, the unfrozen moisture content increased.

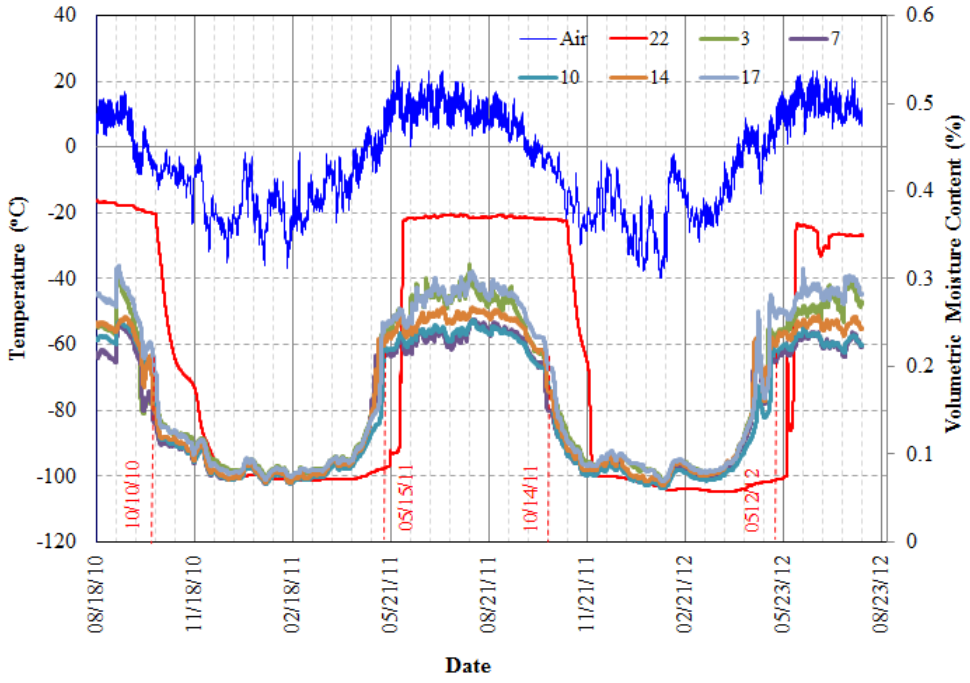

Figure 69. Volumetric water content changes at 1.5 feet below the road surface

Table 3 is a summary of the moisture content of soils at different sensor locations at 1.5 ft below the road surface, before the soil froze and after it thawed. The table indicates that after the soil thawed, slight increases in moisture content occurred at nearly all sensor locations. Soil moisture content did not exceed the saturated water content. After the soil thawed, the moisture content at these sensor locations increased gradually with the increase in air temperature until the end of July and then decreased gradually with the decrease in daily air temperature until the next freezing process. Normally, temperature increase has two effects on soil moisture: first, it tends to cause an increase in soil moisture by thawing the frozen soils to provide more water; second, higher temperatures cause high evaporation, which leads to high evaporation rates and drying of the soils. At this test section, it seemed

the first effect dominated. It was found that rainfall events had limited influence on soil moisture content.

Table 3. Moisture content of soils 1.5 feet below the road surface

Date	Sensor					Note
	3	7	10	14	17	
10/10/2010	0.157	0.152	0.198	0.180	0.219	Before Frozen
5/15/2011	0.235	0.212	0.220	0.229	0.244	After Thawed
10/4/2011	0.217	0.205	0.202	0.219	0.233	Before Frozen
5/12/2012	0.277	0.232	0.230	0.208	0.240	After Thawed

Table 3 shows that during the two-year study period, when the soils were unfrozen, moisture content was far below the saturation moisture content, indicating that there was no frost heave in the first 1.5 ft of soil, which is why the test section performed well.

Figure 70 shows the air temperature and volumetric water content changes for sensors 1, 4, 8, 11, 15, and 18 at about 2.5 feet below the road surface. Similar to Figure 69, when the soils were frozen, the moisture content for soils at most sensor locations (all but sensor 1) had limited changes, with a pattern similar to the air temperature changes. When the soils were unfrozen, dramatic changes in moisture content occurred. Moisture content at the sensor locations shown in Figure 70 was higher than moisture content at the corresponding locations and 1.5 feet below the soil surface, as shown in Figure 69. Under most situations, the soils closer to the west side (ditch) had higher moisture content. Of all soils, only the soil at sensor location 18 occasionally exceeded the saturation moisture content of sensor 22. Note that sensor 18 was at the edge of the road section and might not be compacted very well. The moisture content of moist soils under most situations was much less than saturation moisture content. The increases in moisture content, if there were any, were usually rapid. The high moisture content status normally did not last long. Instead, the moisture content normally dropped quickly, indicating that the drainage of water was quick in the test section.

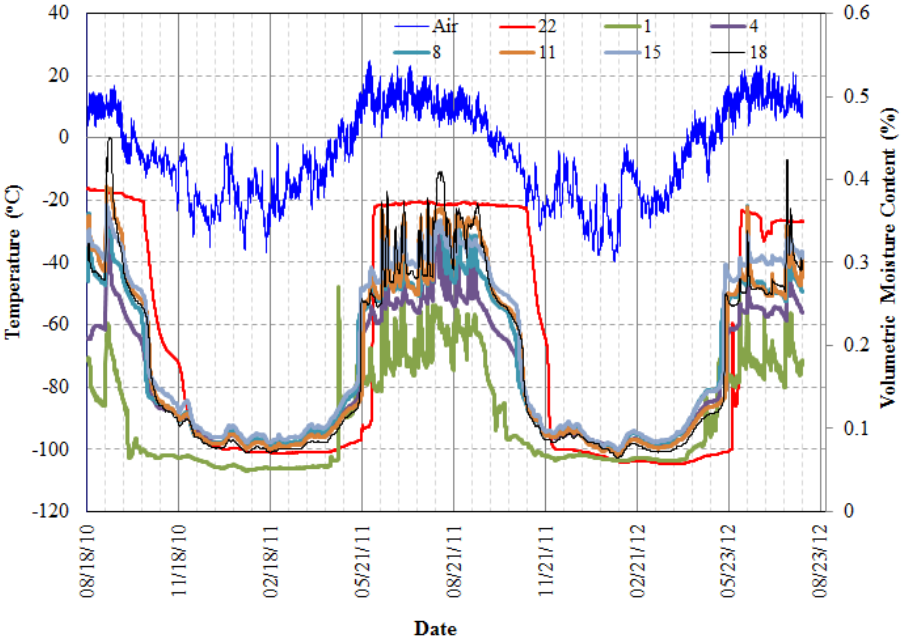

Figure 70. Volumetric water content changes at 2.5 feet below the road surface

Again, sensor 1 was at the shoulder of the road section and was less than 1 ft below the ground soil surface. The moisture content at sensor 1 was much lower than at any other sensor shown in Figure 70, mainly due to the better drainage at that location.

Figure 71 shows the air temperature and volumetric water content changes for sensors 2, 5, 9, 12, 16, 19, and 21 at about 3.5 feet below the road surface. Compared with Figure 70, the soils in Figure 71 had higher moisture content, and the higher moisture content was maintained for a longer time. The soils at the edges of the road section had higher moisture content than those in the center of the road section.

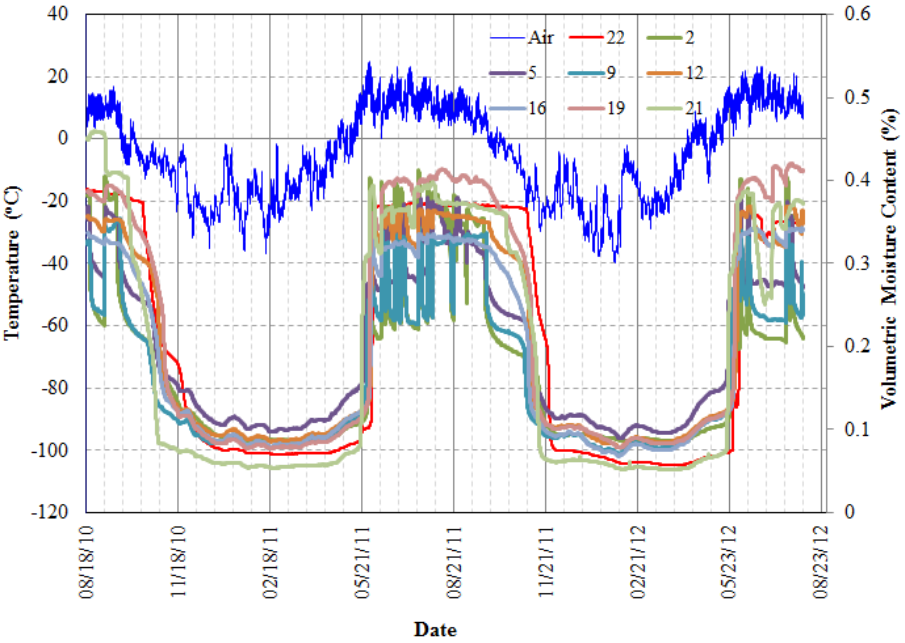

Figure 71. Volumetric water content changes at 3.5 feet below the road surface

Figure 72 shows the air temperature and volumetric water content changes for sensors 5, 9, 12, and 16 only. Comparing Figure 71 with Figure 72, it can be seen that during the summer months the locations with higher moisture content were soils at the edge of the road section such as sensor locations 2, 19, and 21. Note that sensor locations 19 and 21 were close to the ditch and had elevations only slightly higher than the bottom of the ditch. During the winter months, the variations of unfrozen moisture content in all soils were small and smooth. Similar to previous discussions, the unfrozen moisture content of all soils shown in Figure 71 decreased dramatically when the soils were freezing, and increased significantly when they were thawing.

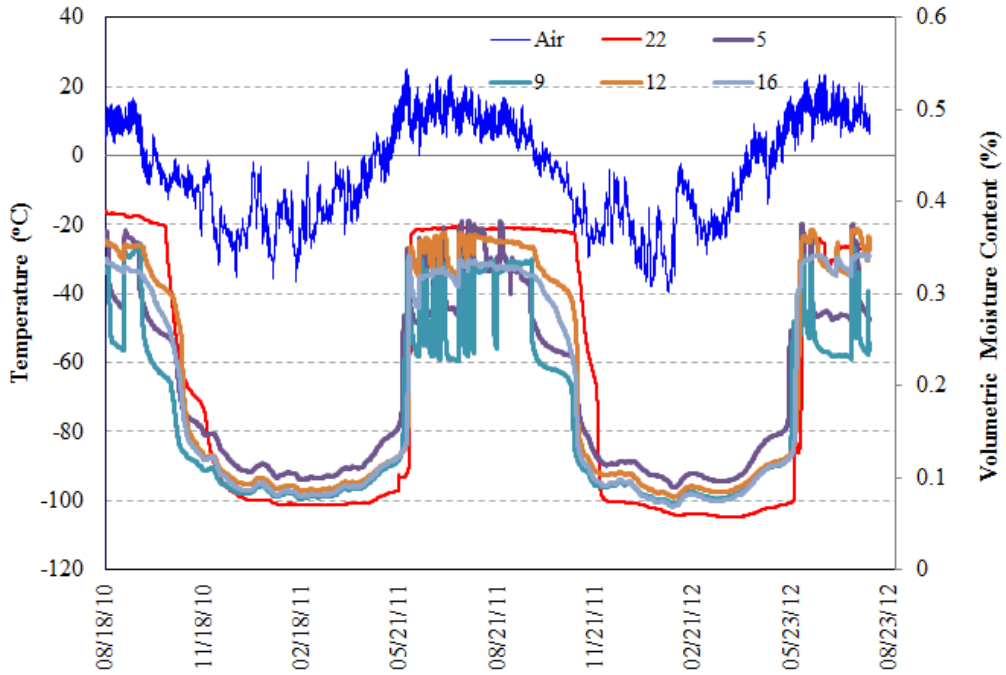

Figure 72. Volumetric water content changes at 3.5 feet below the road surface

Figure 73 shows the air temperature and volumetric water content changes for sensors 6, 13, and 20 at about 6 feet below the road surface. Soils at sensor 6 had lower moisture content than those at sensor locations 3 and 20, mainly due to better drainage at the location of sensor 6. As described in Chapter 3, sensor 20 was installed under water. Figure 73 indicates that the moisture content of soils at sensor 20 was higher than that of the soils at sensor 22 in August 2010. The soil moisture content kept decreasing until to became completely frozen in December 2010. The average unfrozen water content during winter 2010–2011 was about 10%, which is 2% higher than soils at sensor 22. Soils at sensor 20 thawed in June 2011; the moisture content was close to the soils at sensor 22 and decreased slightly with time. The average unfrozen water content for soils at sensor 20 during winter 2011–2012 was similar to that of the previous winter at the same location. When the soils thawed in June 2012, the moisture content of the soils was close to that of the soils at sensor 22 and remained constant. From these observations, it seems that soils at sensor location 20 were not fully compacted during the construction process and became more compacted with time due to the freeze-thaw cycle.

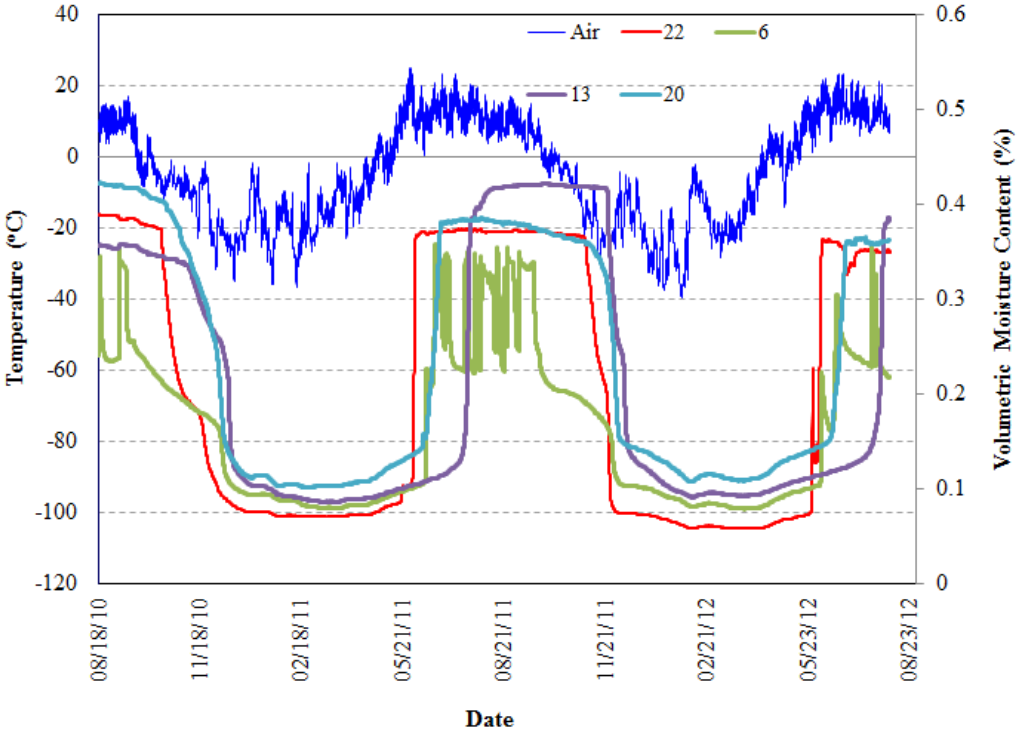

Figure 73. Volumetric water content changes at 6 feet below the road surface

Variations of moisture content for soils at sensor location 13 had a trend opposite of that for soils at sensor location 20. Soils at sensor 13 had moisture content lower than soils at sensor 22 in August 2010. Moisture content continued decreasing until the soil was completely frozen in December 2010. The average unfrozen water content during winter 2010–2011 was similar to soils at sensor location 22. Soils at sensor 13 thawed in July 2011, and the moisture content was 41.9%, which is 5% higher than soils at sensor 22 during the same period. The average unfrozen water content for soils at sensor 13 during winter 2011–2012 was similar to that of the previous winter at the same location. From these observations, it seems that soils at sensor location 13 experienced some frost heave, causing the soil to become loose. The variations in moisture content for soils at sensor location 13 during August and September 2012 were unknown due to the lack of available data at the time of writing this report.

Figure 74 shows the moisture content changes for sensors 10 through 13 at the center of the road section but at different depths. It can be seen that with an increase in depth, moisture content at thawed conditions increased. However, moisture content for soils 3.5 feet below the road surface was lower than saturation most of the time.

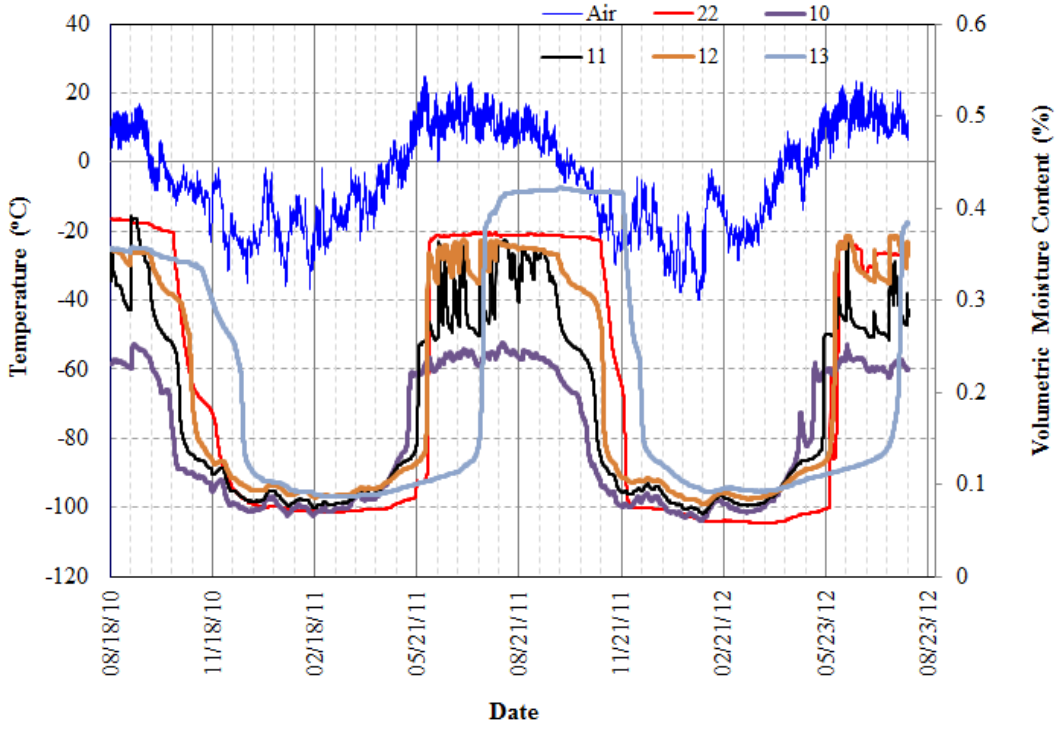

Figure 74. Volumetric water content at the center of the road with different depths

TEMPERATURE AND MOISTURE CONTOURS

The hourly temperature and moisture data at different sensor locations were used to generate temperature and moisture contours to analyze spatial distribution of the temperature and moisture to evaluate the performance of the H2Ri wicking fabric. Appendix I shows snapshots of these contours at noon for each day.

As shown in Figure 75, on August 18, 2010, two weeks after the test section was constructed, the soils at 6 feet below the road surface were completely unfrozen. The soil temperatures decreased with increase in depth, varying from 40°C to 12°C. The isothermal lines were approximately parallel to the configuration of the road section. The moisture content contour was not related to the temperature contour, but depended on groundwater flow. At sensor locations 19 to 22 close to the ditch, the soils were saturated. Soils at sensor locations 12 and 13 were also saturated, while the soils at sensor locations 14 through 16 were unsaturated. The saturated soil protrusion coincided with the excavation pit for sensor installation at the center of the road, which implies that compaction at the excavation pit was not good and resulted in a channel with relatively high permeability. At the east shoulder of the road from sensors 5 to 2, a narrow zone of soils had high moisture content. It was close to the exit of the H2Ri wicking fabric.

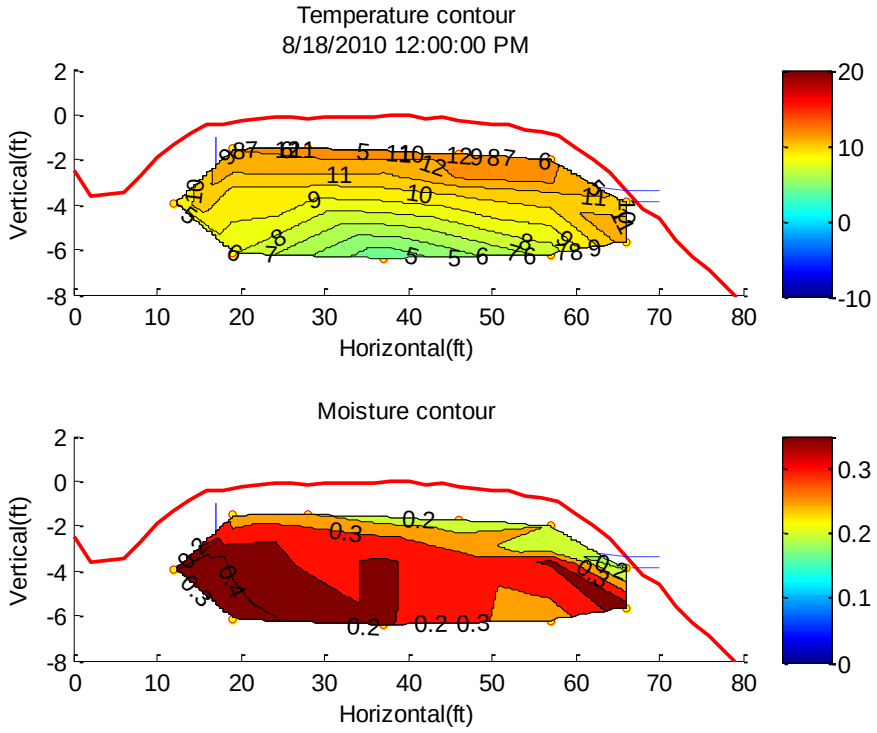

Figure 75. Temperature and moisture content contours at noon on August 18, 2010

As shown in Figure 76, the relative humidity on August 19, 2010, from 3:00 a.m. to 9:00 a.m. was 100%, indicating that a rainfall event occurred. This event was consistent with changes in the moisture content contour at noon on August 19, 2010, as shown in Figure 77. Compared with the previous day, there was a clear increase in the moisture content in the test section, especially along the H2Ri at 3 feet below the road surface. At the east shoulder of the road from sensors 5 to 2, moisture content increased for soils close to the exit of the H2Ri wicking fabric. This was a clear indication that the H2Ri provided a good channel for water transport.

The relative humidity data indicate that no rainfall occurred during the following two weeks. Compared with Figure 75 and Figure 77, the moisture content in the test section clearly decreased, as shown in Figure 78 and Figure 79, especially in the east lane of the road. The soils at the exit of the H2Ri wicking fabric were the driest. A decrease in moisture content in the west lane of the road was clear, although it was not as dramatic a decrease as in the east lane. The high moisture content protrusion at the center of the road, which was reduced significantly until August 26, 2010 (Figure 78), nearly disappeared on September 4, 2010 (Figure 79). The soils remained saturated at sensor locations 20 to 22, close to the ditch.

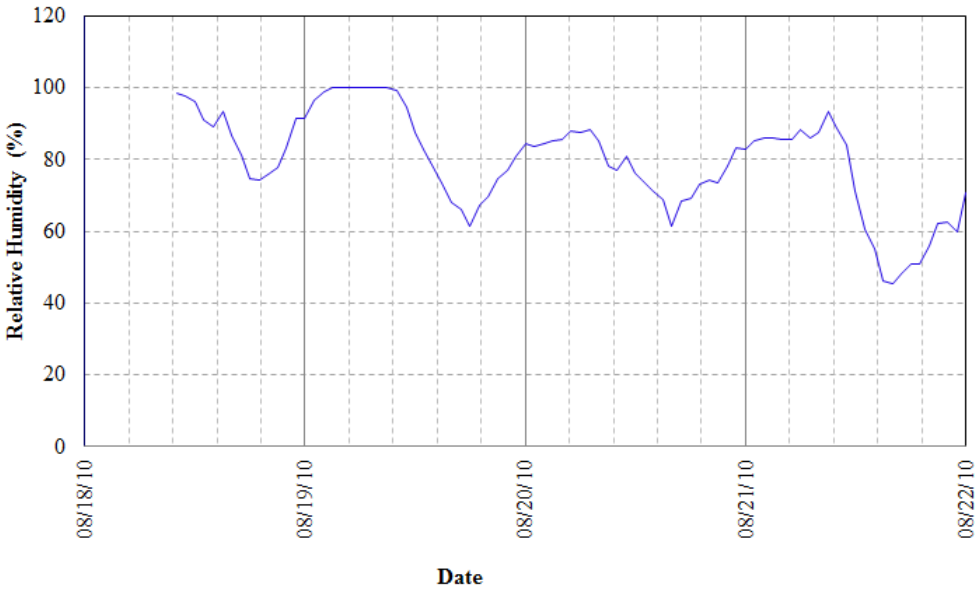

Figure 76. Hourly relative humidity data for August 18–22, 2010

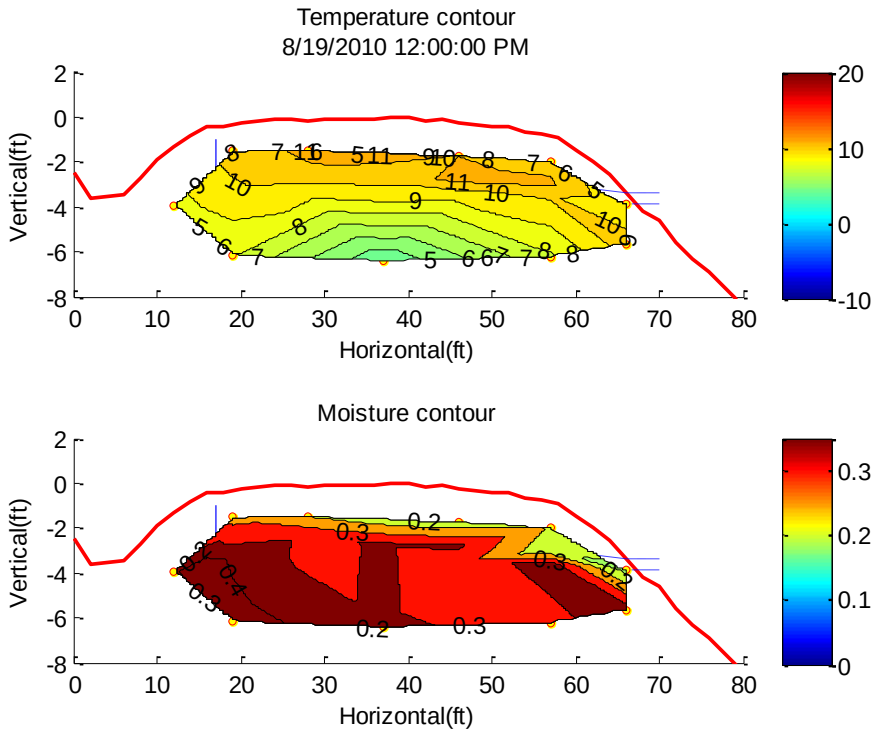

Figure 77. Temperature and moisture content contours at noon on August 19, 2010

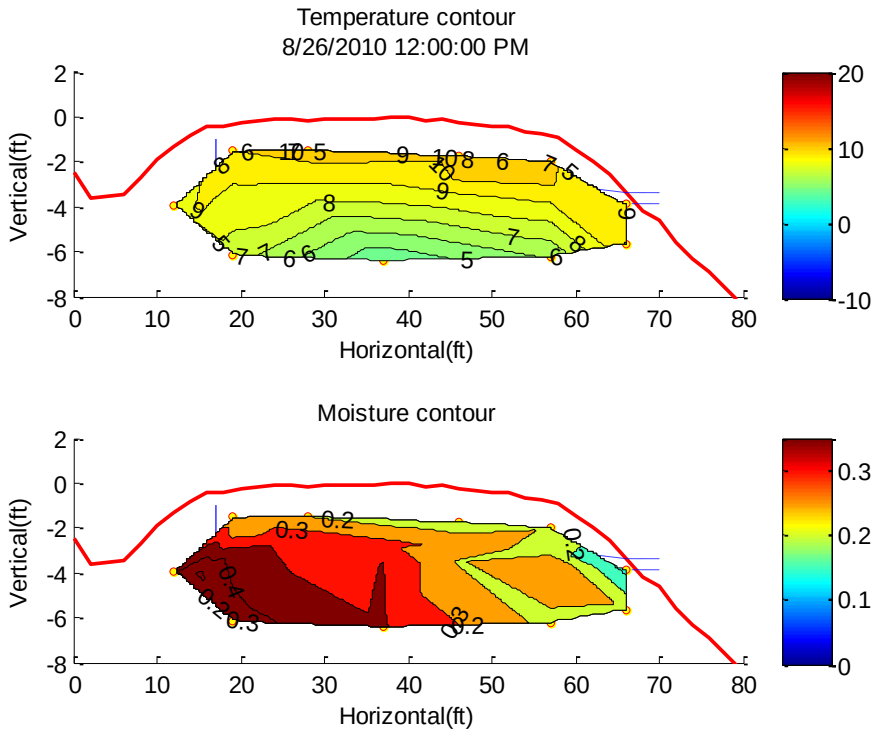

Figure 78. Temperature and moisture content contours at noon on August 26, 2010

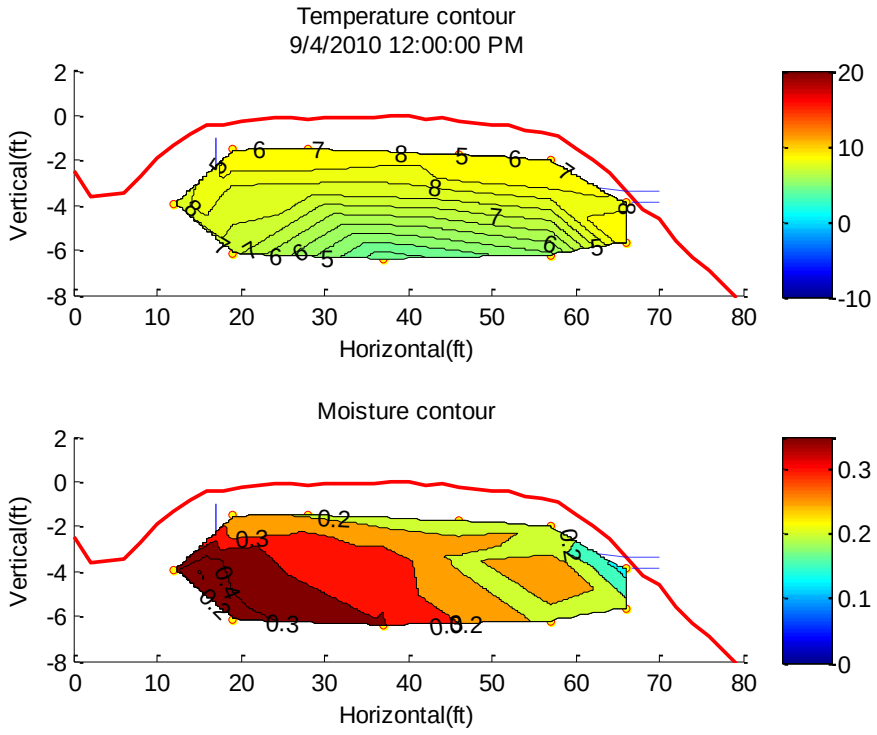

Figure 79. Temperature and moisture content contours at noon on September 4, 2010

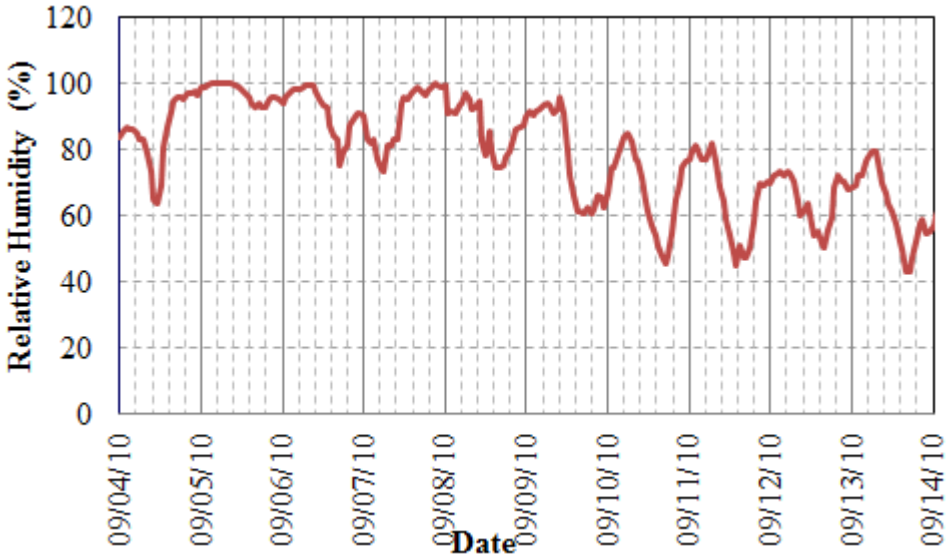

Figure 80. Hourly relative humidity data for September 4–14, 2010

The hourly relative humidity data indicate that several rainfall events occurred during the period of September 5–8, 2010 (Figure 80). As a result, the soil moisture content of the road section quickly increased. On September 6, 2010, soils in the road section were nearly saturated for all soils 3 feet below the road surface (Figure 81). From September 5–8, 2010, alternating increases and decreases in moisture content occurred in the road section. However, soil moisture content during this period was generally high for soils 3 feet below the road surface (Figure 82). From September 9–14, 2010, the relative humidity at the test site generally decreased (Figure 80). As a result, moisture content in the road section decreased, as indicated in Figure 83. As seen in Figure 83, soils dried from the east side to the west side along the H2Ri wicking fabric, and a high moisture-content zone formed near the exit of the H2Ri wicking fabric. While soils below 5.5 feet remained saturated, a low moisture-content zone was observed at sensors 19, 16, 12, 13, and 20 at the west lane of the road section at a depth of 3.5 to 5.5 eeft.

Figure 84 shows an unexpected increase in moisture content in the road section on September 13, 2010, compared with the moisture content contour in Figure 83 and relative humidity in Figure 80. The water supply seemed to be related to groundwater at deeper depth (water seemed to flow along sensors 20→13→12→9→5→1). Once again, the water was flowing along the H2Ri wicking fabric. The soils near the exit of the H2Ri were dry, while the soils below the H2Ri were wet.

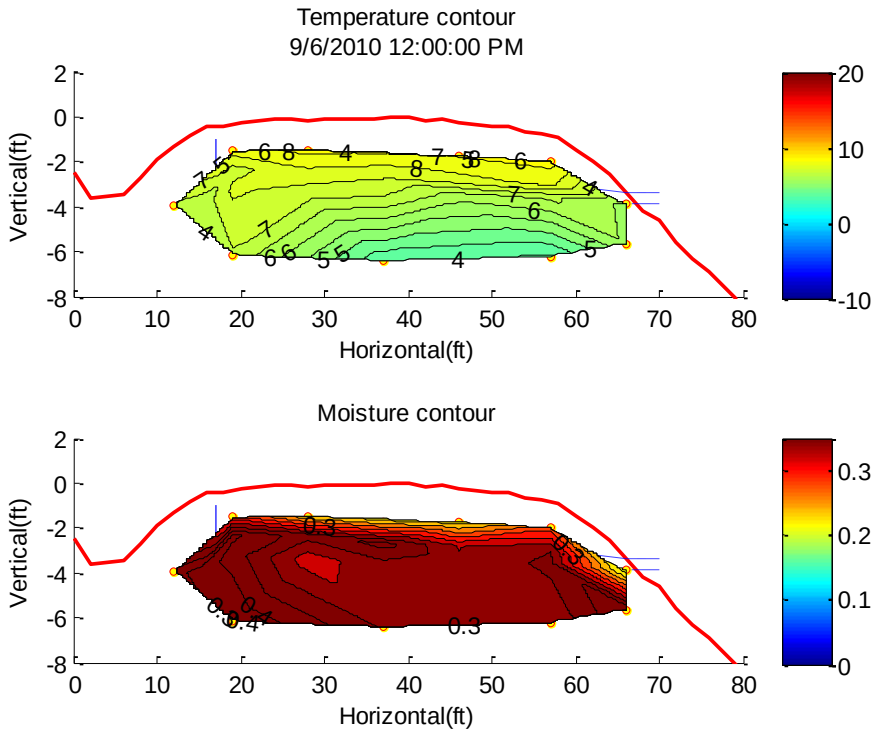

Figure 81. Temperature and moisture content contours at noon on September 6, 2010

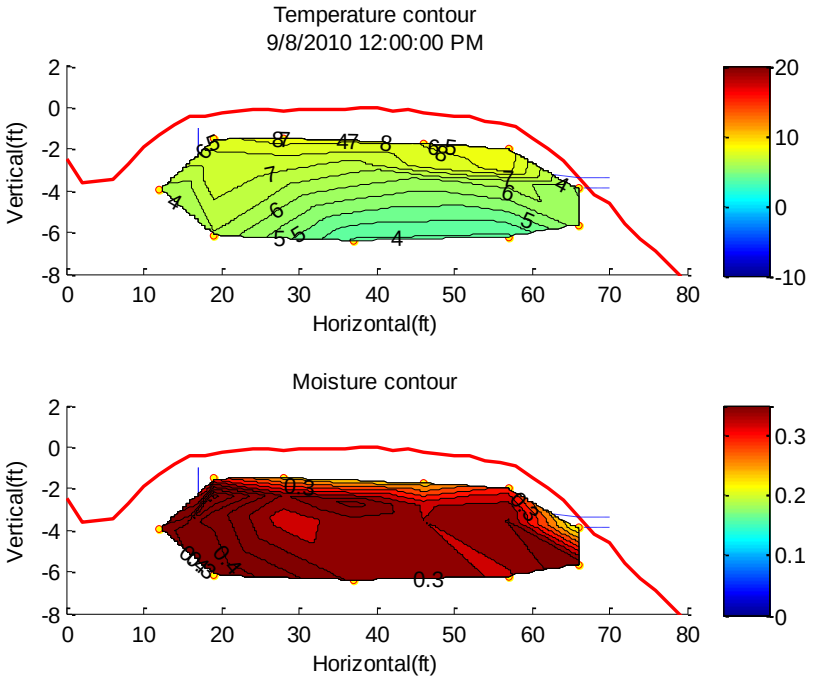

Figure 82. Temperature and moisture content contours at noon on September 8, 2010

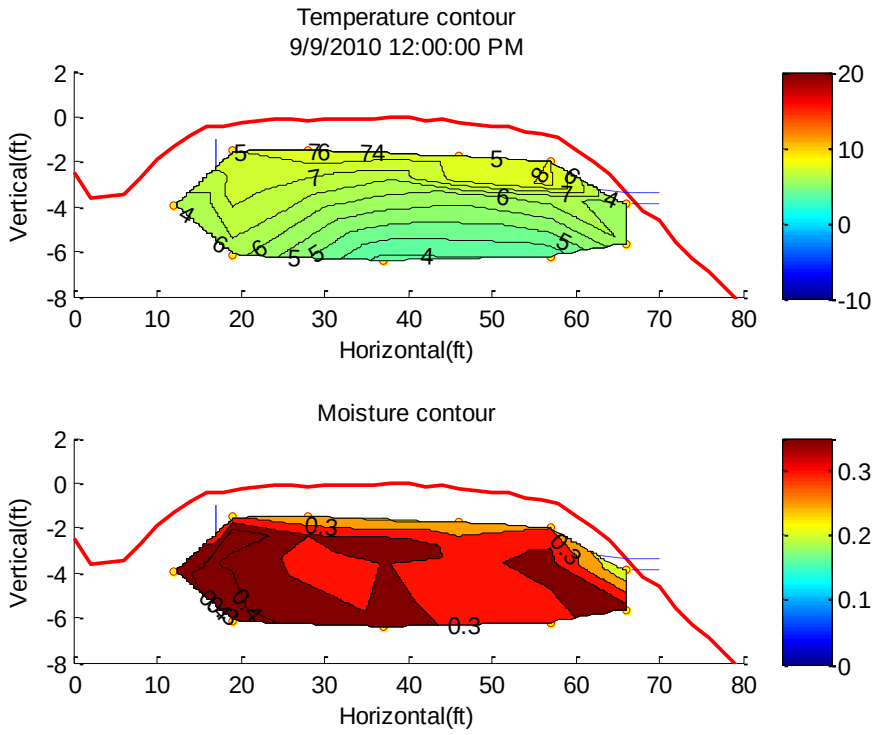

Figure 83. Temperature and moisture content contours at noon on September 9, 2010

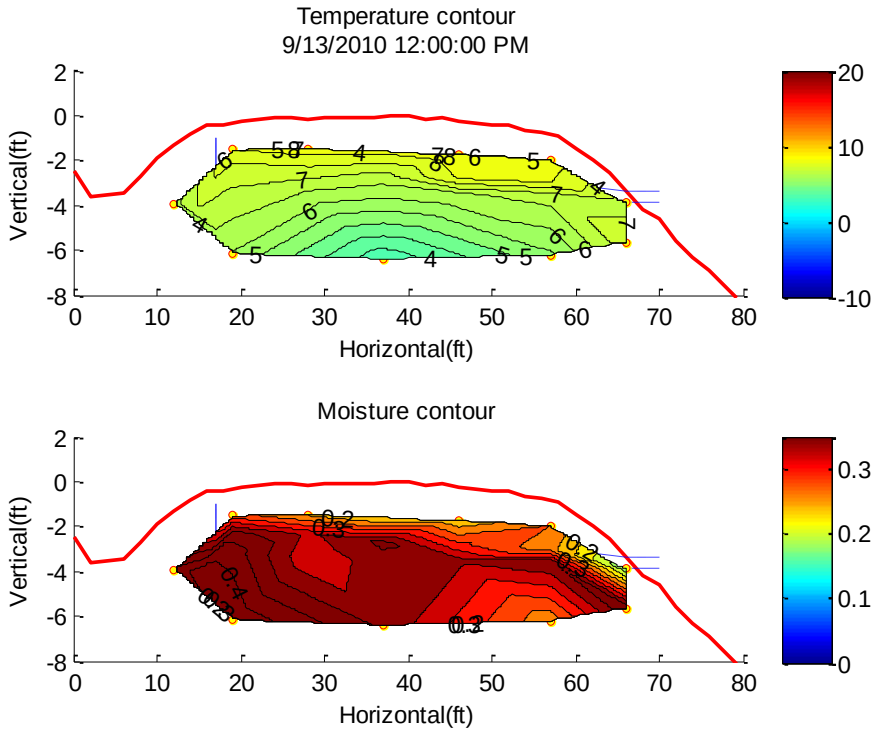

Figure 84. Temperature and moisture content contours at noon on September 13, 2010

From September 13 to 22, 2010, the relative humidity at the test site was lower than 90%, indicating that most likely no rainfall occurred during this period. The moisture content in the road section kept decreasing, as demonstrated in Figure 85 by the moisture content

contour on September 22, 2010. As shown previously, the air temperature at the test site dropped to below 0°C on September 23, 2010. Freezing reduced free water in the soil and, subsequently, in the groundwater supply. As a result, the moisture content in the road section was further decreased, as shown in Figure 86 by the moisture content contour on September 24, 2010.

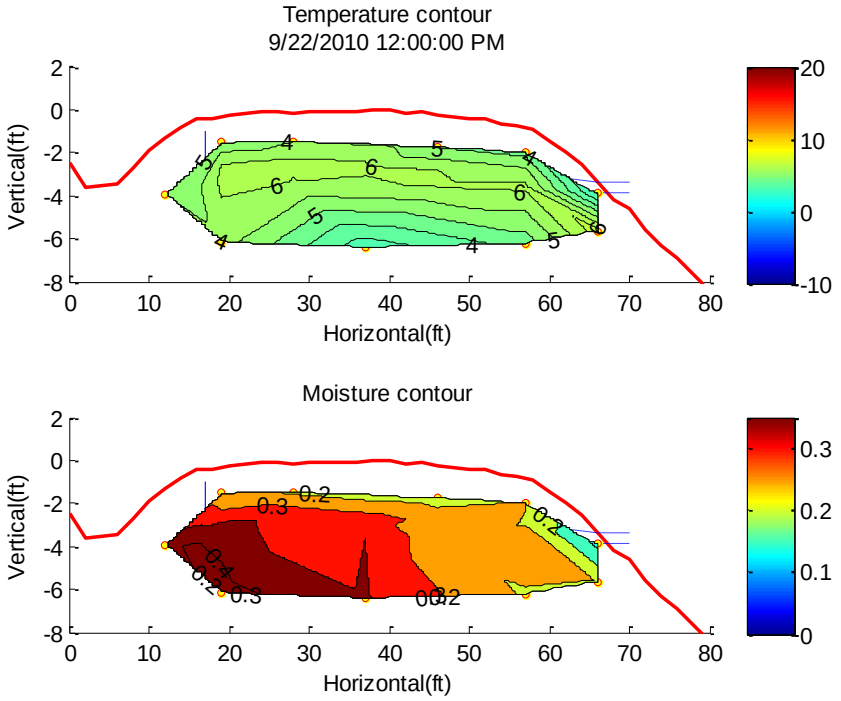

Figure 85. Temperature and moisture content contours at noon on September 22, 2010

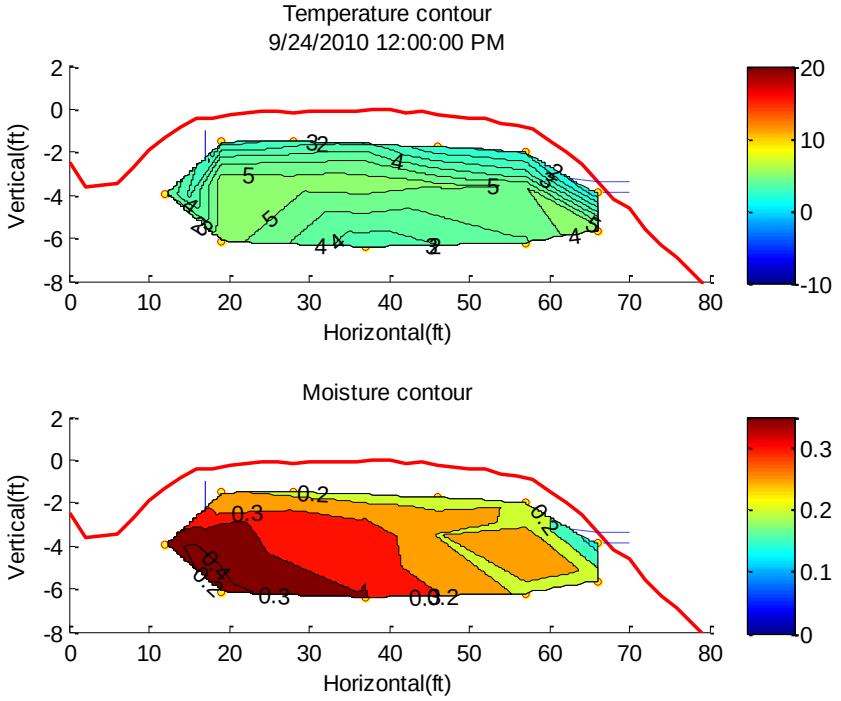

Figure 86. Temperature and moisture content contours at noon on September 24, 2010

Figure 87 through Figure 90 show the temperature and moisture content contours for the road section when the freezing front penetrated to approximately 1.5 ft, 2.5 ft, 3.5 ft, and 6 feet below the road surface on October 10, 2010, October 17, 2010, October 26, 2010, and November 9, 2010, respectively. It can be seen from these figures that the temperature and moisture contours for frozen soils are similar (as shown later, it seemed that unfrozen moisture content for partially frozen soils depended upon temperature only). For soils in the unfrozen zone, no clear relationship appeared between the temperature and moisture content contours. Figure 87–Figure 90 show that before the soils were frozen, moisture content had significantly reduced. Possible reasons for this phenomenon include (1) reduced water supply from the upward tundra, (2) increased drainage due to a drier environment, and (3) upward movements of water due to frost heaving. The third reason is related to the frost boil/soft spot problem. Available data at this time can only eliminate possibility 2, since the soils at the exit of the H2Ri wicking fabric were frozen the earliest, as shown in Figure 87–Figure 90. Analysis of the spring 2011 thawing data indicates that no frost heave occurred during this period. As a result, the conclusion is that there was reduced water supply from the upward tundra.

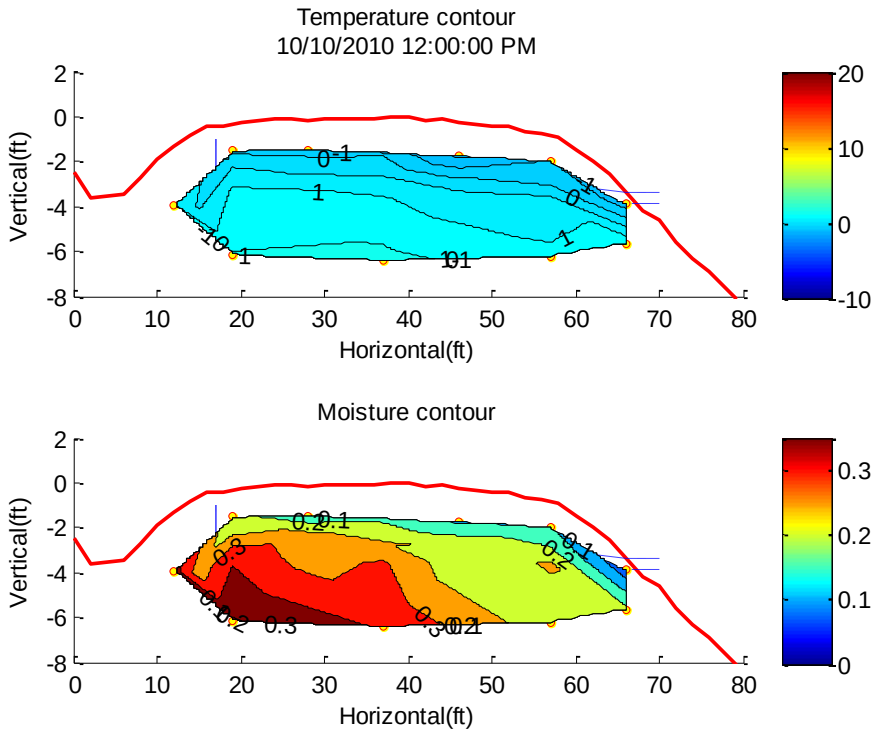

Figure 87. Temperature and moisture content contours at noon on October 10, 2010

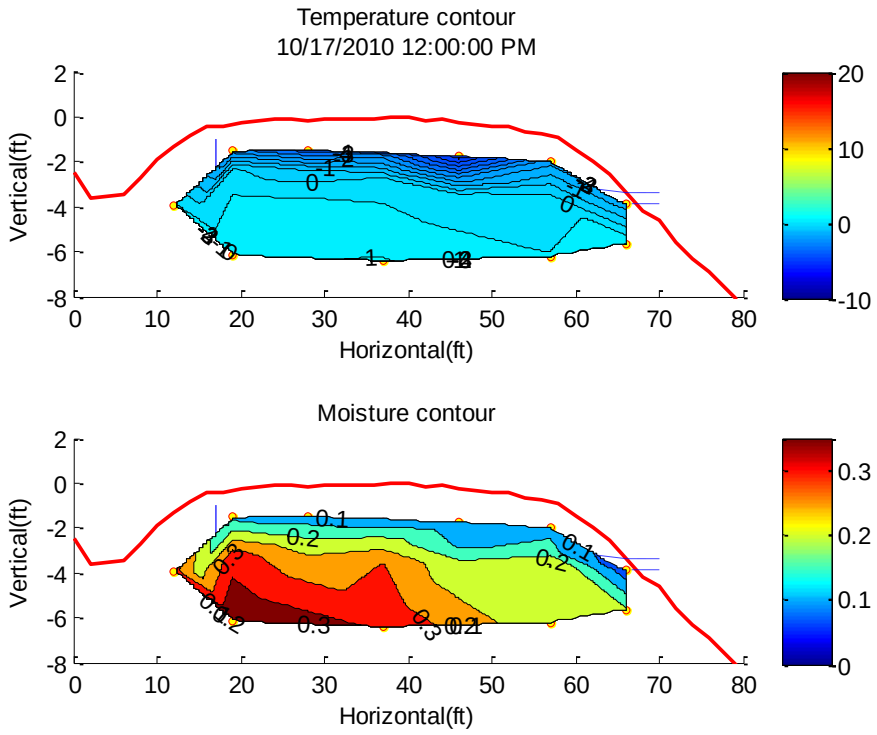

Figure 88. Temperature and moisture content contours at noon on October 17, 2010

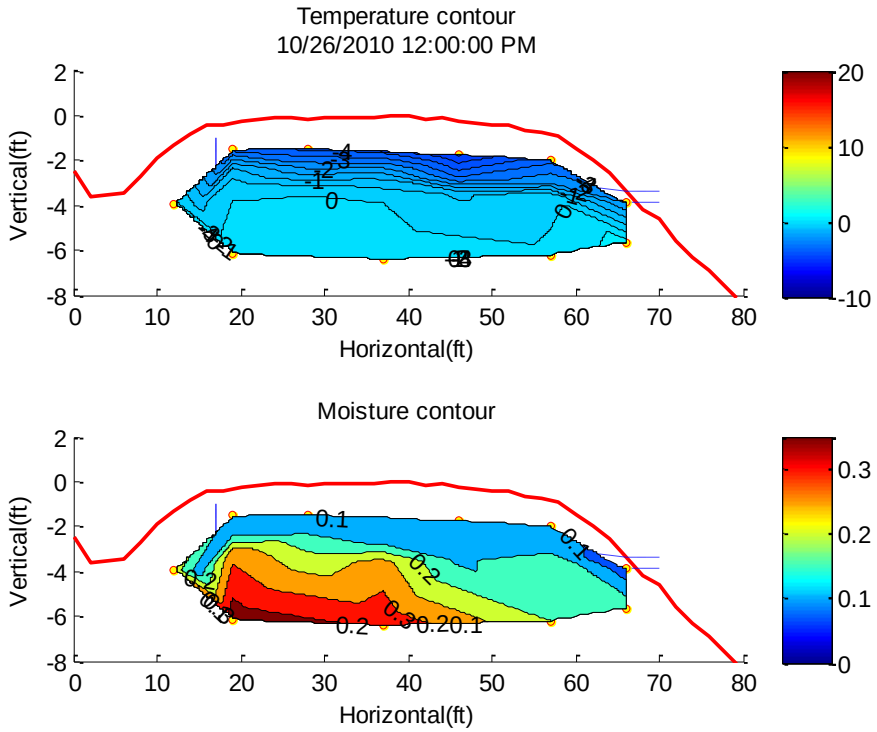

Figure 89. Temperature and moisture content contours at noon on October 26, 2010

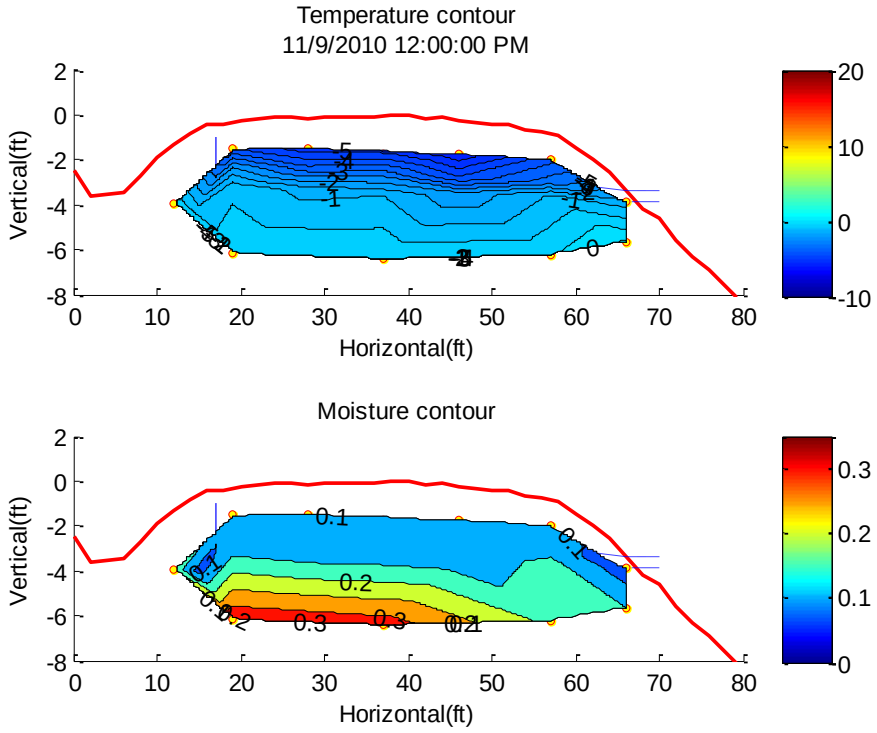

Figure 90. Temperature and moisture content contours at noon on November 9, 2010

Figure 91 shows the temperature and moisture content contours for the road section on March 12, 2011, when the whole road section was completely frozen during the field trip (Figure 54). The moisture content was not above 10% anywhere.

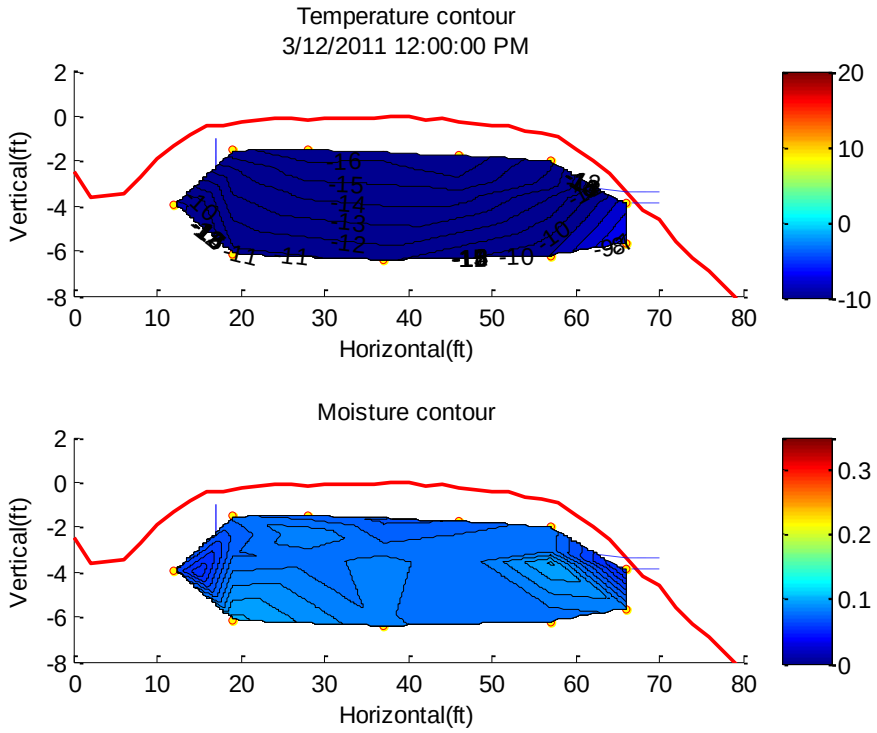

Figure 91. Temperature and moisture content contours at noon on March 12, 2011

When the air temperature rose to above zero on April 26, 2011, the whole road test section remained frozen, and the unfrozen moisture content was very low, as shown in Figure 92. Figure 93 and Figure 94 show the temperature and moisture content contours of the road section on May 15 and May 22, 2011, when the thawing depths were 1.5 feet and 2.5 feet below the road surface. Appendix I shows that during this period, although the moisture content in the range of 1.5–2.5 feet below the road surface increased, the soils did not reach saturation anyplace. Soils at sensor 22 near the ditch remained frozen. Note that in previous years, frost boils/soft spots were apparent at this time. We concluded, therefore, that in previous years frost boils/soft spots in early spring each year at the Beaver Slide were not likely caused by groundwater; they were more likely caused by thawing of in situ water in the soils. Since an excess amount of water is needed to form frost boils/soft spots, it must come from thawing of ice lenses caused by frost heave. Figure 93 and Figure 94 as well as the figures in Appendix I for the period of April 26 to May 22, 2011, indicate that the soil moisture content in the road section remained low, which implies that there was no frost heave 2.5 feet below the road surface. In other words, the H2Ri wicking fabric successfully eliminated frost heave and subsequent thaw weakening in early spring 2011.

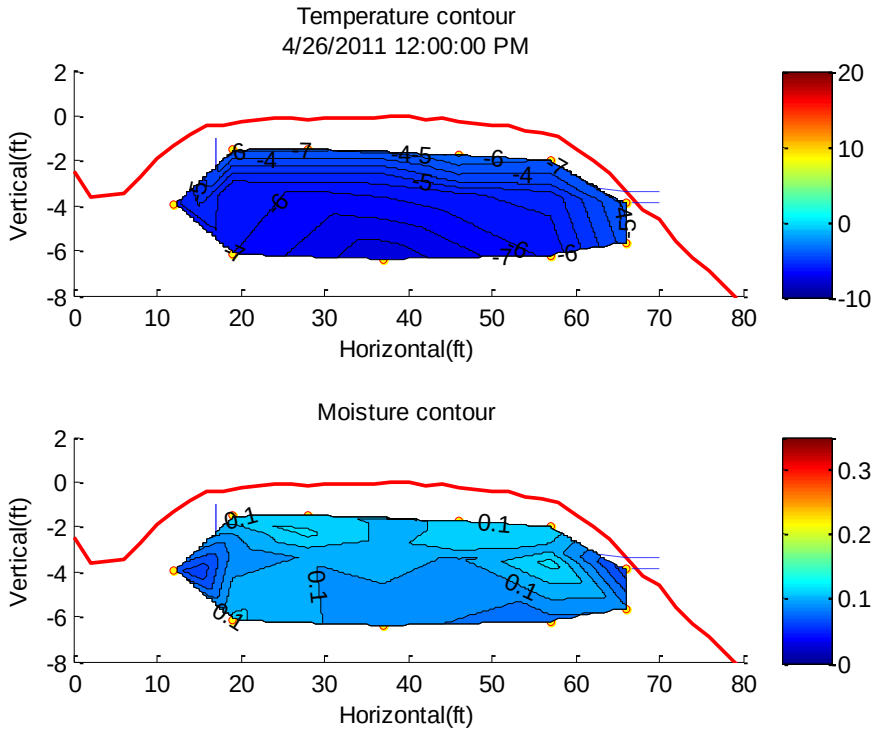

Figure 92. Temperature and moisture content contours at noon on April 26, 2011

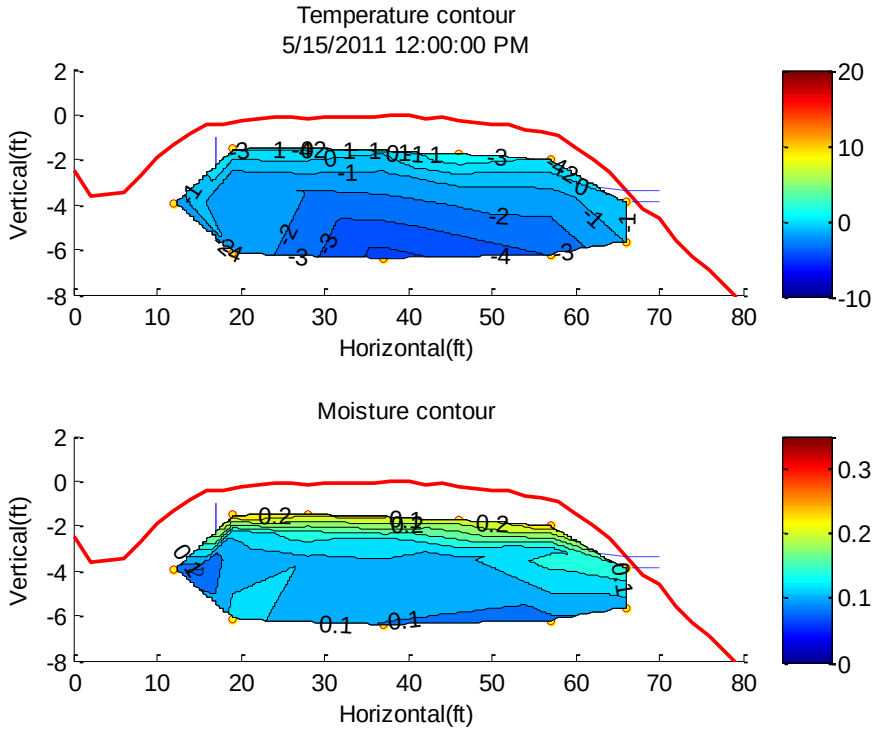

Figure 93. Temperature and moisture content contours at noon on May 15, 2011

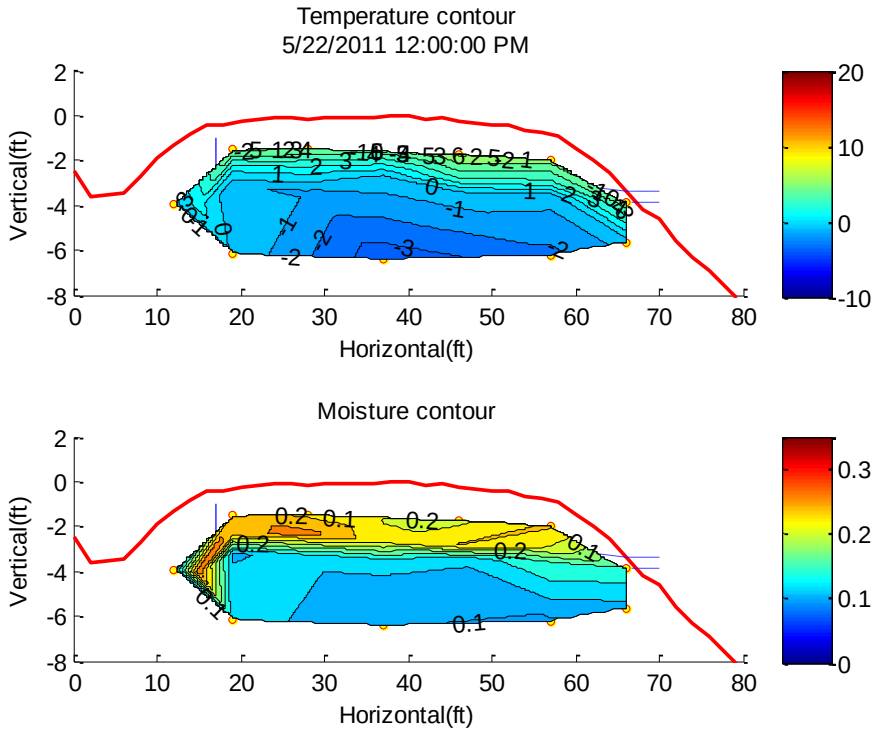

Figure 94. Temperature and moisture content contours at noon on May 22, 2011

Figure 95 shows the temperature and moisture content contours of the road section on May 29, 2011. The east lane of the road section had higher soil temperatures and thawed to a

depth of 6 feet below the road surface, while the west lane of the road thawed to a depth of 4.5 ft. In Figure 95, it can be seen that soils at sensor locations 2, 5, 8, 9, 19, 21, and 22 were nearly saturated. There was a frozen soil protrusion at sensor locations 20, 16, 11, 12, and 13, seen more clearly in Figure 96, which shows the temperature and moisture content contours of the road section on May 30, 2011. The frozen soil protrusion reduced at the center of the road where sensors 12 and 13 were located. On both sides of the frozen soil protrusion, soils were near saturation at the depth of 4 feet below the road surface. Compared with Figure 95, the soils at the east lane of the road were much drier, as shown in Figure 96. The soils at 6 feet below the road surface remained frozen.

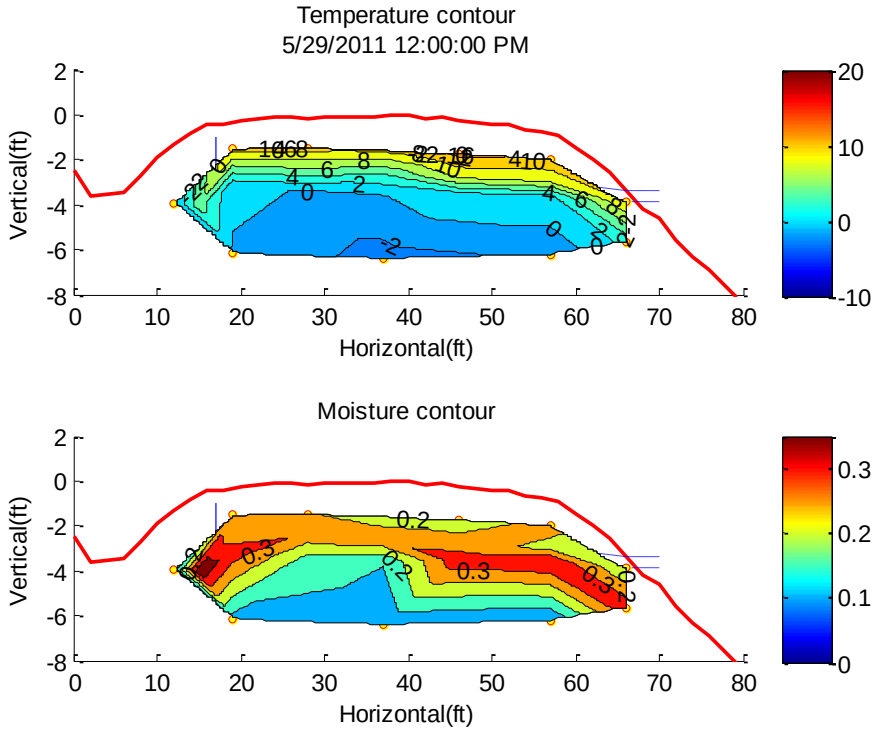

Figure 95. Temperature and moisture content contours at noon on May 29, 2011

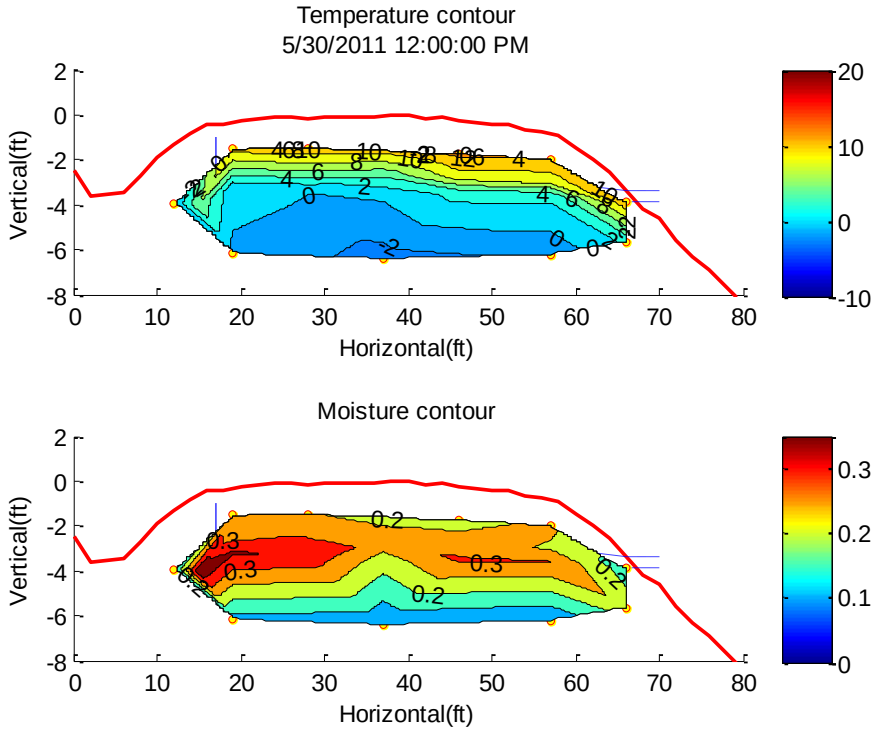

Figure 96. Temperature and moisture content contours at noon of May 30, 2011

From April 17 to June 8, 2011, there was no clear indication of any rainfall event. The groundwater was mainly from thawing of frozen soils from the hill. On the morning of June 9, 2011, a rainfall event occurred. As a result, the water content of the road section increased. As shown in Figure 97, there was a high water content channel at 3 to 5 feet below the road surface where the two layers of H2Ri wicking fabric were installed. The soils 5 feet below the road surface remained frozen, and was considered an impermeable layer. The soils above 3.0 feet below the road surface had moisture content of less than 30%.

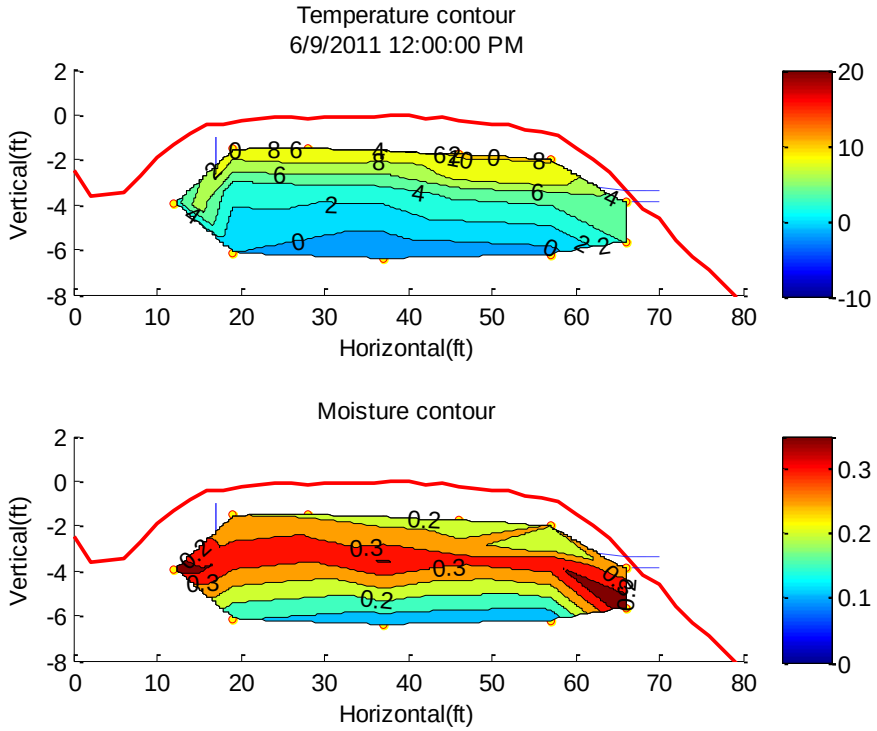

Figure 97. Temperature and moisture content contours at noon on June 10, 2011

Figure 98 shows the temperature and moisture content contours at noon on July 1, 2011, after a possible rainfall event in the morning of the same day. There were three saturated soil zones in the moisture content contour: one near the ditch, one at the center, and one at the east lane. Below the saturated soil zone at the center was a frozen soil core with low (unfrozen) water content, which seems to imply that non-uniform thawing of the soils caused ponding of water at the center of the road. With the installed wicking fabric, the road section dried out in a few days. Figure 99 shows the temperature and moisture content contours at noon on July 5, 2011. Comparing Figure 98 and Figure 99, it can be seen that the wicking fabric works as a siphon to drain the ponded water caused by non-uniform thawing. This is consistent with the results from the laboratory tests as discussed in Chapter 2.

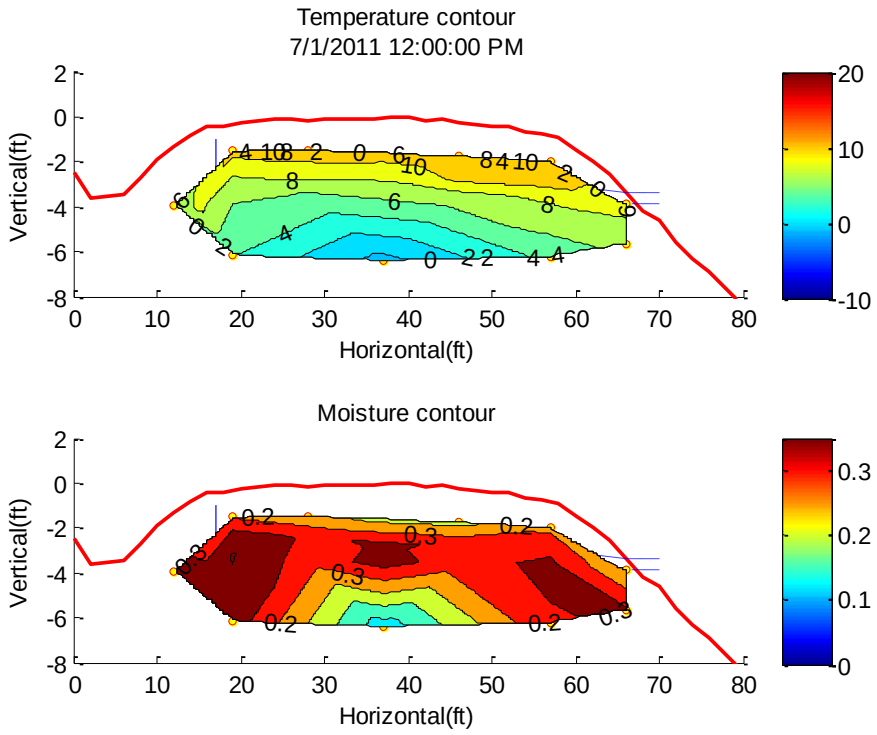

Figure 98. Temperature and moisture content contours at noon on July 1, 2011

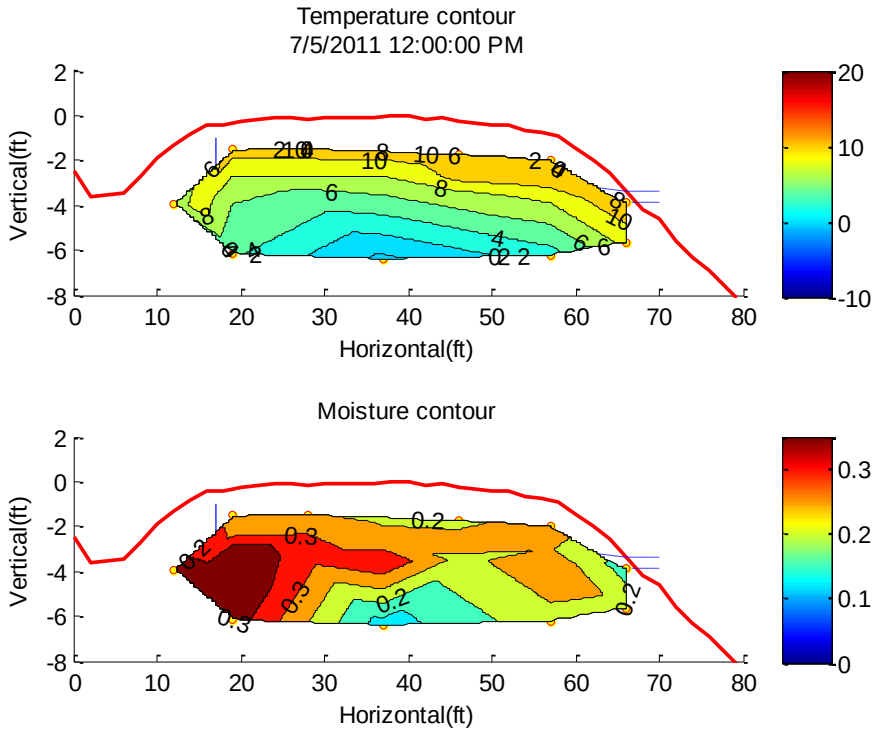

Figure 99. Temperature and moisture content contours at noon on July 5, 2011

Figure 100 shows the temperature and moisture content contours at noon on July 18, 2011, after a possible rainfall event in the morning of the same day. There were three

saturated soil zones at the same locations as those in Figure 98, which confirmed the conclusion that the wicking fabric works as a siphon to drain the ponded water caused by non-uniform thawing. Comparing Figure 98 and Figure 100, it can be seen that the frozen soil core had been reduced significantly.

Figure 101 shows the temperature and moisture content contours at noon on July 21, 2011, when the road section was completely thawed. The soils at 6 feet below the center of the road became saturated. The moisture content contour was similar but not identical to the ones in Figure 75, Figure 77, and Figure 85 for the previous year. The difference might imply that the freeze-thaw cycle changed the soil structure in the road section. Specifically, it seemed that the soils at the west lane of the road between sensor locations 13 and 22 had been loosened and had higher moisture content compared with the previous year. The soils at the east lane of the road were significantly drier than soils at the west lane.

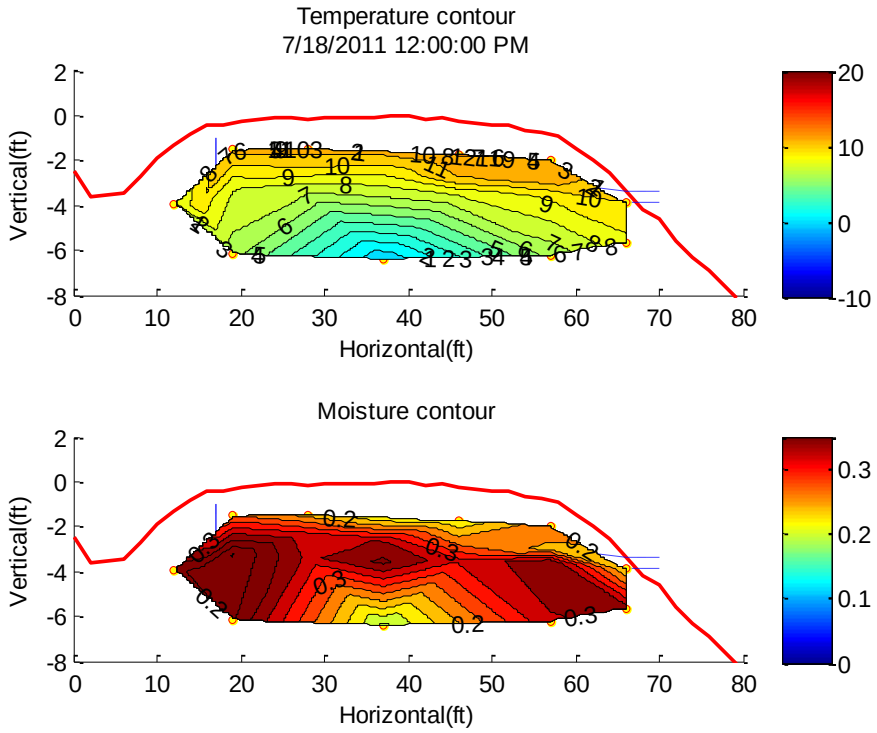

Figure 100. Temperature and moisture content contours at noon on July 18, 2011

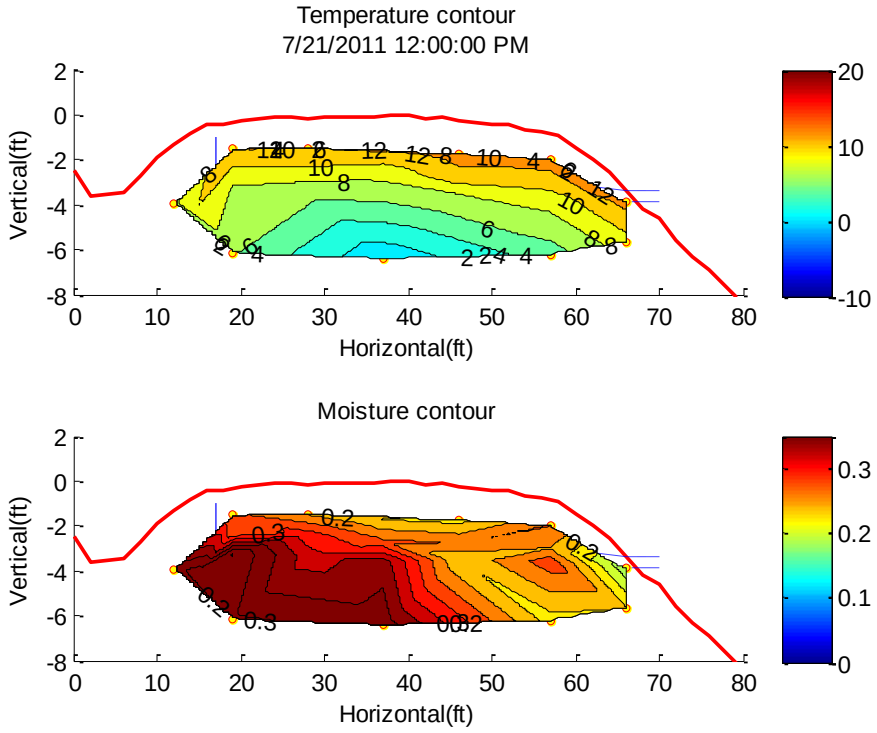

Figure 101. Temperature and moisture content contours at noon on July 21, 2011

Several rainfall events as well as the continuous thawing of frozen soils on the hill kept the road section relatively wet in August and early September 2011. Figure 102, Figure 103, Figure 104, and Figure 105 show the temperature and moisture content contours at noon on July 31, August 3, August 15, and August 24, 2011, respectively, after a rainfall event on each day. The first 3 feet of soils below the surface, however, was always unsaturated with lower water content. In addition, after a rainfall event, the road section on the east lane dried out in a few days along the horizontal direction where the wicking fabric was installed. All the moisture content contours clearly show that water moved along the wicking fabric out of the road structure.

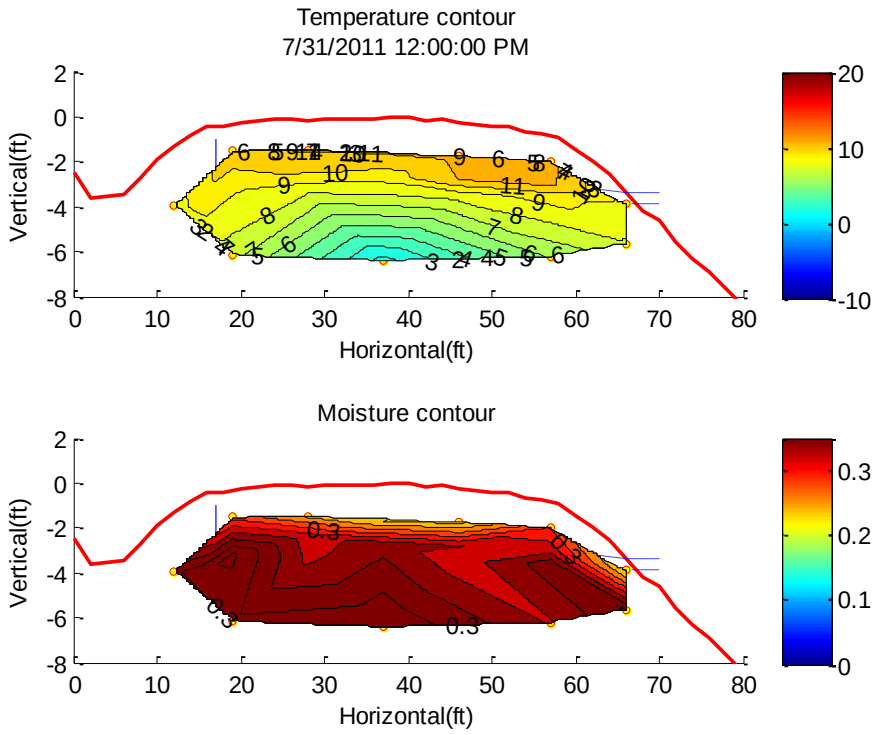

Figure 102. Temperature and moisture content contours at noon on July 31, 2011

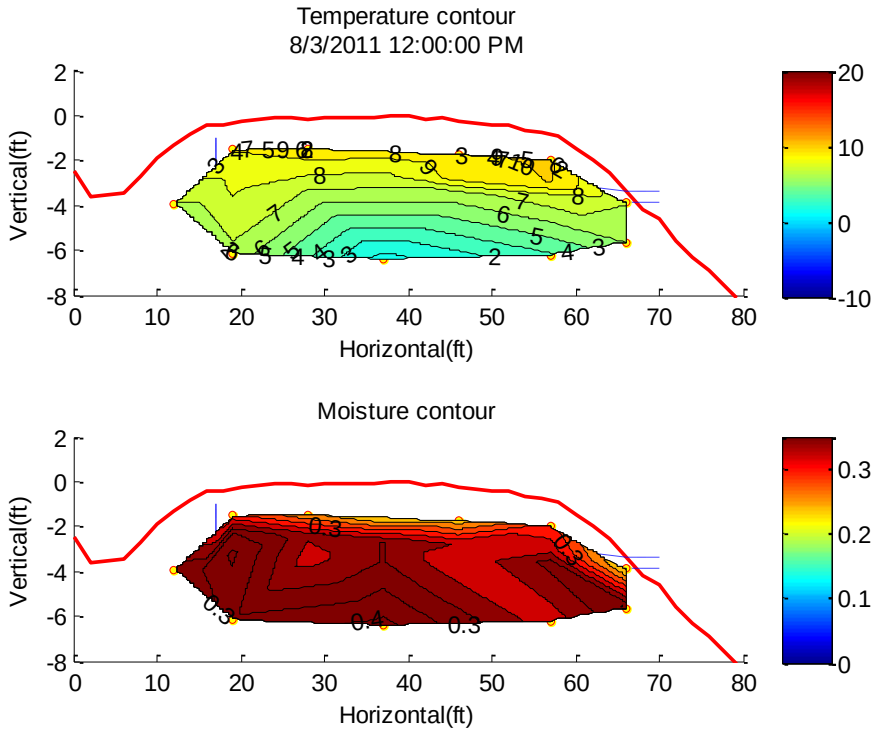

Figure 103. Temperature and moisture content contours at noon on August 3, 2011

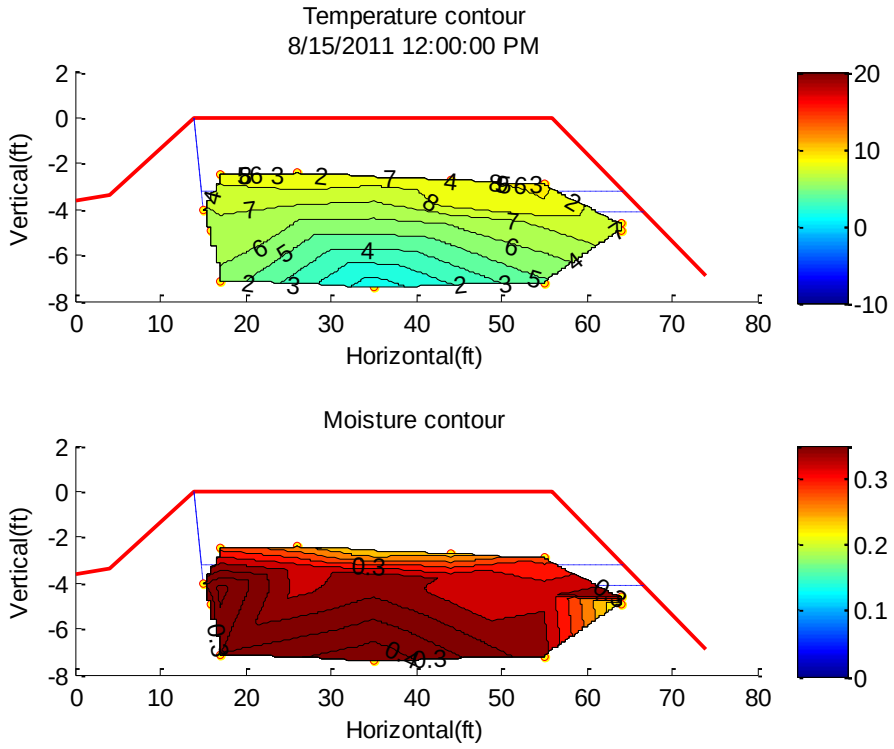

Figure 104. Temperature and moisture content contours at noon on August 15, 2011

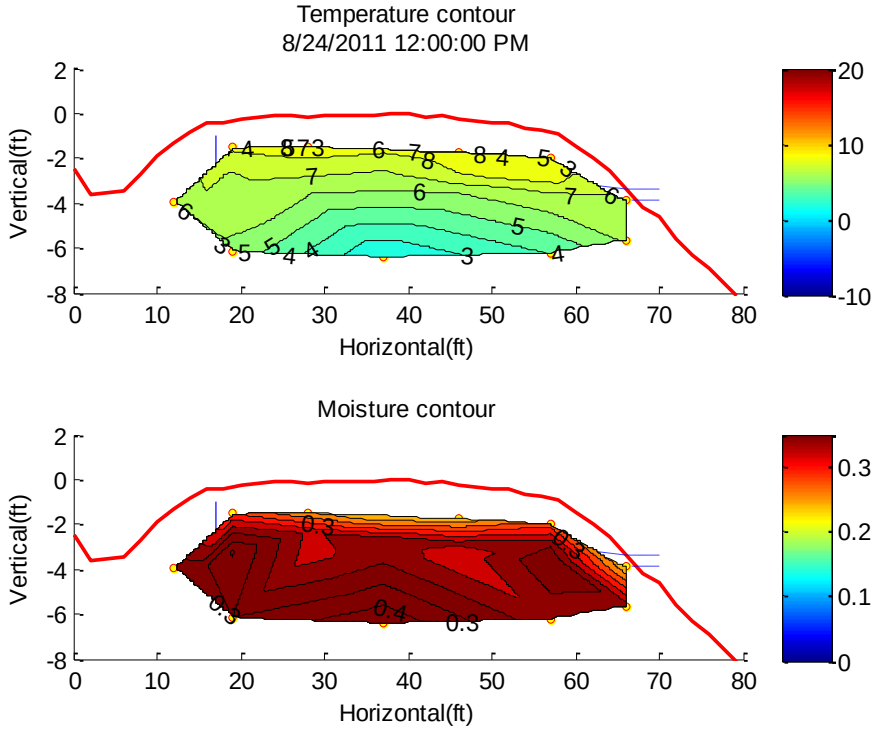

Figure 105. Temperature and moisture content contours at noon on August 24, 2011

In 2011, the air temperature dropped to zero on September 23. The corresponding temperature and water content contours are shown in Figure 106. Before the soil froze, water

had drained out, and the moisture content in most of the road section was low, especially in the first 3.5 feet below the road surface, where the soil moisture content was generally less than 20%, corresponding to a degree of saturation less than 50%. Because the soils were relatively dry, frost heave was not expected to occur in the first 3.5 feet of soils.

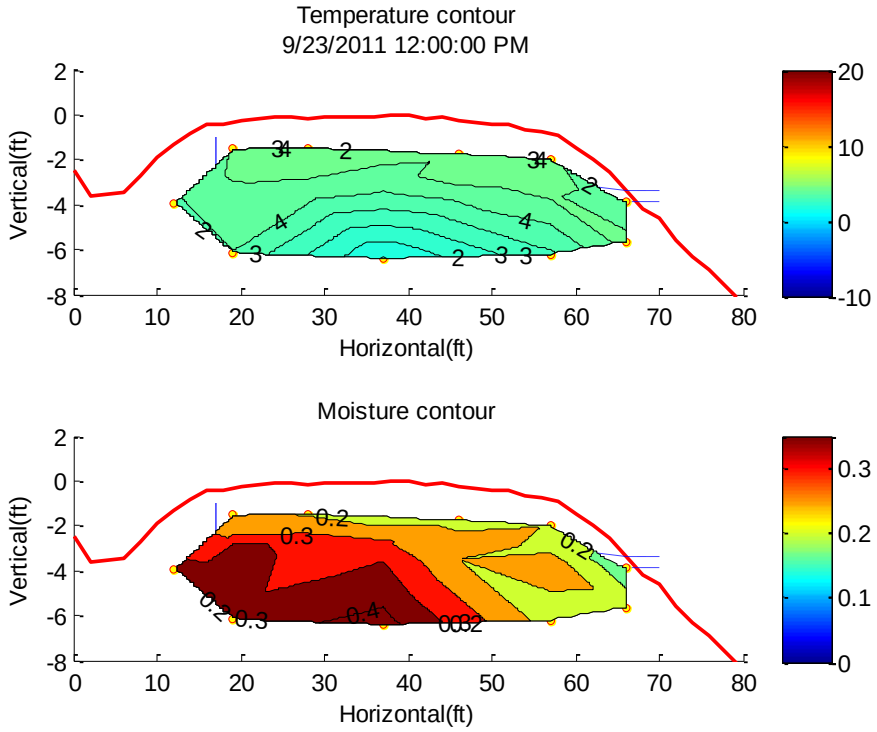

Figure 106. Temperature and moisture content contours at noon on September 23, 2011

Figure 107, Figure 108, Figure 109, and Figure 110 show the temperature and moisture contours when the freezing front penetrated to 1.5 ft, 2.5 ft, 3.5 ft, and 6 feet below the road surface, respectively. There was concern that the wicking fabric would lose function when the exit at the edge froze. Such a scenario seemed not to happen. Once the air temperature dropped to zero and the soils started freezing, the water supply from the uphill slope was reduced. Consequently, the soil water content in the road section was reduced during the freezing process, as shown in Figure 107–Figure 110. Figure 111 shows the temperature and moisture contours when the road section was completely frozen. The unfrozen moisture content in the whole road section dropped to 10% or less.

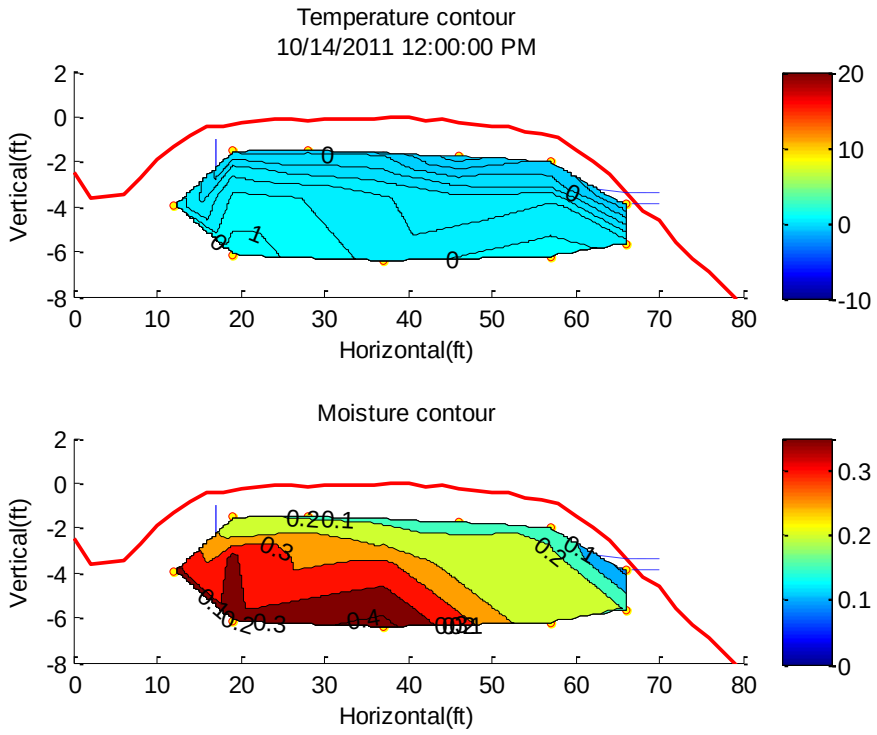

Figure 107. Temperature and moisture content contours at noon on October 14, 2011

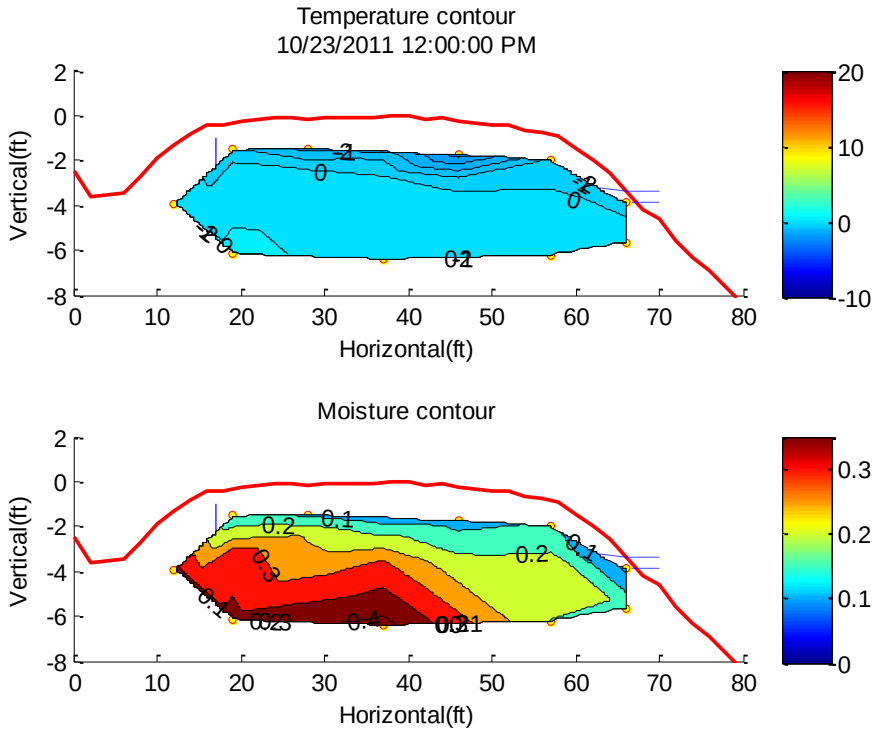

Figure 108. Temperature and moisture content contours at noon on October 23, 2011

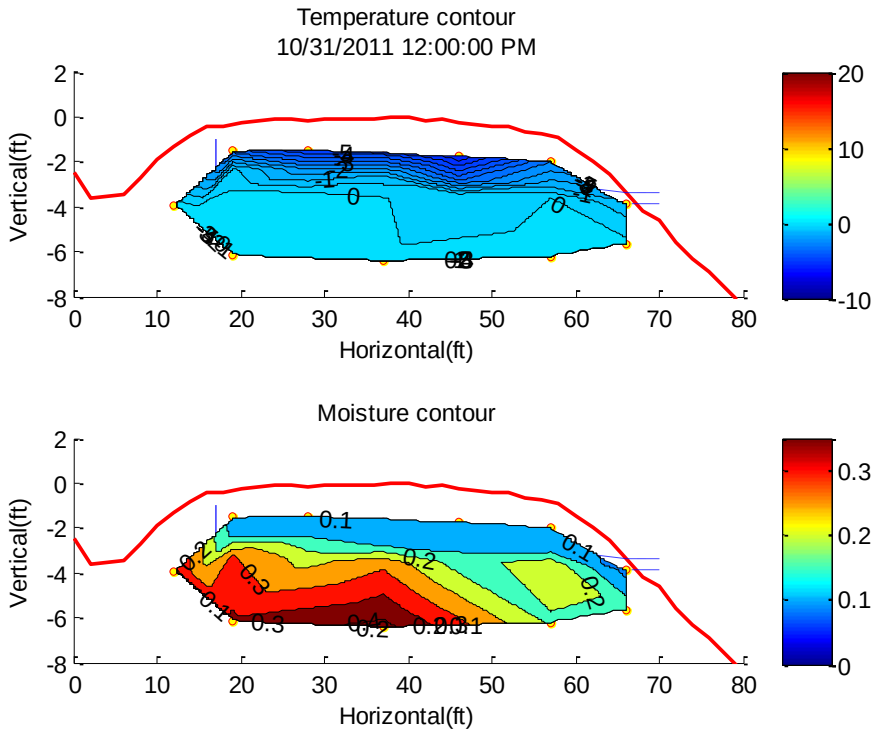

Figure 109. Temperature and moisture content contours at noon on October 31, 2011

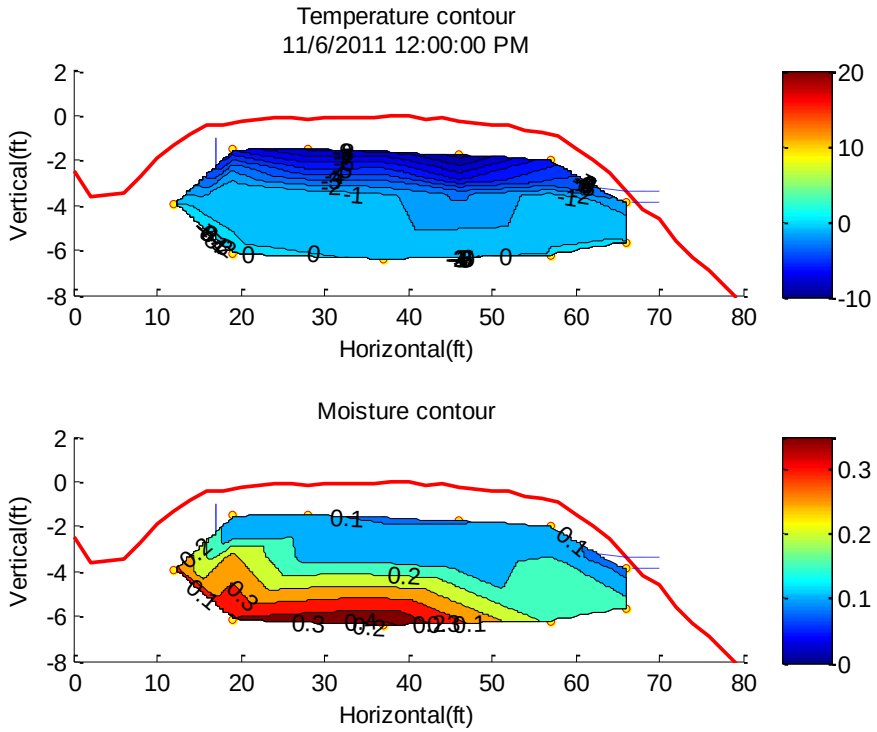

Figure 110. Temperature and moisture content contours at noon on November 6, 2011

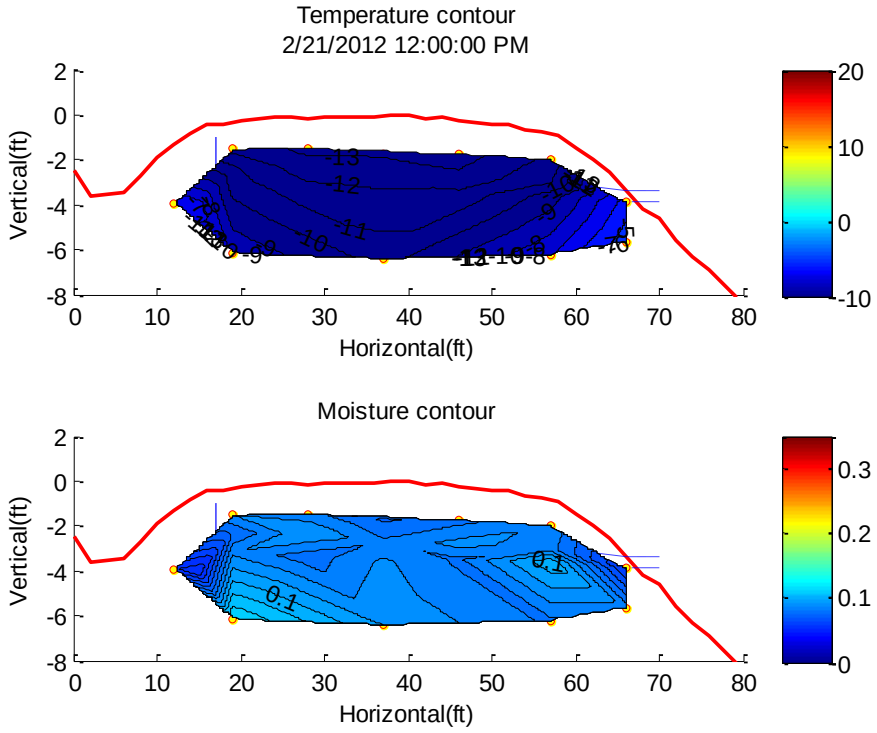

Figure 111. Temperature and moisture content contours at noon on February 21, 2012

Figure 112 shows the temperature and moisture contours when the air temperature first rose to above zero in 2012. It was found that the road section was completely frozen and the unfrozen moisture content was at 10% or less. Figure 113 and Figure 114 show the temperature and moisture contours when the thawing front penetrated to 1.5 feet and 2.5 feet below the road surface on May 12 and 22, 2012, respectively. This period corresponded to frost boils in early spring. The moisture contours during this period did not indicate any saturated soil zone, which was an indication of no frost heave in the previous year. Figure 115 shows the temperature and moisture contours when the thawing front penetrated to 3.5 feet below the road surface on May 29, 2012. Soils at sensor locations 19 and 21 near the ditch were saturated, while soils at other locations were below saturation. Similar to 2011, a frozen soil core was present at the bottom center of the road. The moisture content contour indicates that water was flowing from the ditch to the east edge along the wicking fabric.

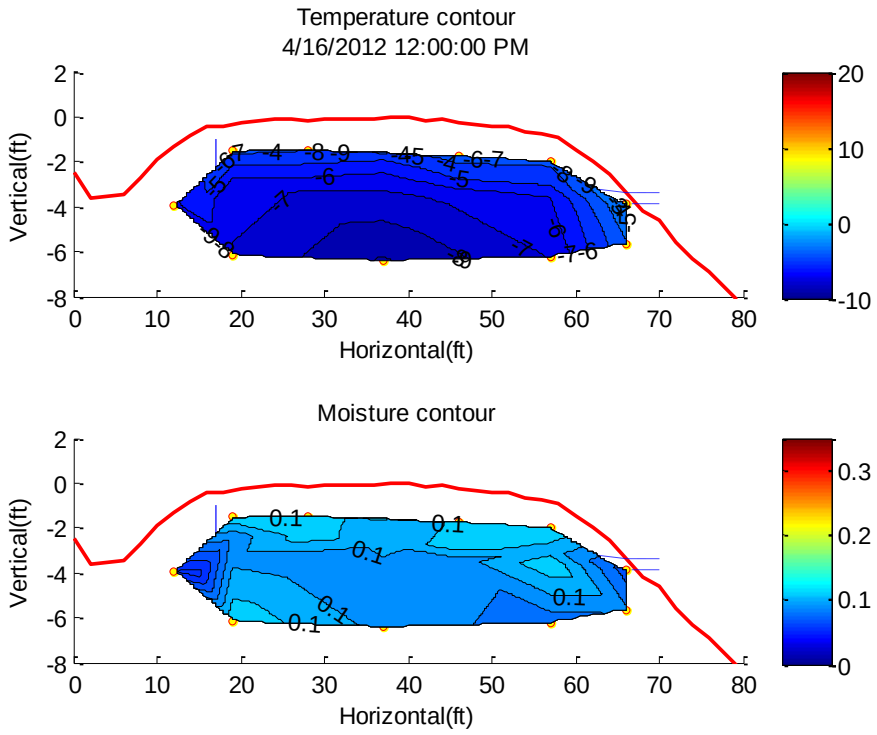

Figure 112. Temperature and moisture content contours at noon on April 16, 2012

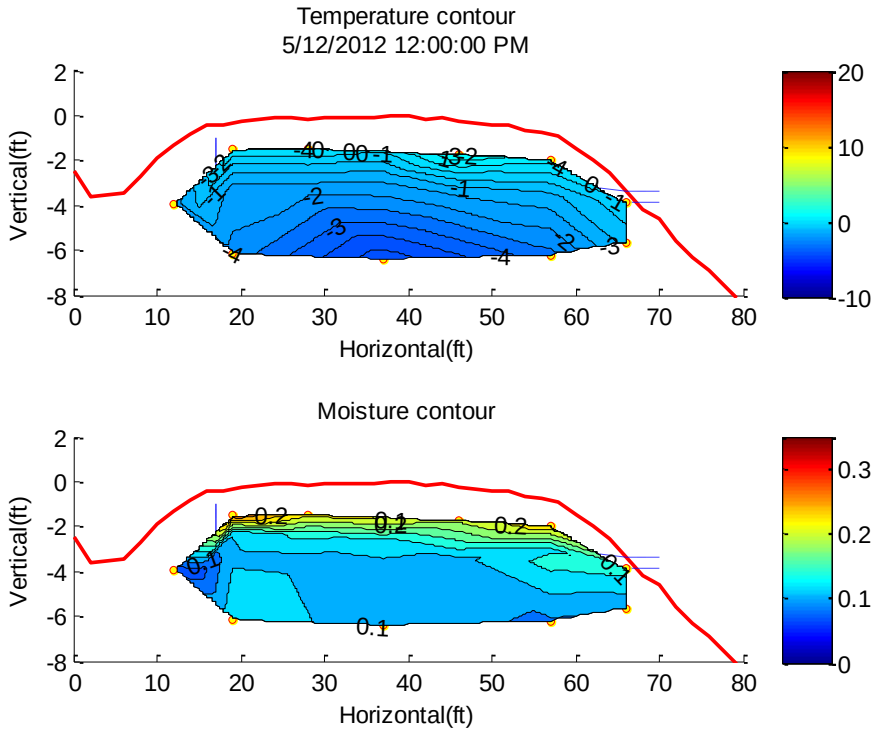

Figure 113. Temperature and moisture content contours at noon on May 12, 2012

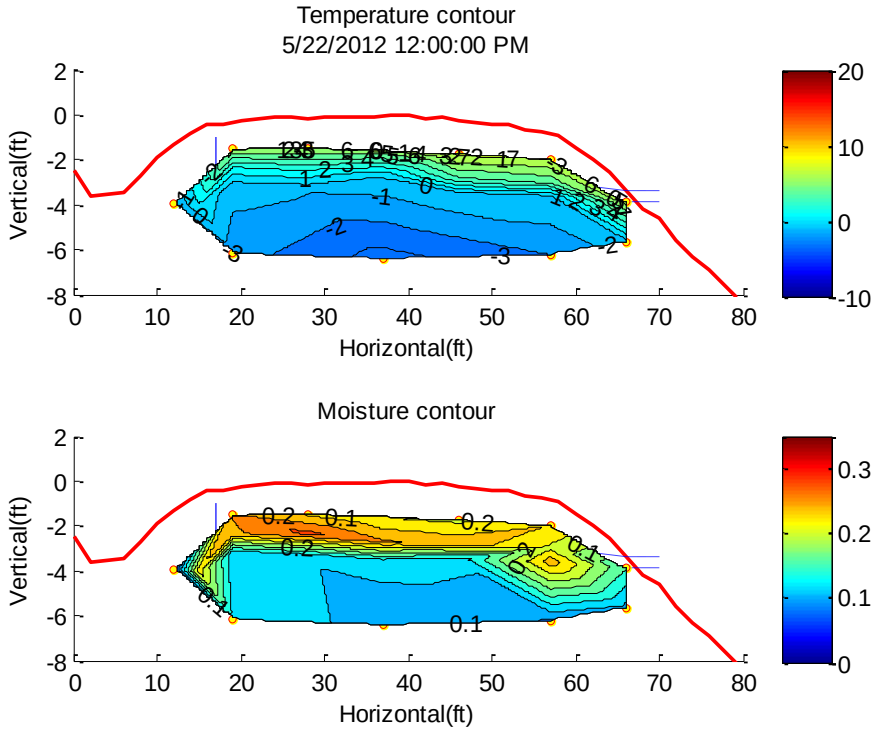

Figure 114. Temperature and moisture content contours at noon on May 22, 2012

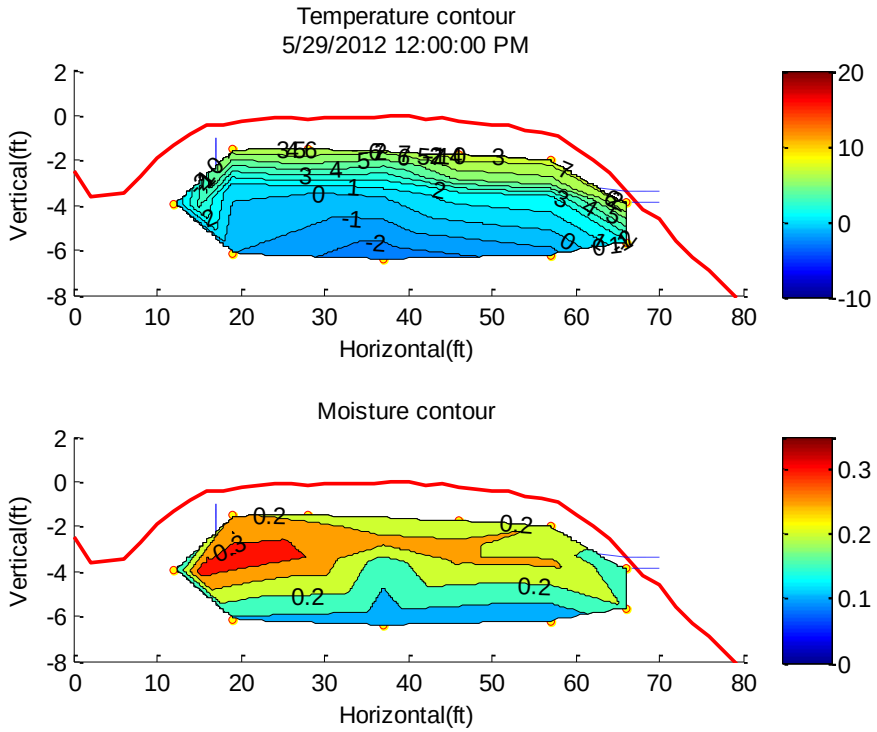

Figure 115. Temperature and moisture content contours at noon on May 29, 2012

Figure 116 shows the temperature and moisture contours on July 20, 2012, after a rainfall event. The moisture content in the road section significantly increased in comparison

with the previous days. There were three discontinuous saturated soil zones similar to those in Figure 98 on July 1, 2011, which demonstrates the non-uniform thawing of the soils and the associated ponding of water. The moisture contours in the following days (as shown in Appendix I) indicate that the ponding water drained out of the road structure along the direction of the installed wicking fabric. Figure 117 shows the temperature and moisture contours when the test section was completely thawed on July 30, 2012. The frozen soil core, as shown in Figure 116, was completely gone and the soils at the same area were saturated. In the east lane of the road, the moisture content between the two layers of wicking fabric was higher than the surrounding area, indicating the water was draining along the wicking fabric.

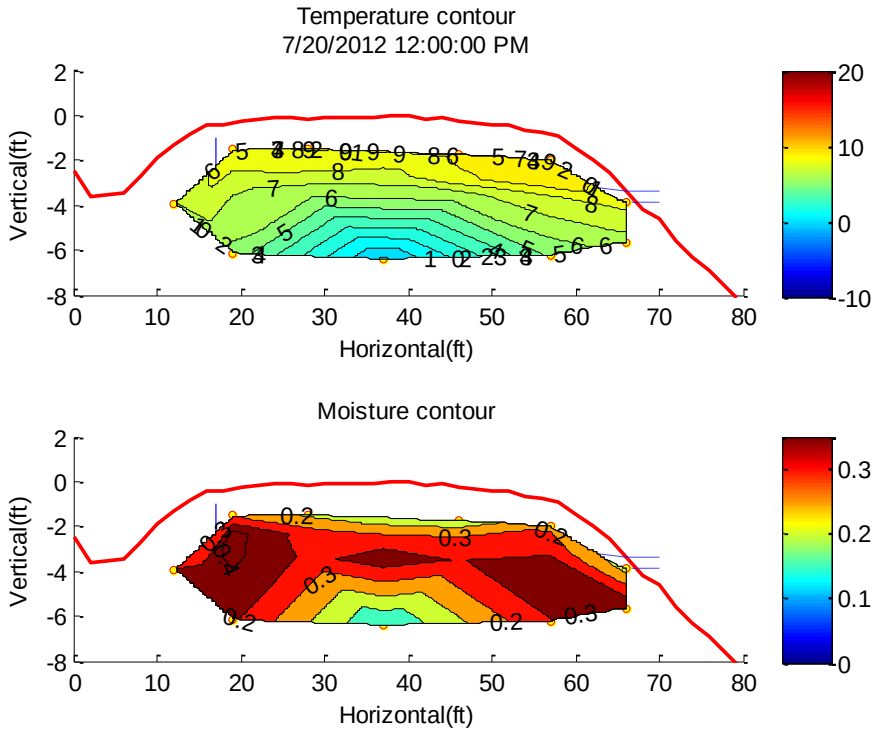

Figure 116. Temperature and moisture content contours at noon on July 20, 2012

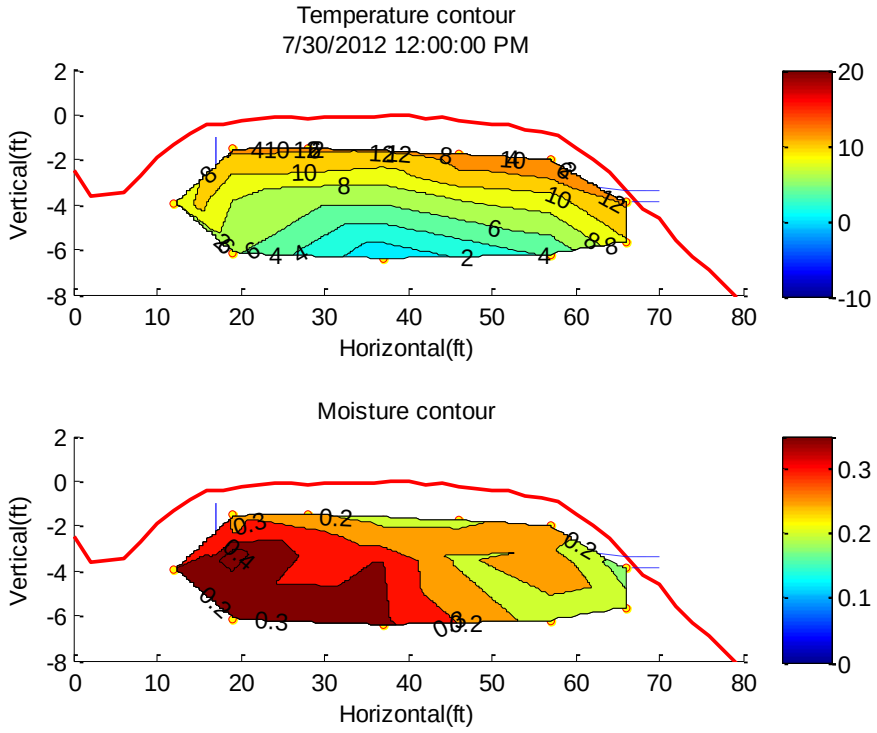

Figure 117. Temperature and moisture content contours at noon on July 30, 2012

UNFROZEN WATER CONTENT VERSUS TEMPERATURE RELATIONSHIP

Unfrozen volumetric water content was plotted against temperatures at the same location at the same time for each pair of sensors. Figure 118 shows the unfrozen water content versus temperature curve for soil at sensor location 3; it indicates that there was no clear relationship between moisture content and temperature when the soil was at temperatures above zero (unfrozen). Moisture content when the soil was unfrozen was more related to a balance between the water supply and drainage. In contrast, a clear relationship appeared between the unfrozen water content and subzero temperatures. Although such a relationship is not unique, the variation was small. Consistent with conclusions reported in much of the existing literature, freezing of water did not take place at a certain freezing point (specifically 0°C). Instead, the freezing process occurred over a range of temperatures. Figure 118 indicates that even when the soil temperature reached -23°C, 7% of the water still remained unfrozen. In temperatures ranging from 0°C to -0.4°C, the unfrozen moisture content reduced rapidly from 23% to 14%. From a temperature of -0.4°C to -23°C, the unfrozen moisture content reduced from 14% to 7% at a relatively constant rate.

Figure 119, Figure 120, Figure 121, and Figure 122 show the unfrozen water content versus temperature curve for soils at different depths of the road section. All the curves show patterns similar to that in Figure 118. Except for soils at sensor locations 1, 6, 13, and 20, the remaining soils had relationships close to the same, indicating that the soils at the road section were relatively uniform.

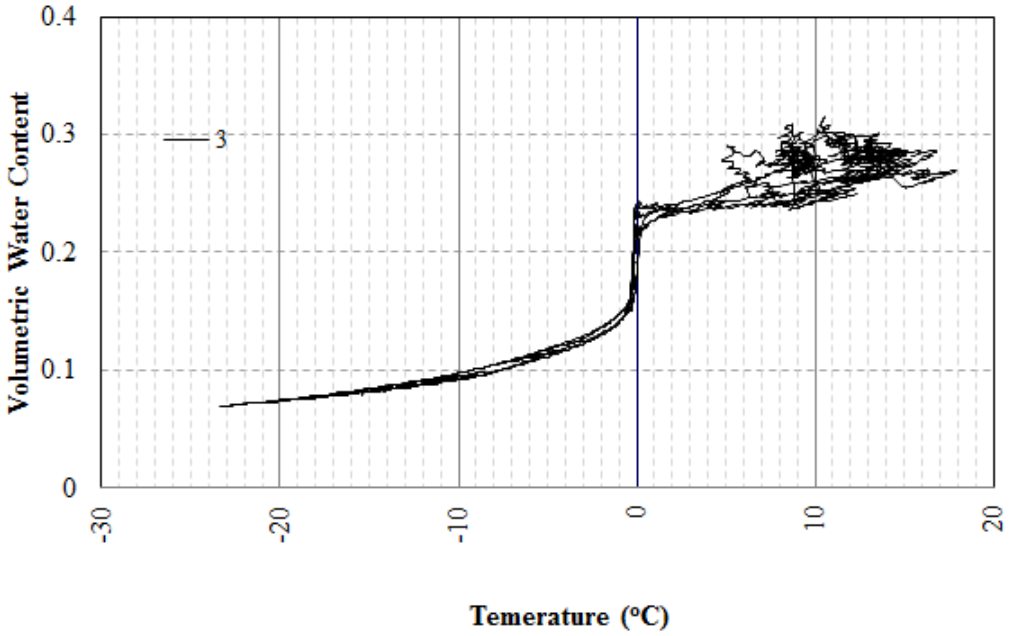

Figure 118. Unfrozen moisture content versus temperature relation at the sensor location 3

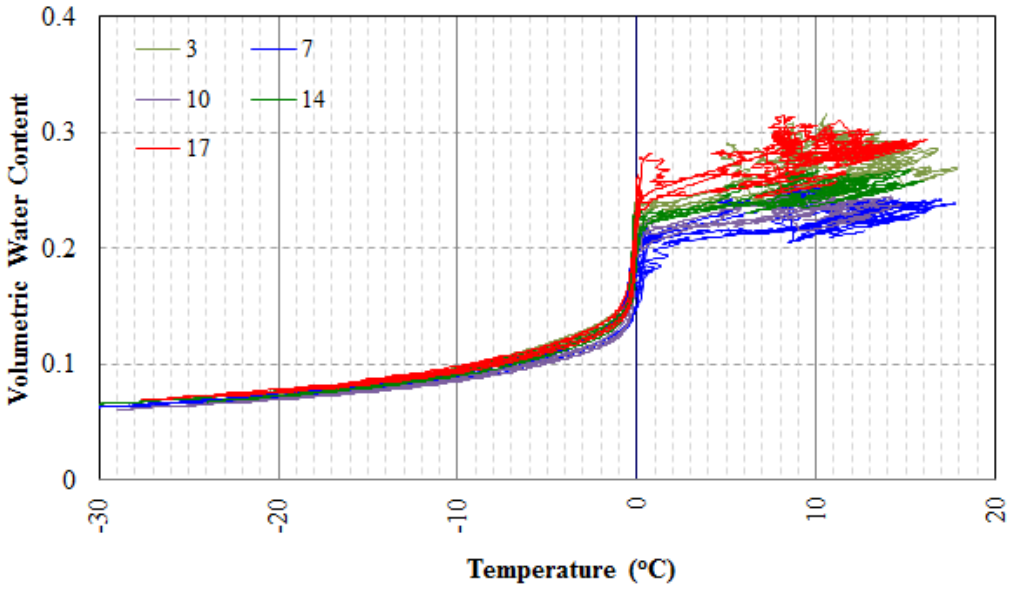

Figure 119. Unfrozen moisture content versus temperature relation for soils at 2 feet below the road surface

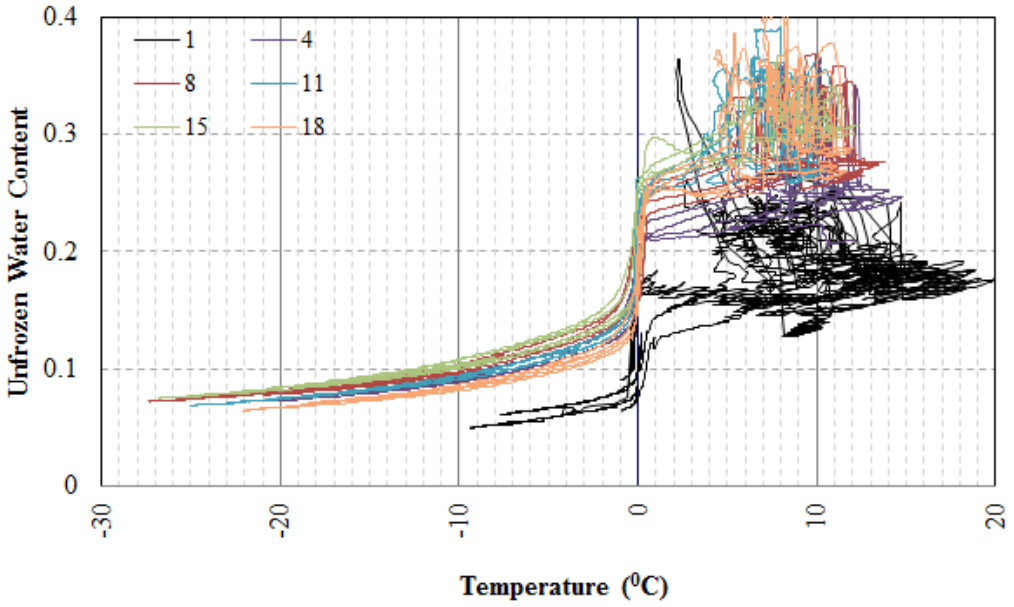

Figure 120. Unfrozen moisture content versus temperature relation for soils 3 feet below the road surface

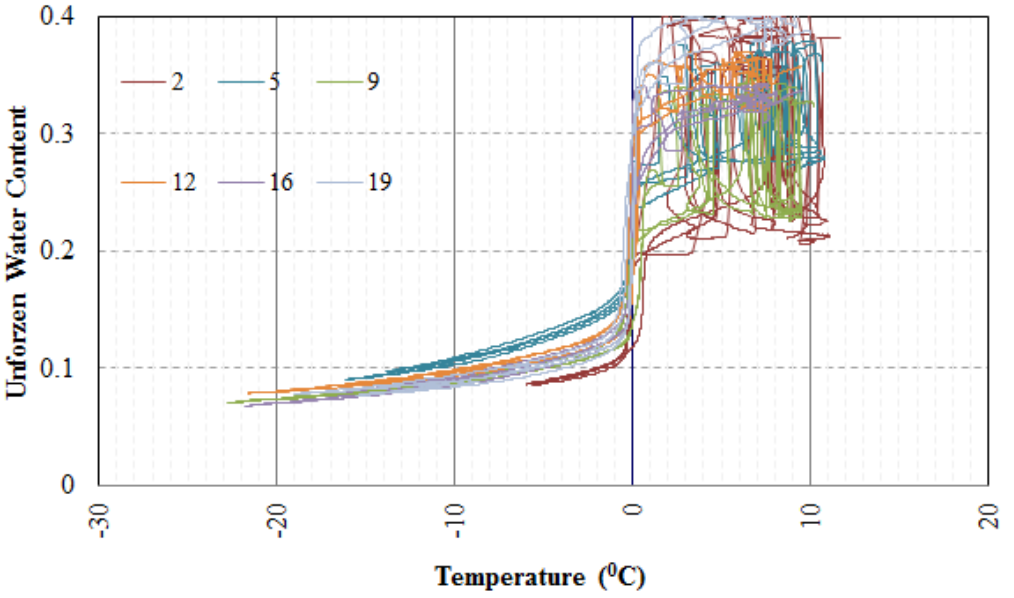

Figure 121. Unfrozen moisture content versus temperature relation for soils 4 feet below the road surface

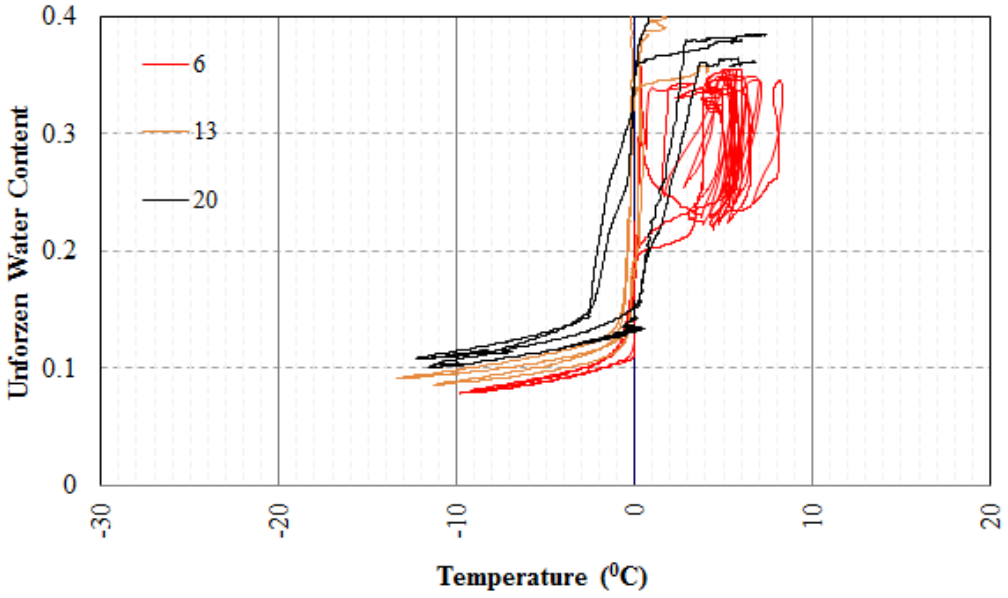

Figure 122. Unfrozen moisture content versus temperature relation for soils 7 feet below the road surface

DISCUSSION

Mechanisms of the Frost Boils/Soft Spots

Employees with DOT&PF M&O reported that frost boils occur from the end of April until mid-May each spring. As shown in Figure 112–Figure 114, soils remained frozen at 3 feet below the road surface until the end of May. Thus, the water that causes frost boils/soft spots is unlikely to be coming from the drainage ditch, which is 3.6 ft below the road surface. Instead, the water has to come from thawing of in situ water in the road structure. To form soft spots (shown in Figure 2), the soils must first be fully saturated, and excess water must be available. The excess water can only come from thawing ice lenses in the road structure. In other words, frost heave must have occurred the previous winter. For this reason, we conclude that frost boils that occur in early spring are due to frost heave and subsequent thaw weakening (see Figure 123a).

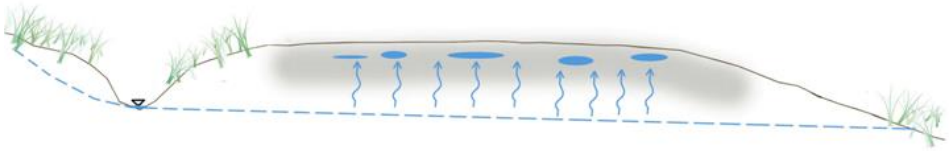

(a) Frost heave and subsequent thaw weakening during early spring (transverse direction)

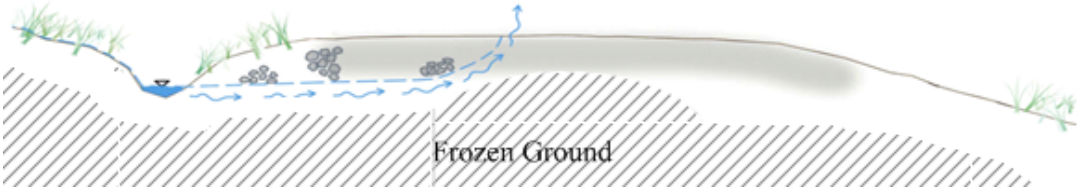

(b) Pressurized groundwater flow after lengthy rains (transverse direction)

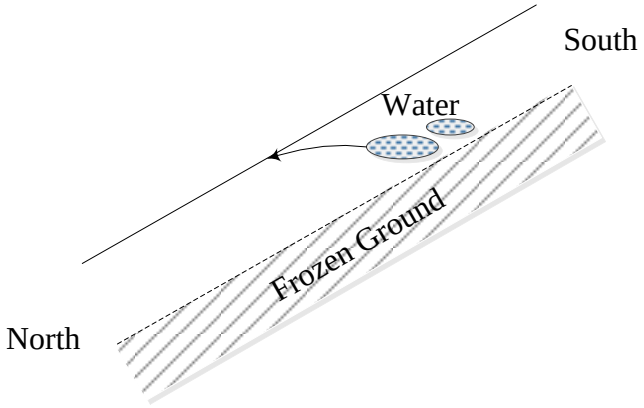

(c) Water flow in the longitudinal direction

Figure 123. Mechanism of frost boils/soft spots

Employees with DOT&PF M&O also reported that soft spots remain all summer and go away after freeze-up. Soft areas will heal if there are periods with no rain, but as soon as a significant amount of rain falls, they reappear. Figure 81–Figure 85 show variations in moisture content during a rainfall event. It was found that soils 2 feet below the road surface never reach saturation. Careful examination of moisture contours from the two-year study period indicate that soil wetting was not due to water coming from the road surface (infiltration). Instead, water was found coming from the west side of the road near the drainage ditch. Since the road prism is built on a side hill, it is natural for water to flow from the high side (west) to the low side (east). Pressurized groundwater can easily rise to the road surface in the transverse direction of the road, especially when there is a frozen (impermeable) soil core, as shown in Figure 123b. Figure 101 and Figure 117 indicate that the road section did not completely thaw until mid-July in 2011 and 2012.

For scenarios depicted in either Figure 123a or Figure 123b, it is natural for the Beaver Slide road section to form frost boils or soft spots. Figure 123c indicates the reason; it

schematically shows the Beaver Slide road section in the longitudinal direction. The Beaver Slide slopes downhill when heading north, with a gradient of approximately 11%. When water is in the road section, as shown in Figure 123c, the easiest way for free water to drain is to flow out of the road surface under the influence of gravity, because the flow path is shortest and the associated hydraulic gradient is largest.

Mechanisms of the H2Ri Wicking Fabric to Mitigate Frost Boils/Soft Spots at the Beaver Slide

It seems that H2Ri wicking fabric successfully eliminated the frost heave problem at the Beaver Slide test section. The potential mechanism involves draining water out of the road embankment and forming a capillary barrier, as discussed in the Literature Review. Figure 86 and Figure 106 show that before the soils were frozen, moisture content in the test section was low, especially in the east lane, where the volumetric moisture content was lower than 20% for most soils, corresponding to a degree of saturation of 54%. For soils with such a low degree of saturation, the unsaturated permeability of the soils is normally very low. Consequently, when heat loss occurs at the road surface with subsequent freezing downward, the water supply from the lower soils is not sufficient to sustain ice crystal growth in the freezing front. Thus, most of the ice in the frozen soils comes from freezing of in situ water in the unsaturated soils. Table 3 shows a slight increase in water content for soils 1.5 ft below the road surface after the thaw in 2011. However, the increased water content did not cause the soil to reach saturation. As mentioned in the Literature Review, frost heaving requires substantially more water than is naturally available in soil pores (Taber 1929). By draining water out of the road embankment and keeping the top soils dry, the H2Ri wicking fabric worked as a capillary barrier and eliminated frost heave in the test section, as suggested by Henry and Holtz (2001).

The H2Ri wicking fabric is an excellent material for transporting water from the road structure. As shown in Figure 19, the H2Ri wicking fabric was purposely sloped during installation. The slope helps drain water only when the soils are saturated. Note that when the soils are unsaturated, the H2Ri wicking fabric relies on the suction gradient generated by evaporation to drain water from the road embankment. Figure 124 shows the suction in the air at the Beaver Slide, which is calculated using hourly air temperature and relative humidity in the air.

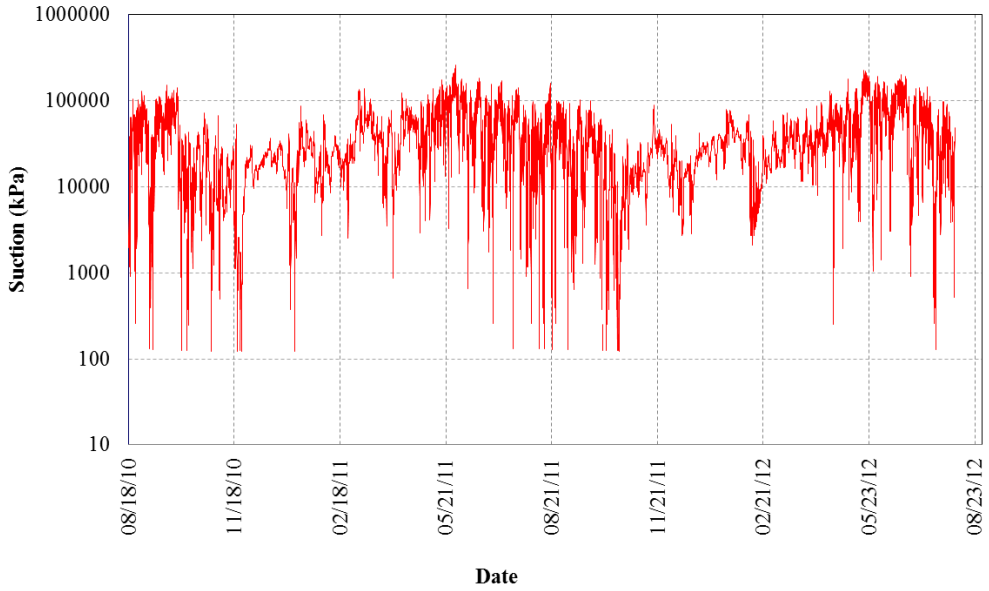

Figure 124. Suction in the Air at the Beaver Slide

Compared with thousands of kilopascal of suction in the air, the unsaturated soils in the pavement structure have suction values normally less than 1,000 kPa. The difference in suction is the driving force of H2Ri in moving water out of the road section, which is why it is important to have at least 3 feet of the H2Ri wicking fabric exposed to the air (see Figure 19).

Under situations where it is not convenient or it is impossible to install H2Ri wicking fabric with a slope, having the exposed exit portion of H2Ri lower than the road section is important. Figure 98 and Figure 99 indicate that the H2Ri wicking fabric can siphon water out if there is water ponding.

CHAPTER 5: CONCLUSIONS AND RECOMMENDATIONS

This study was an evaluation of H2Ri wicking fabric and its field performance in mitigating frost boils/soft spots at the Beaver Slide area of the Dalton Highway. Here we present the conclusions that followed from this research as well as recommendations for the use of H2Ri wicking fabric to mitigate frost boils/soft spots.

CONCLUSIONS

1. The obtained data indicate that there are two mechanisms in the formation of frost boils/soft spots at the Beaver Slide: (a) frost heave and subsequent thaw weakening which occurs in early spring, and (b) upward pressurized water flow to the road surface, similar to artesian water, during lengthy rainy periods.
2. The test section was built at an area where the most soft spots had occurred in previous years. Surface observations by the ADOTP&F M&O crew for the Dalton Highway indicate that H2Ri was able to eliminate the damage caused by both mechanisms. The test section performed very well during the two-year study period. No soft spots or frost boils occurred in the test section treated with H2Ri, but soft spots or frost boils were observed during early spring or a particularly rainy period just beyond the upper and lower ends of the test section. The M&O personnel claim they can clearly see where the road has been treated with H2Ri based on the road surface performance.
3. The animation of the change in volumetric water content clearly indicated that water flows along the direction of the wicking fabric to the shoulder of the road. Field observations indicated that soil at the shoulder was damp.
4. The animation of the change in volumetric water content and temperature in the road structure tends to indicate that frost boils in early spring are due to thaw weakening only, since the soil above the ditch line was still frozen when frost boils appeared.
5. H2Ri successfully eliminated frost heave and thaw weakening in the first 3.5 feet below the road surface (below the second layer of H2Ri). The observed volumetric moisture content indicated that the soils did not reach saturation in the test section. The D-1 material used in the Beaver Slide indicated no frost heave at all. However, soils at 4.5 ft below the center road surface, beyond the treated zone, indicated excess water due to frost heave, though this depth was too great to cause damage to the road structure.
6. H2Ri is an excellent material for draining water out of the road structure if used properly. The material itself has high ability to absorb water from surrounding soils and to transport water under differential water pressure. The pressure difference can be generated by exposing H2Ri to the atmosphere.
7. The obtained data indicate that the instrumented sensors functioned well and the data were consistent with each other. The whole data-acquisition system functioned well

during the two-year study period and could be used for a longer monitoring period if needed.

RECOMMENDATIONS

The following recommendations are made regarding the use of H2Ri wicking fabric to mitigate frost boils/soft spots.

1. H2Ri is an excellent material for draining water out of the road structure. It has high ability to absorb water from the surrounding soils due to its high specific surface area. It seems that H2Ri can maintain saturation in a high-suction (dry) environment and, therefore, high permeability under both saturated and unsaturated conditions. However, H2Ri itself does not provide the driving force for water to move. Proper design should generate a hydraulic head difference for water to move. This can be done by installing H2Ri on a slope or exposing it to air at the exit.
2. Installation of H2Ri with a slope will have the best effect in draining water out of the road structure when soils are saturated. Exposing H2Ri to the air works best when the soils are unsaturated. A combination of both features is expected to have the best effect.
3. Under situations where it is not convenient or is impossible to install H2Ri wicking fabric with a slope, it is important to have the exposed exit portion of the fabric lower than the fabric in the road section. H2Ri wicking fabric can siphon water out if there is water ponding.
4. It is recommended that long-term performance of H2Ri be investigated. Several concerns should be addressed, one being the degradation of the wicking fabric under sunshine exposure, and another being the possible clogging of the multiple channels in the fabric. Generally, soil clogging might be a problem,
5. When the width of H2Ri is not sufficient for one application, it is recommended that the wicking fabric be overlapped to maintain continuous water transport. An overlap of 18 inches is recommended for this purpose.

REFERENCES

DOT&PF (2004). *Alaska Department of Transportation and Public Facilities Standard Specification for Highway Construction.*

Allen, T., Bell, J. R., and Vinson, T. S. (1983). "Properties of Geotextiles in Cold Regions Applications." Report 83-6. Transportation Research Institute, Oregon State University, Corvallis.

Beskow, G. (1946). "Supplement: Some results of Scandinavian soil frost research 1935–1946." In Soil freezing and frost heaving with special applications to roads and railroads. Swedish Geological Society, Series Cv, No. 375, Year Book 3.

Casagrande, L. (1938). "Examination of the sub-soil of roads." In *Proceedings of the 8th International Road Congress*, The Hague, pp. 1–27.

Esch, D. (1994). "Long-Term Evaluations of Insulated Roads and Airfields in Alaska." *FHWA_AK_RD_94_18 Final Report.* Alaska Department of Transportation and PublicFacilities. http://www.dot.state.ak.us/stwddes/research/assets/pdf/fhwa_ak_rd_94_18.pdf

Guthrie, W.S., and Hermansson, Å. (2006). "Saturation of granular base material due to water vapor flow during freezing." In *Proceedings of the American Society of Civil Engineers 13th International Conference on Cold Regions Engineering*. CD-ROM. Orono, Maine, July 2006.

Henry, K.S. (1990). Geotextiles as capillary barriers." *Geotechnical Fabrics Report* 8(2): 30–36.

Henry, K.S., (1995). "The use of geosynthetic capillary barriers to reduce moisture migration in soils." *Geosynthetics International* 2(5): 883–888.

Henry, K.S. (1996). "Geotextiles to mitigate frost effects in soils: A critical review." *75th Annual Meeting of the Transportation Research Board*, Washington, DC. Paper no. 1534 (94 pp.), pp. 5-11

Henry, K.S. (1998). "The use of geosynthetics to mitigate frost heave in soils." *Ph.D. dissertation*, Civil Engineering Department, University of Washington, Seattle.

Henry, K.S., and Holtz, R.D. (2001). "Geocomposite capillary barrier to reduce frost heave in soils." *Canadian Geotechnical Journal* 38: 678–694.

Henry, K.S., and Stormont, J.C. (2002). "Geocomposite barrier drain for limiting moisture changes in pavement subgrades and base courses,. *Final Report for NCHRP-IDEA Project 68*, The National Academies, Washington, DC, 24 pp.

Hoover, J. M., Pitt, J. M., Handfelt, L. D., and Stanley, R. L.(1981). "Performance of Soil-Aggregate-Fabric Systems in Frost-Susceptible Roads, Linn County, Iowa. In Transportation Research Record 827, TRB, National Research Council, Washington, D.C., 1981, pp. 6–14.

Jay, T. (2002). “Use of Terram to mitigate frost heave: Terram Frost Blanket.” *Terram Guidance Note,* September.

Rengmark, F. (1963). “Highway pavement design in frost areas in Sweden.” *Highway Research Record* 33, Pavement Design in Frost Areas II. Design Considerations, pp. 137–157.

Taber, S. (1929). “Frost heaving.” *Journal of Geology* 38: 303–317. In Historical perspectives in frost heave research. CRREL Special Report 91-23, U.S. Army Cold Regions Research and Engineering Laboratory, Hanover, NH, pp. 29–35.

Taivenen, O.A. (1963). “Preventive measure to reduce frost action on highways in Finland.” *Highway Research Record* 33, pp. 202–216.

Zhang, X., and Belmont, N. (2011). “Use of Wicking Fabric to Help Prevent Differential Settlements in Expansive Soil Embankments.” Geo‐Frontiers 2011: Advances in Geotechnical Engineering, Dallas, TX, USA. ASCE doi:10.1061/41165(397)400.

APPENDIX I